Constraining Anthropogenic and Biogenic Emissions Using Chemical Ionization Mass Spectrometry

Thesis by

Kathleen M. Spencer

In Partial Fulfillment of the Requirements

for the Degree of

Doctor of Philosophy

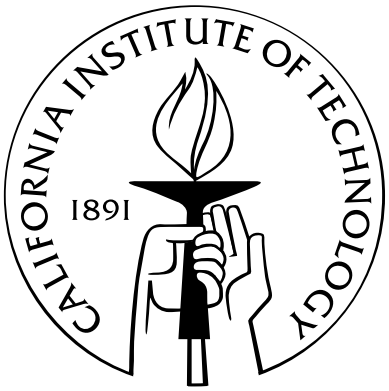

California Institute of Technology

Pasadena, California

2011

(Defended May 31, 2011)

Acknowledgements

I have many people to thank for the wonderful experience I have had at Caltech. Their guidance and support made this work possible.

First and foremost, I would like to express my sincere gratitude to my advisor, Paul Wennberg. His vast knowledge and scientific insight are truly astounding, and I am grateful to have had the opportunity to learn from him. As a member of the Wennberg Group, I have grown immensely both as a scientist and as a person.

I would like to thank Mitchio Okumura, my co-advisor. I have greatly benefited from his insight and sound advice. I also thank my committee members, Jack Beauchamp, Geoff Blake, and John Seinfeld for their diligence in overseeing my Ph.D. progress.

During my time in the Wennberg Group, I had the pleasure of working with many wonderful scientists, who became friends as well. John Crounse, Jason St. Clair, and Melinda Beaver have been invaluable resources for instrumental and scientific questions. I have learned a great deal from them and enjoyed myself during the process. I would also like to thank Coleen Roehl, Fabien Paulot, Nathan Eddingsaas, Alan Kwan, and David McCabe for many interesting discussions and knowledge shared. I am indebted to Debra Wunch for the many things she has taught me in MATLAB and LaTeX and the general interest she took in me. I was fortunate to have a wonderful officemate and friend, Gretchen Keppel-Aleks, whom I will miss very much. Gretchen has provided laughter, empathy, and perspective during my time at Caltech.

I would like to thank the members of the Okumura Group, both past and present, all of whom significantly added to my experience at Caltech. I am particularly grateful to Matt Sprague for his help and insight over the years.

I would like to thank Evelyn Novello for the support and guidance she has provided me. She made a challenging road much easier to navigate.

I have had the great fortune of making many wonderful friends while at Caltech. I am grateful to Havala Pye, Andrew Metcalf, Arthur Chan, Chethana Kulkarni, Eric Olmon, and Claire Farnsworth for their support, encouragement, patience, and friendship. I would like to thank Nathan Honsowetz for being such an important part of my life. My experience at Caltech has been greatly enhanced by the conversations, adventures, and time I have shared with these wonderful people.

I cannot adequately express my gratitude to Stephanie Rasines, Richard Norton, and Jacob Norton, my surrogate family. I am thankful for the years of encouragement, support, generosity, and perspective.

Most importantly, I cannot thank my family enough for their unconditional love and unfailing support. My Mom, my Dad, Sarah, and Anne have been there every step of the way, and for this, I am so grateful.

Abstract

Numerous gas-phase anthropogenic and biogenic compounds are emitted into the atmosphere. These gases undergo oxidation to form other gas-phase species and particulate matter. Whether directly or indirectly, primary pollutants, secondary gas-phase products, and particulate matter all pose health and environmental risks. In this work, ambient measurements conducted using chemical ionization mass spectrometry are used as a tool for investigating regional air quality.

Ambient measurements of peroxynitric acid (HO_2NO_2) were conducted in Mexico City. A method of inferring the rate of ozone production, P_{O3}, is developed based on observations of HO_2NO_2, NO, and NO_2. Comparison of this observationally based P_{O3} to a highly constrained photochemical box model indicates that regulations aimed at reducing ozone levels in Mexico City by reducing NO_x concentrations may be effective at higher NO_x levels than predicted using accepted photochemistry.

Measurements of SO_2 and particulate sulfate were conducted over the Los Angeles basin in 2008 and are compared to measurements made in 2002. A large decrease in SO_2 concentration and a change in spatial distribution are observed. Nevertheless, only a modest reduction in sulfate concentration is observed at ground sites within the basin. Possible explanations for these trends are investigated.

Two techniques, single and triple quadrupole chemical ionization mass spectrometry, were used to quantify ambient concentrations of biogenic oxidation products, hydroxyacetone and glycolaldehyde. The use of these techniques demonstrates the advantage of triple quadrupole mass spectrometry for separation of mass analogues, provided the collision-induced daughter ions are sufficiently distinct. Enhancement ratios of hydroxyacetone and glycolaldehyde in Californian biomass burning plumes are presented as are concentrations of these compounds at a rural ground site downwind of Sacramento.

Contents

List of Tables

List of Figures

Chapter 1

Introduction

Trace gases represent less than 1% of atmospheric mass. Despite their small concentrations, these gases are much more reactive than the major atmospheric constituents N_2, O_2, and Ar. Due to their reactivity, trace gases play a central role in controlling the chemical properties of the atmosphere. The concentration and spatial distribution of these gases are determined, in part, by emissions at Earth's surface.

Both anthropogenic and biogenic processes release gases to the atmosphere. Significant anthropogenic emissions of NO_x ($NO_x = NO + NO_2$), SO_2, and volatile organic compounds (VOCs) result from fossil fuel combustion, chemical processing, and industrial activities (Seinfeld and Pandis, 2006). Biogenic sources, such as plants and trees, emit substantial amounts of VOCs also. Once emitted to the atmosphere, these gas-phase species are altered by oxidation, driven by photolysis. The lifetime of gas-phase compounds ranges from seconds to years, depending on the reactivity of the compound and the concentrations of other atmospheric species.

Many urban areas are impacted by a pall of ozone, particulate matter (PM), and other oxidants. Although ozone (O_3) in the stratosphere ($\sim$10 – 50 km altitude) is beneficial and protects life at Earth's surface by absorbing UV radiation, O_3 is harmful to people, animals, and plants due to its ability to oxidize biological tissue (Jacob, 1999). The production of ozone is controlled by a complex cycling of HO_x ($HO_x = OH + HO_2$) and NO_x radicals and requires sunlight, NO_x, and hydrocarbons.

Particulate matter (also termed aerosol) is an important constituent of the atmosphere and poses both health and environmental risks. PM is typically classified by diameter: PM_{10} are particles less than 10 µm in diameter and $PM_{2.5}$ are particles less than 2.5 µm in diameter. While most particles are filtered out in the nose and throat, $PM_{2.5}$ can become lodged in the lungs and is associated with increased incidents of asthma, lung cancer, and cardiopulmonary mortality (Pope et al., 2002). Increased concentrations of PM are responsible for reduced visibility and contribute to global climate change (Forster et al., IPCC, 2007; Ramanathan et al., 2001). PM can be emitted directly into the atmosphere, but the majority of fine aerosol ($PM_{2.5}$) is produced from gas-phase precursors such as VOCs, SO_2, and NO_x.

Because of their ability to harm human health, air quality guidelines for O_3, NO_2, SO_2, and PM have been established by the World Health Organization (WHO, 2006). In the United States, the Environmental Protection Agency (EPA) sets National Ambient Air Quality Standards (NAAQS) for acceptable exposure to air pollutants. The current NAAQS for O_3 is a maximum 8-hour mean concentration of 75 ppbv not to be exceeded more than three days per year (USEPA, 2006). The current NAAQS for $PM_{2.5}$ is a maximum annual mean concentration of 15 µg m^{-3} and a maximum 24-hour mean concentration of 35 µg m^{-3} (USEPA, 2004). Compliance with these standards can be challenging as ozone production is influenced by many factors and particulate matter has many anthropogenic and biogenic sources.

Ambient measurements are central to determining air quality compliance. Additionally, such measurements offer an opportunity to evaluate our current understanding of atmospheric processes. This thesis presents in situ measurements of several important trace gases conducted using CF_3O^- chemical ionization mass spectrometry. In this technique, analytes react with the reagent ion CF_3O^- to form charged molecules, which are separated based on their mass-to-charge ratios. CF_3O^- enables the detection of many atmospherically relevant species, such as HO_2NO_2, SO_2, HCN, HNO_3, H_2O_2, and many biogenic oxidation products. Aircraft measurements were conducted over Mexico City, Mexico and the state of California. Ground-based measurements were performed at a rural site on the western slope of the Sierra Nevada. Ambient observations are presented and discussed in terms of the broader picture of regional air quality.

Chapter 2 describes a method of calculating the instantaneous photochemical ozone production rate using in situ measurements of peroxynitric acid (HO_2NO_2) obtained simultaneously with measurements of NO and NO_2. Ambient concentrations were measured from the NCAR C-130 aircraft over Mexico City in March 2006. Measured concentrations of HO_2NO_2 are compared to those predicted by the NASA Langley highly constrained photochemical time-dependent box model. Overall, modeled values are consistent with observations, however, at higher NO_x levels, the photochemical box model underpredicts HO_2NO_2 observations. As a result, the ozone production rate calculated using measured HO_2NO_2 is faster than predicted using accepted photochemistry. This result implies

regulations aimed at reducing NO_x, with the intention of reducing ozone, will likely be effective at higher NO_x levels than predicted by the model.

Chapter 3 details trends in SO_2 and particulate sulfate concentrations in the Los Angeles basin between 2002 and 2008 as determined from aircraft and ground-based measurements. A large decrease in SO_2 concentration and a change in the SO_2 spatial distribution were observed. The effects of meteorology and different measurement techniques on the observed changes are discussed. Although a corresponding reduction in sulfate concentration is expected to accompany a decrease in SO_2 levels, aircraft observations indicate an increase in sulfate concentrations between 2002 and 2008. This is contrary to the modest reduction indicated by ground-based measurements. Possible explanations for the trends in SO_2 and sulfate are investigated using the EPA Community Multiscale Air Quality model.

Chapter 4 describes the development of a new method for the in situ detection and quantification of hydroxyacetone and glycolaldehyde, critical oxidation products of biogenic precursors. Two approaches for quantification of hydroxyacetone are described. Tandem mass spectrometry is shown to provide direct separation of glycolaldehyde and acetic acid, two isobaric compounds. Ambient measurements of these compounds were conducted during two field intensives—the first an aircraft campaign over California and the second a ground-based campaign at a rural site in northern California. Observations from the first intensive are used to calculate enhancement ratios of hydroxyacetone and glycolaldehyde in biomass burning plumes, while observations from the second are compared to box model predictions of biogenic volatile organic compound oxidation at the experiment site.

Bibliography

Forster, P., Ramaswamy, V., Artaxo, P., Berntsen, T., Betts, R., Fahey, D. W., Haywood, J., Lean, J., Lowe, D. C., Myhre, G., Nganga, J., Prinn, R., Raga, G., Schulz, M., and Van Dorland, R.: Changes in atmospheric constituents and in radiative forcing, in: Climate Change 2007: The Physical Science Basis. Contribution of Working Group I to the Fourth Assessment Report of the Intergovernmental Panel on Climate Change, edited by: Solomon, S., Qin, D., Manning, M.,

Chen, Z., Marquis, M., Averyt, K. B., Tignor, M., and Miller, H.L., Cambridge University Press, Cambridge, United Kingdom and New York, NY, USA, 2007.

Jacob, D. J.: Introduction to Atmospheric Chemistry, Princeton University Press, 1999.

Pope, C. A., Burnett, R. T., Thun, M. J., Calle, E. E., Krewski, D., Ito, K., and Thurston, G. D.: Lung cancer, cardiopulmonary mortality, and long-term exposure to fine particulate air pollution, Journal of the American Medical Association, 287, 1132–1141, 2002.

Ramanathan, V., Crutzen, P. J., Kiehl, J. T., and Rosenfeld, D.: Atmosphere — Aerosols, climate, and the hydrological cycle, Science, 294, 2119–2124, 2001.

Seinfeld, J. H., and Pandis, S. N.: Atmospheric Chemistry and Physics, 2nd ed., John Wiley & Sons, 2006.

United States Environmental Protection Agency (USEPA): Air Quality Criteria for Particulate Matter (Final Report, 2004), Environmental Protection Agency, Washington, DC, EPA 600/P-99/002aF-bF, 2004.

United States Environmental Protection Agency (USEPA): Air Quality Criteria for Ozone and Related Photochemical Oxidants (Final Report, 2006), Environmental Protection Agency, Washington, DC, EPA 600/R-05/004aF-cF, 2006.

World Health Organization (WHO): WHO Air quality guidelines for particulate matter, ozone, nitrogen dioxide and sulfur dioxide: Global update 2005, Summary of risk assessment, WHO Press, Geneva, Switzerland, 2006.

Chapter 2

Inferring Ozone Production in an Urban Atmosphere Using Measurements of Peroxynitric Acid *

*Reproduced with permission from "Inferring ozone production in an urban atmosphere using measurements of peroxynitric acid" by K. M. Spencer, D. C. McCabe, J. D. Crounse, J. R. Olson, J. H. Crawford, A. J. Weinheimer, D. J. Knapp, D. D. Montzka, C. A. Cantrell, R. S. Hornbrook, R. L. Mauldin III, and P. O. Wennberg, *Atmospheric Chemistry and Physics*, 9 (11), 3697-3707, 2009.

2.1 Abstract

Observations of peroxynitric acid (HO_2NO_2) obtained simultaneously with those of NO and NO_2 provide a sensitive measure of the ozone photochemical production rate. We illustrate this technique for constraining the ozone production rate with observations obtained from the NCAR C-130 aircraft platform during the Megacity Initiative: Local and Global Research Observations (MILAGRO) intensive in Mexico during the spring of 2006. Sensitive and selective measurements of HO_2NO_2 were made in situ using chemical ionization mass spectrometry (CIMS). Observations were compared to modeled HO_2NO_2 concentrations obtained from the NASA Langley highly constrained photochemical time-dependent box model. The median observed-to-calculated ratio of HO_2NO_2 is 1.18. At NO_x levels greater than 15 ppbv, the photochemical box model underpredicts observations with an observed-to-calculated ratio of HO_2NO_2 of 1.57. As a result, we find that at high NO_x, the ozone production rate calculated using measured HO_2NO_2 is faster than predicted using accepted photochemistry. Inclusion of an additional HO_x source from the reaction of excited state NO_2 with H_2O or reduction in the rate constant of the reaction of OH with NO_2 improves the agreement.

2.2 Introduction

Peroxynitric acid, HO_2NO_2, is an important reservoir of both HO_x ($HO_x = OH + HO_2$) and NO_x ($NO_x = NO + NO_2$) radicals. These radicals are of primary atmospheric importance as they influence the production and degradation of tropospheric ozone and numerous volatile organic compounds (Murphy et al., 2004). Ozone production in urban environments is initiated by OH radicals and requires sunlight, NO_x, and hydrocarbons. The relative amounts of these species control the rate of ozone production (Seinfeld and Pandis, 2006).

The only known pathway for the formation of HO_2NO_2 in the atmosphere is the association reaction of HO_2 and NO_2 (R2.1) (Niki et al., 1977). HO_2NO_2 is lost via thermal decomposition (reverse of R2.1) (Graham et al., 1977, 1978; Zabel et al., 1995; Gierczak et al., 2005); UV and visible/near-IR photolysis (R2.2) (Macleod et al., 1988; Roehl et al., 2002; Knight et al., 2002); and

reaction with OH radical (R2.3) (Trevor et al., 1982; Smith et al., 1984; Barnes et al., 1986; Jimenez et al., 2004).

$$HO_2 + NO_2 + M \rightleftharpoons HO_2NO_2 + M \quad \text{(R2.1)}$$

$$HO_2NO_2 + h\nu \rightarrow \text{products} \quad \text{(R2.2)}$$

$$HO_2NO_2 + OH \rightarrow H_2O + NO_2 + O_2 \quad \text{(R2.3)}$$

The relative importance of the HO_2NO_2 sinks depends on temperature, pressure, OH radical concentration, and the UV/IR radiation field. The lifetime of HO_2NO_2 with respect to thermal decomposition varies due to the strong temperature dependence of this process (Kim et al., 2007). As temperature decreases, loss due to photolysis and reaction with OH radical become increasingly important. At altitudes greater than 7 km, photolysis and reaction with OH become the dominant loss mechanisms (Roehl et al., 2002). The formation of HO_2NO_2 followed by its loss via reaction with OH forms a NO_x-catalyzed sink of HO_x radicals (Roehl et al., 2002).

The role of HO_2NO_2 in photochemistry of the lower troposphere has been less explored, in part because of a paucity of observations of this compound. In situ measurements of HO_2NO_2 have been obtained previously in the free troposphere during the 2004 INTEX-NA campaign (Kim et al., 2007) and in Antarctica (Slusher et al., 2001). An indirect estimate of the HO_2NO_2 abundance was obtained from the sum of peroxynitrate observations during the 2000 TOPSE campaign (Murphy et al., 2004).

Here, we present in situ measurements of HO_2NO_2 in and around Mexico City. These measurements were made in March of 2006 from the NCAR C-130 aircraft platform during the MILAGRO field experiment. One goal of the MILAGRO mission, and the focus of the C-130 flights, was to investigate the processing and outflow of pollution from Mexico City. Most flights occurred during the daytime hours at altitudes below 7 km and temperatures between 260 and 300 K. The majority

of the data are between 270 and 283 K. This study is limited to six of the MILAGRO flights (8, 22, 23, 26, 28, and 29 March) during which all necessary species were measured. A photochemical steady state approximation of HO_2NO_2 under MILAGRO conditions is discussed, and measured HO_2NO_2 concentrations are compared to those predicted by the NASA LaRC box model. A simplified method of estimating the rate of ozone production using HO_2NO_2 is compared to full NASA LaRC box model calculations of the rate of ozone production.

2.3 Method

2.3.1 Instrumentation

NO and NO_2 mixing ratios were measured by photofragmentation/chemiluminescence. The precision of these measurements is ∼15 pptv and the overall uncertainties are ±(7% of the mixing ratio + 15 pptv) and ±(10% of the mixing ratio + 15 pptv), respectively (Campos et al., 1998; Weinheimer et al., 1998). CH_2O mixing ratios were measured by tunable diode laser absorption spectroscopy with an uncertainty of 15% (Fried et al., 2003; Wert et al., 2003). HO_2 mixing ratios were determined by chemical-conversion/chemical ionization mass spectroscopy with an uncertainty of 35% (Cantrell et al., 2003). Non-methane hydrocarbons (NMHC) were measured using whole air sampling (WAS), and subsequent analysis was conducted by gas chromatography/mass spectrometry/flame ionization detection/electron capture detection (Colman et al., 2001; Blake et al., 2003). H_2O mixing ratios were calculated using the ambient water vapor pressure and corrected static pressure. These measurements and the ambient temperature measurements are included in the NCAR C-130 standard airborne scientific measurements and are discussed in RAF Bulletin No. 9 (Miller and Friesen, 1985). The full details of measurements taken during MILAGRO from the NCAR C-130 aircraft platform can be found at http://mirage-mex.acd.ucar.edu/Measurements/C130/index.shtml.

Negative ion chemistry of CF_3O^- has been shown to provide sensitive and selective detection of many inorganic and organic acids (Huey et al., 1996; Amelynck et al., 2000a,b; Crounse et al., 2006) and was exploited in this work to detect HO_2NO_2. The Caltech chemical ionization mass

spectrometry (CIMS) instrument consists of a flow tube controlled at 35 mbar total pressure where a reagent ion, CF_3O^-, interacts with ambient air diluted 1:4 with dry nitrogen. Ions are sampled from the flow tube into a quadrupole mass filter and detected with a channel electron multipler.

The reaction of CF_3O^- with acids follows several pathways. Reaction with strong acids proceeds via fluoride ion transfer (Huey et al., 1996) while reaction with weaker acids yields clusters of reagent ion and analyte (Amelynck et al., 2000a). HO_2NO_2 reacts with CF_3O^- via fluoride ion transfer (R2.4), clustering (R2.5) (Crounse et al., 2006), and HF elimination (R2.6), providing three distinct ion signals. R2.4 – R2.6 are complicated by competing reactions with the one-water cluster of CF_3O^- ($CF_3O^- \cdot H_2O$). Each mass-to-charge ratio is observed for ∼0.5 seconds. HO_2NO_2 masses were monitored every ∼15 seconds. Further instrument details are given in Crounse et al. (2006).

$$CF_3O^- + HO_2NO_2 \rightarrow HF \cdot OONO_2^- \ (m/z\ 98) + CF_2O \tag{R2.4}$$

$$CF_3O^- + HO_2NO_2 \rightarrow CF_3O^- \cdot HO_2NO_2 \ \ (m/z\ 164) \tag{R2.5}$$

$$CF_3O^- + HO_2NO_2 \rightarrow CF_2O \cdot OONO_2^- \ \ (m/z\ 144) + HF \tag{R2.6}$$

2.3.1.1 Sensitivity and Calibration

Due to differences in reactivity of CF_3O^- and its water cluster, the sensitivity of the CIMS instrument to the ion products of the three channels (R2.4, R2.5, R2.6) is dependent on the mixing ratio of water vapor in the flow tube (Crounse et al., 2006). This dependence is quantified via laboratory measurements. A small quantity of HO_2NO_2 was introduced into the flow tube. The flow tube humidity was controlled using mass flow controllers to adjust the ratio of air saturated with water vapor to dry zero air. Humidity was quantified by Fourier Transform Infrared (FTIR) spectroscopy using HITRAN line lists (Rothman et al., 2005) and the nonlinear NLM4 software developed by Griffith (1996). The sensitivity of the instrument to the fluoride ion transfer and cluster channels

of HO_2NO_2 was determined as a function of humidity and is presented in Fig. 2.1. Sensitivity is expressed in ion counts, normalized by the ion counts of the ^{13}C isotope of the reagent ion and its one-water cluster ($^{13}CF_3O^-$ and $^{13}CF_3O^- \cdot H_2O$), per pptv of HO_2NO_2. The yield of R2.6 is typically one-third that of R2.5. Due to the low reaction yield, R2.6 is not used to quantify the ambient observations of HO_2NO_2.

During calibration, the concentration of HO_2NO_2 in the flow tube was determined by thermally decomposing the HO_2NO_2 into NO_2 (reverse of R2.1) and quantifying the resultant NO_2 using CIMS with SF_6^- as the reagent ion (R2.7) (Huey et al., 1995):

$$SF_6^- + NO_2 \rightarrow SF_6 + NO_2^- \quad (m/z\ 46). \tag{R2.7}$$

NO_2 is not detected with high sensitivity using CF_3O^-.

Synthesis of HO_2NO_2 was performed offline using the procedure described in Roehl et al. (2002); gas-phase HO_2NO_2 was produced by flowing dry N_2 over the solution of HO_2NO_2. A small portion of this flow was directed through a critical orifice into a PTFE three-way valve, which directed the flow through either a heated or unheated glass inlet tube (6 mm OD). The heated inlet tube was kept at 190° C, a temperature at which 99.8% of the HO_2NO_2 decomposed, as determined by monitoring the signal with CF_3O^- at m/z 98. The unheated inlet was maintained at room temperature. The sensitivity of the CIMS to NO_2 was quantified using a dilute mixture of NO_2 in N_2; the concentration of NO_2 in this mixture was quantified with FTIR using HITRAN line lists (Rothman et al., 2005) and the nonlinear NLM4 software developed by Griffith (1996).

The CIMS sensitivity to HO_2NO_2 was determined by back-to-back measurements of the products of R2.4, R2.5, and R2.7. HO_2NO_2 was added through the room temperature inlet and measured using CF_3O^- as the reagent ion. Next, HO_2NO_2 was added through the heated inlet and NO_2 was measured using SF_6^- as the reagent ion (R2.7). Background NO_2 from NO_2 impurity in the HO_2NO_2 solution was measured using SF_6^- by passing the HO_2NO_2 through the room temperature inlet; this background signal was subtracted from the NO_2 signal when the heated inlet was used. The signals from R2.4 and R2.5 obtained using the room temperature inlet were also corrected for

the small amount of HO_2NO_2 that did not dissociate in the heated inlet and other backgrounds (see below) by monitoring those masses using CF_3O^- as the reagent ion with the heated inlet in use. This procedure was repeated at a number of humidities to obtain water-dependent calibration functions for each ion product. Postmission laboratory calibrations for HO_2NO_2 were conducted. During flight, isotopically labeled HNO_3 was periodically added to the flow tube to monitor the stability of the instrument sensitivity. Sensitivity of the instrument to HNO_3 was consistent and comparable during flight and laboratory calibrations indicating the sensitivity of the instrument to HO_2NO_2 was consistent.

In the absence of HO_2NO_2, ion signals at *m/z* 98 and *m/z* 164 are nonzero, and these background signals must be accounted for in the data analysis. These background signals were measured during flight by periodically passing ambient air through a filter consisting of alumina pellets coated with palladium and nylon wool coated with sodium bicarbonate, quantitatively removing HO_2NO_2. This technique is described in Crounse et al. (2006).

2.3.1.2 Ambient HO_2NO_2 Concentration

HO_2NO_2 concentrations are calculated from the signals observed at *m/z* 98 and *m/z* 164 after normalization by the amount of reagent ion signal, subtraction of background signals, and application of the appropriate sensitivity factor for HO_2NO_2.

Acetate in the form $HF \cdot CH_3C(O)O^- \cdot H_2O$ is a known interference in the *m/z* 98 signal. $HF \cdot CH_3C(O)O^- \cdot H_2O$ is seen at *m/z* 97, with approximately 2.5% of the *m/z* 97 signal appearing at *m/z* 98 due to heavy isotopes of the ion. Because the *m/z* 97 signal was not monitored during these flights, the interference at *m/z* 98 was estimated from the monitored signal of the acetate-fluoride transfer ion ($HF \cdot CH_3C(O)O^-$) at *m/z* 79 and ambient water levels, using a function derived through postmission laboratory measurements. There are no interferences of which we are aware at *m/z* 164. Background signals were measured (as described above) about every 15 minutes and are used to model background levels during the flight.

A scatter plot of the independent determinations of HO_2NO_2 calculated from the *m/z* 98 and

the m/z 164 signals is shown in Fig. 2.2. During the flight, there is an ∼8 second delay between a m/z 98 measurement and the corresponding m/z 164 measurement. Only observations obtained when the measured NO_y differs by less than 10% between m/z 98 and m/z 164 sampling times are included in Fig. 2.2. The slope of the robust fit line (DuMouchel and O'Brien, 1989; Street et al., 1988) is 0.76, and the intercept is 0.90 pptv. $R^2 = 0.94$. These independent measurements are in good agreement, providing confidence in the use of this ion chemistry to quantify HO_2NO_2.

The concentration of HO_2NO_2 used in the subsequent analysis is determined by combining the independent measurements from m/z 98 and m/z 164 as follows. When the water mixing ratio in the flow tube is less than or equal to 200 ppmv, the m/z 98 measurement is used because the sensitivity at m/z 164 is low (Fig. 2.1). When the water mixing ratio in the flow tube is between 200 and 500 ppmv, the mean of the m/z 98 and the m/z 164 measurements is used. At water vapor mixing ratios greater than 500 ppmv, the m/z 164 measurement is used exclusively. Although the sensitivity is somewhat lower at m/z 164 than at m/z 98 for water mixing ratios between 500 and 1000 ppmv, higher backgrounds and interference from acetate at m/z 98 make the cluster ion (m/z 164) a more robust measure of HO_2NO_2 at these higher water mixing ratios.

The uncertainty in the PNA measurements is approximately ±(30% + 30 pptv). The uncertainty reflects the sum of the precision of the data determined by the counting statistics of the ions, the variability of the background signal, and the uncertainty in the sensitivities shown in Fig. 2.1.

2.3.2 Photochemical Time-Dependent Box Model

Calculated concentrations of HO_2, NO_2, and HO_2NO_2 and rates of ozone production were obtained from a highly constrained photochemical time-dependent box model—NASA Langley Research Center (LaRC) box model (Olson et al., 2006). The modeling approach used is based on the assumption of a diurnal equilibrium (Olson et al., 2006, 2004; Frost et al., 2002; Jaegle et al., 2000). Model inputs include observations of atmospheric parameters such as temperature, pressure, water vapor, and critical long-lived chemical precursor species (O_3, CO, NO, CH_4, non-methane hydrocarbons, acetone). With the exception of NO and the radiation field, the atmospheric

state is held constant throughout the model run. NO varies diurnally; however reactive nitrogen, NO_y=NO + NO_2 + NO_3 + $2N_2O_5$ + HONO + HO_2NO_2, is held constant with partitioning as determined by the model. The amount of total reactive nitrogen is determined so that NO matches the observed value at the time of the measurement. Additional constraints are implemented if data are available. These additional constraints include methanol, ethanol, H_2O_2, CH_3OOH, HNO_3, PAN, acetic acid, and formic acid. Concentrations of these species are computed by the model when data are unavailable. While a discrepancy between calculated and observed values of acetaldehyde (CH_3CHO) does exist and has the potential to impact HO_x levels, constraining the model to observed CH_3CHO values suggests that this uncertainty propagates to impact OH mixing ratios by 5%–10% and HO_2 mixing ratios by less than a few percent.

The model chemistry includes HO_x−NO_x−CH_4 gas-phase reactions based on the recommendations of Atkinson et al. (2004) and Sander et al. (2003). In addition, the model uses the rate for $O(^1D)$ quenching by N_2 suggested by Ravishankara et al. (2002), temperature-dependent quantum yields for acetone photolysis from Arnold et al. (2005), and the parameterization for near-IR photolysis of HO_2NO_2 described by Roehl et al. (2002). Nonmethane hydrocarbon chemistry is based on the condensed mechanism of Lurmann et al. (1986) with modifications included to address remote low-NO_x conditions. Explicit chemistry is included for C_2H_6, C_3H_8, C_2H_4, isoprene, and benzene. C_4 and higher alkanes are lumped together, as are C_3 and higher alkenes, and aromatics other than benzene. Reactions of lumped C_3 and higher alkenes are assumed to be predominantly propene. The assumed aldehyde product is CH_3CHO and reaction rates are based on those for propene. Photolysis rate coefficients are based on spectroradiometer measurements (Shetter and Muller, 1999). The diurnal profiles of the photolysis rates are computed by a DISORT four-stream implementation of the Tropospheric Ultraviolet and Visible (TUV) radiative transfer code (Madronich and Flocke, 1998). These calculated profiles are then normalized to match the instantaneous observations at the time of measurement.

Model calculations use the 1-minute merged data set available on the INTEX-B public data archive (http://www-air.larc.nasa.gov). In this study, we limit the analysis to those points that

include direct measurement of NMHCs.

2.3.3 Photochemical Steady State

Due to the short lifetime of HO_2NO_2 with respect to thermal decomposition for the conditions experienced during the MILAGRO flights, photochemical steady state of HO_2NO_2 was assumed. To verify the validity of this assumption with respect to HO_2NO_2, the model was run in a non-steady state mode. A large, polluted perturbation was introduced into the model and allowed to decay over several days. A second set of calculations was performed in which each point was solved along the decay of the plume using steady state assumptions. While some species were not in equilibrium during this model run, the mixing ratios of HO_2NO_2 were consistent with the steady state run. This is attributed to the very short lifetime of HO_2NO_2 for the temperature range in the data set. NO_x is directly input into the model while HO_x varies rapidly enough to represent the instantaneous precursor condition. At photochemical steady state, production and loss of HO_2NO_2 are equal and R2.1 – R2.3 yield (Kim et al., 2007)

$$[HO_2NO_2]_{ss} = \frac{k_1[HO_2][NO_2]}{J_2 + k_{-1} + k_3[OH]}. \tag{2.1}$$

For the conditions experienced during the MILAGRO flights, the median lifetime of HO_2NO_2 with respect to thermal decomposition was five minutes while the lifetime with respect to reaction with OH and UV/IR photolysis was on the order of 10 hours and 6 days, respectively. Under these conditions, the steady state concentration of HO_2NO_2 simplifies to

$$[HO_2NO_2]_{ss} \approx \frac{k_1[HO_2][NO_2]}{k_{-1}}. \tag{2.2}$$

To evaluate whether the simplified assumption for steady state (Eq. 2.2) is robust for MILAGRO conditions, NASA LaRC box model predictions of HO_2 and NO_2 were used in the right-hand side of Eq. 2.2 to calculate HO_2NO_2 using the steady state assumption ($[HO_2NO_2]_{ss}$). $[HO_2NO_2]_{ss}$ was then compared to the full diurnal equilibrium model predictions of HO_2NO_2 (shown in Fig. 2.3).

The slope of the robust fit line is 1.02, and the intercept is 0.10 pptv. $R^2 = 0.99$.

The HO_2 mixing ratio measurements measured from the C-130 were not sufficiently precise to provide for a direct comparison between the measurements of HO_2NO_2 and the steady state calculation of $[HO_2NO_2]_{ss}$ using observed HO_2 and NO_2; however, the mean observed concentration of HO_2 was within 15% of the mean concentration of the NASA LaRC box model estimate for each of the flights used in this analysis.

2.4 Comparisons with NASA LaRC Photochemical Box Model

An example time trace for HO_2NO_2 is illustrated in Fig. 2.4. During this flight (29 March 2006), the C-130 flew in and out of airmasses heavily impacted by pollution from Mexico City. Variations in the measured and modeled HO_2NO_2 mixing ratio closely follow variations in NO_2.

Observed HO_2NO_2 mixing ratios, colored by NO_x mixing ratios, are compared to the NASA LaRC box model calculation of HO_2NO_2 mixing ratios in Fig. 2.5. The slope of the robust fit line is 0.81, and the intercept is 6.74 pptv. Although overall agreement is good ($R^2 = 0.82$), there is a tendency for the model to underpredict HO_2NO_2 concentrations at NO_x levels greater than 15 ppbv (shown by the red and orange colors in Fig. 2.5). Underprediction of HO_2NO_2 at elevated NO_x levels are in agreement with previous findings of Murphy et al. (2004) and Kim et al. (2007).

2.5 Ozone Production

Photochemical ozone production is the result of oxidation of CO and hydrocarbons in reactions involving NO_x and HO_x. The instantaneous rate of photochemical ozone production can be calculated using Eq. 2.3 (Jacob, 1999).

$$P_{O3} = k_{RO_2+NO}[RO_2][NO] + k_{HO_2+NO}[HO_2][NO] \tag{2.3}$$

The rate constants for the reactions of peroxyradicals (including HO_2) with NO are similar, so P_{O3} can be approximated as

$$P_{O3} \approx k_{HO_2+NO}[NO]([RO_2] + [HO_2]). \quad (2.4)$$

In polluted atmospheres, HO_2 is produced primarily from the reaction of RO_2 with NO and therefore, the sum of all non-HO_2 peroxy radicals will be closely and linearly related to the concentration of HO_2 (e.g., Jacob, 1999).

$$P_{O3} = Zk_{HO_2+NO}[HO_2][NO], \quad (2.5)$$

where Z is a number generally close to 2 in polluted air. Setting $K_{eq} = k_1/k_{-1}$, solving Eq. 2.2 for $[HO_2]$, and substituting into Eq. 2.5 yields

$$P_{O3} = \frac{Zk_{HO_2+NO}[HO_2NO_2][NO]}{K_{eq}[NO_2]}. \quad (2.6)$$

In Fig. 2.6, we plot P_{O3} from the NASA LaRC box model versus $k_{HO_2+NO}[HO_2NO_2][NO]/K_{eq}[NO_2]$ to estimate Z. Using the NASA LaRC box model, we examined the predictions of Eq. 2.6. We limit this analysis to times when the solar zenith angle is $<80^\circ$. The slope of the best-fit line, Z, in Fig. 2.6 is 1.77. The correlation is high ($R^2 = 0.99$) suggesting that the production of ozone under MILAGRO conditions can be estimated directly from Eq. 2.6 using measured HO_2NO_2, NO, and NO_2 with Z = 1.77.

2.6 Discussion and Conclusions

The rate of ozone production is sensitive to the rate of HO_x production and the amount of NO_x present. At a fixed HO_x production rate, the rate of ozone production increases with NO_x until NO_x reaches a level where the rate of nitric acid formation via R2.8 reduces HO_x levels and photochemistry slows.

$$OH + NO_2 + M \rightarrow HNO_3 + M \quad (R2.8)$$

This behavior can be seen in the model chemistry (Fig. 2.7, center panel). Ozone production rates for these MILAGRO flights calculated by the NASA LaRC box model are plotted versus NO levels and colored by the mixing ratio of CH_2O. CH_2O is used as a proxy for HO_x production rate (Seinfeld and Pandis, 2006). At low NO, the ozone production rate increases with NO at a fixed level of CH_2O, i.e., NO_x-limited behavior. At high NO, the ozone production rate becomes independent of or even decreases with NO at a fixed level of CH_2O, i.e., NO_x-saturated behavior.

In contrast to NASA LaRC box model calculations, the rate of ozone production estimated from observed HO_2NO_2, NO, and NO_2 does not show a saturation behavior (Fig. 2.7, left panel). At high NO, the rate of ozone production continues to increase with NO, in contrast to model predictions (Fig. 2.7, right panel). This suggests that the NASA LaRC box model underestimates the HO_2 levels and therefore either the HO_x production/loss rate is under/overestimated at elevated NO levels. This is consistent with observed HO_2NO_2 mixing ratios greater than NASA LaRC model predictions at NO_x levels greater than 15 ppbv shown in Fig. 2.5.

Observed values of HO_2NO_2, and hence HO_2, greater than those predicted by the NASA LaRC box model are consistent with a number of urban measurements of HO_2. Several recent studies have pointed to possible missing HO_x sources in urban air. At high NO_x concentrations, HO_2 levels calculated using highly constrained box models were significantly less than those measured in Nashville, Birmingham, and New York City in the summer (Martinez et al., 2003; Heard et al., 2004; Emmerson et al., 2005; Ren et al., 2003) and in New York City and Tokyo in the winter (Ren et al., 2006; Kanaya et al., 2007). Martinez et al. (2003) reported daytime HO_2 levels 1.56 times modeled values in Nashville in 1999. The difference between measured and modeled HO_2 was positively correlated with high NO_x mixing ratios. In Birmingham, England in the summer of 1999 and winter of 2000, Heard et al. (2004) observed HO_2 levels 1.78 and 2.04 times modeled values, respectively. They found that the observed HO_2 concentrations were particularly insensitive to changes in NO_x levels. Summertime levels of HO_2 in New York City in 2001 were underestimated, with observed levels 1.24 times modeled values. The difference between measured and calculated HO_2 depended on the time of day. At midday, the observed and modeled values were found to agree

very well while the model tended to underestimate the observations when NO_x was high, usually during the morning hours (Ren et al., 2003). Similar results were found in Tokyo during the winter of 2004. Daytime HO_2 concentrations were underestimated, with observed HO_2 levels 2.08 times modeled values. These comparisons were sensitive to the assumed hydrocarbon levels. When the concentration of alkenes and reactive alkanes used in the model was increased by a factor of 3 and 5, respectively, the observed-to-modeled HO_2 ratio decreased to 1.13. Continued underestimation of HO_2 concentrations occurred at high NO_x mixing ratios (Kanaya et al., 2007). The higher than expected levels of HO_2 suggest higher rates of ozone production than can be accounted for using known chemistry.

It should be noted that the discrepancy between observed and modeled values of HO_2NO_2 at high NO_x found in this study appears to be distinct from the underprediction of HO_x values correlated with isoprene. Ren et al. (2008) found the observed-to-modeled OH ratio in the boundary layer to be strongly dependent on isoprene during the INTEX-A summer 2004 campaign, with divergence occurring at isoprene levels greater than 100 pptv. Isoprene mixing ratios were well below 100 pptv for the vast majority of the data used in this analysis.

Not all studies have found excess HO_2. Indeed, several studies have found overpredictions of HO_2 levels by photochemical box models even at high NO_x concentrations. HO_2 concentrations were overestimated in the Los Angeles basin, Mexico City, and summertime Tokyo (George et al., 1999; Shirley et al., 2006; Kanaya et al., 2007). George et al. (1999) reported daytime HO_2 levels 0.67 times calculated values downwind of Los Angeles in 1993. The agreement of observed and calculated HO_2 was quite good in the early morning hours, but calculated HO_2 concentrations were found to be significantly higher than observations during midday. In Mexico City in 2003, Shirley et al. (2006) determined that observations of HO_2 were 0.79 times calculated values of HO_2 during the midday. However, they also calculated an observed-to-modeled ratio of 1.17 during morning rush hour, coinciding with the morning rush hour peak in NO_x concentrations. Unlike wintertime findings, summertime HO_2 concentrations in Tokyo were overestimated. An observed-to-modeled HO_2 ratio of 0.78 was reported. Trends at high NO_x levels were not discussed as NO mixing ratios

greater than 20 ppbv were not seen during this sampling period (Kanaya et al., 2007).

HO_2, HO_2NO_2, and hence the rate of ozone production may be underpredicted at high NO due to errors in calculated NO_x-dependent HO_x sources and sinks. We have investigated several possible sources of error. One possibility is an overestimate of the rate constant of R2.8, a sink of HO_x. The accepted rate constant for R2.8 has been subject to numerous revisions in the last decade (DeMore et al., 1997; Sander et al., 2000, 2003, 2006). In addition, a recommended rate constant for the reaction of OH and NO_2 to form pernitrous acid (HOONO) is included for the first time in the 2006 JPL critical evaluation. Recent laboratory work at the Jet Propulsion Laboratory and the California Institute of Technology (Okumura and Sander, 2005) suggests that the 2000 JPL critical evaluation recommendation (Sander et al., 2000) may be closer to the true rate of R2.8 than the current recommendation (Sander et al., 2006). The 2000 JPL critical evaluation recommended rate constant for R2.8 is approximately 30% lower for MILAGRO conditions than the current evaluation. The explicit rate constant for HNO_3 formation was used in the model. The model does not include the HOONO branch of the OH + NO_2 + M reaction due to the short lifetime (seconds to minutes) of HOONO under MILAGRO conditions. The formation and breakdown of HOONO is considered to be a null cycle under these conditions (Fry et al., 2004). A reduction in the rate constant for R2.8 leads to an increase in OH and NO_2 mixing ratios, leading to an increase in HO_2NO_2 levels. To test the importance of this modified rate constant on HO_2NO_2 levels, the 2000 JPL critical evaluation recommended rate constant for R2.8 was substituted into the model. Fig. 2.8 (top panel) illustrates the sensitivity of the modeled HO_2NO_2 mixing ratio to a change in the rate constant for R2.8. At high NO levels, use of the 2000 JPL recommended rate constant increases the mixing ratio of calculated HO_2NO_2, leading to better agreement between measured and calculated HO_2NO_2.

HO_2NO_2 mixing ratios and hence the rate of ozone production may also be underpredicted at high NO_x due to missing calculated HO_x sources at high NO_x. Li et al. (2008) recently reported significant HO_x production from the reaction of excited-state NO_2 (NO_2^*) with H_2O:

$$NO_2^* + H_2O \rightarrow OH + HONO. \qquad \text{(R2.9)}$$

NO_2^* is formed through the excitation of NO_2 at wavelengths longer than 420 nm. These direct and indirect (via HONO photolysis) OH sources lead to increased concentrations of HO_x at elevated NO_x levels. Including this process in the box model (using the rate of R2.9 determined by Li et al.), improves agreement with observed HO_2NO_2. As seen in Fig. 2.8 (center panel), the inclusion of R2.9 increases the mixing ratio of modeled HO_2NO_2, again leading to better agreement between measured and modeled HO_2NO_2. Including both the reduced rate of R2.8 and the Li et al. (2008) process leads to increased levels of modeled HO_2NO_2 (Fig. 2.8, bottom panel). Increased levels of calculated HO_2NO_2 are in better agreement with observations. These two recently suggested ideas lead to better, not perfect, agreement between observed and calculated HO_2NO_2.

The transition to NO_x saturation appears to occur at higher NO_x levels than estimated by the NASA LaRC box model for Mexico City. This may have implications for engineering of improvements in air quality in the basin. If generally true, it suggests that further NO_x controls will yield reductions in smog levels. Significant uncertainties remain, however. It is unclear why the HO_x levels are generally underestimated. Although we identify several possible deficiencies in the photochemical mechanism that may contribute to an underprediction of HO_x, these are not sufficient to account for the discrepancy. Each is uncertain and requires additional laboratory work to test these mechanisms (e.g., Wennberg and Dabdub, 2008). Additionally, NO_x levels are generally much higher at the surface and so it is unclear if NO_x-limited conditions also apply.

2.7 Acknowledgements

The authors wish to thank C. M. Roehl for synthesizing the peroxynitric acid for calibration. P. Weibring and A. Fried, D. R. Blake, and R. E. Shetter provided formaldehyde, whole air sample, and solar actinic flux measurements, respectively, which provided constrains for the photochemical box model. The authors also wish to thank the C-130 crew and support team. The HO_2NO_2 measurements and their interpretation were made possible with the financial support of NASA (NAG: NNG06GB32B). J.D.C. acknowledges support from the EPA-STAR Fellowship Program (FP916334012). This work has not been formally reviewed by the EPA. The views expressed in this

document are solely those of the authors and the EPA does not endorse any products or commercial services mentioned in this publication.

Bibliography

Amelynck, C., Schoon, N., and Arijs, E.: Gas phase reactions of CF_3O^- and $CF_3O^- \cdot H_2O$ with nitric, formic, and acetic acid, International Journal of Mass Spectrometry, 203, 165–175, 2000.

Amelynck, C., Van Bavel, A. M., Schoon, N., and Arijs, E.: Gas phase reactions of CF_3O^- and $CF_3O^- \cdot H_2O$ and their relevance to the detection of stratospheric HCl, International Journal of Mass Spectrometry, 202, 207–216, 2000.

Arnold, S. R., Chipperfield, M. P., and Blitz, M. A.: A three-dimensional model study of the effect of new temperature-dependent quantum yields for acetone photolysis, Journal of Geophysical Research—Atmospheres, 110, D22305, doi:10.1029/2005JD005998, 2005.

Atkinson, R., Baulch, D. L., Cox, R. A., Crowley, J. N., Hampson, R. F., Hynes, R. G., Jenkin, M. E., Rossi, M. J., and Troe, J.: Evaluated kinetic and photochemical data for atmospheric chemistry: Volume I—gas phase reactions of O_x, HO_x, NO_x and SO_x species, Atmospheric Chemistry and Physics, 4, 1461–1738, 2004.

Barnes, I., Bastian, V., Becker, K. H., Fink, E. H., and Zabel, F.: Pressure-Dependence of the Reaction of OH with HO_2NO_2, Chemical Physics Letters, 123, 28–32, 1986.

Blake, N. J., Blake, D. R., Simpson, I. J., Meinardi, S., Swanson, A. L., Lopez, J. P., Katzenstein, A. S., Barletta, B., Shirai, T., Atlas, E., Sachse, G., Avery, M., Vay, S., Fuelberg, H. E., Kiley, C. M., Kita, K., and Rowland, F. S.: NMHCs and halocarbons in Asian continental outflow during the Transport and Chemical Evolution over the Pacific (TRACE-P) Field Campaign: Comparison with PEM-West B, Journal of Geophysical Research—Atmospheres, 108, 8806, doi:10.1029/2002JD003367, 2003.

Campos, T. L., Weinheimer, A. J., Zheng, J., Montzka, D. D., Walega, J. G., Grahek, F. E., Vay, S. A., Collins, J. E., Wade, L. O., Sachse, G. W., Anderson, B. E., Brune, W. H., Tan, D., Faloona, I., Baughcum, S. L., and Ridley, B. A.: Measurement of NO and NO_y emission indices during SUCCESS, Geophysical Research Letters, 25, 1713–1716, 1998.

Cantrell, C. A., Edwards, G. D., Stephens, S., Mauldin, L., Kosciuch, E., Zondlo, M., and Eisele, F.: Peroxy radical observations using chemical ionization mass spectrometry during TOPSE, Journal of Geophysical Research—Atmospheres, 108, 8371, 2003.

Colman, J. J., Swanson, A. L., Meinardi, S., Sive, B. C., Blake, D. R., and Rowland, F. S.: Description of the analysis of a wide range of volatile organic compounds in whole air samples collected during PEM-Tropics A and B, Analytical Chemistry, 73, 3723–3731, 2001.

Crounse, J. D., McKinney, K. A., Kwan, A. J., and Wennberg, P. O.: Measurement of gas-phase hydroperoxides by chemical ionization mass spectrometry, Analytical Chemistry, 78, 6726–6732, 2006.

DeMore, W. B., Sander, S. P., Golden, D. M., Hampson, R. F., Kurylo, M. J., Howard, C. J., Ravishankara, A. R., Kolb, C. E., and Molina, M. J.: Chemical Kinetics and Photochemical Data for Use in Stratospheric Modeling, Evaluation Number 12, JPL Publication 97-4, NASA Jet Propulsion Laboratory, California Institute of Technology, Pasadena, CA 1997.

DuMouchel, W. H., and O'Brien, F. L.: Integrating a Robust Option into a Multiple Regression Computing Environment, Computer Science and Statistics: Proceedings of the 21st Symposium on the Interface, Alexandria, VA, American Statistical Association, 1989.

Emmerson, K. M., Carslaw, N., Carpenter, L. J., Heard, D. E., Lee, J. D., and Pilling, M. J.: Urban atmospheric chemistry during the PUMA campaign 1: Comparison of modelled OH and HO_2 concentrations with measurements, Journal of Atmospheric Chemistry, 52, 143–164, 2005.

Fried, A., Crawford, J., Olson, J., Walega, J., Potter, W., Wert, B., Jordan, C., Anderson, B., Shetter, R., Lefer, B., Blake, D., Blake, N., Meinardi, S., Heikes, B., O'Sullivan, D., Snow, J., Fuelberg,

H., Kiley, C. M., Sandholm, S., Tan, D., Sachse, G., Singh, H., Faloona, I., Harward, C. N., and Carmichael, G. R.: Airborne tunable diode laser measurements of formaldehyde during TRACE-P: Distributions and box model comparisons, Journal of Geophysical Research—Atmospheres, 108, 8798, doi:10.1029/2003JD003451, 2003.

Frost, G. J., Fried, A., Lee, Y. N., Wert, B., Henry, B., Drummond, J. R., Evans, M. J., Fehsenfeld, F. C., Goldan, P. D., Holloway, J. S., Hubler, G., Jakoubek, R., Jobson, B. T., Knapp, K., Kuster, W. C., Roberts, J., Rudolph, J., Ryerson, T. B., Stohl, A., Stroud, C., Sueper, D. T., Trainer, M., and Williams, J.: Comparisons of box model calculations and measurements of formaldehyde from the 1997 North Atlantic Regional Experiment, Journal of Geophysical Research—Atmospheres, 107, 4060, doi:10.1029/2001JD000896, 2002.

Fry, J. L., Nizkorodov, S. A., Okumura, M., Roehl, C. M., Francisco, J. S., and Wennberg, P. O.: Cis-cis and trans-perp HOONO: Action spectroscopy and isomerization kinetics, Journal of Chemical Physics, 121, 1432–1448, 2004.

George, L. A., Hard, T. M., and O'Brien, R. J.: Measurement of free radicals OH and HO_2 in Los Angeles smog, Journal of Geophysical Research—Atmospheres, 104, 11643–11655, 1999.

Gierczak, T., Jimenez, E., Riffault, V., Burkholder, J. B., and Ravishankara, A. R.: Thermal decomposition of HO_2NO_2 (peroxynitric acid, PNA): Rate coefficient and determination of the enthalpy of formation, Journal of Physical Chemistry A, 109, 586–596, 2005.

Graham, R. A., Winer, A. M., and Pitts, J. N.: Temperature dependence of the unimolecular decomposition of pernitric acid and its atmospheric implications, Chemical Physics Letters, 51, 215–220, 1977.

Graham, R. A., Winer, A. M., and Pitts, J. N.: Pressure and temperature-dependence of unimolecular decomposition of HO_2NO_2, Journal of Chemical Physics, 68, 4505–4510, 1978.

Griffith, D. W. T.: Synthetic calibration and quantitative analysis of gas-phase FT-IR spectra, Applied Spectroscopy, 50, 59–70, 1996.

Heard, D. E., Carpenter, L. J., Creasey, D. J., Hopkins, J. R., Lee, J. D., Lewis, A. C., Pilling, M. J., Seakins, P. W., Carslaw, N., and Emmerson, K. M.: High levels of the hydroxyl radical in the winter urban troposphere, Geophysical Research Letters, 31, L18112, doi:10.1029/2004GL020544, 2004.

Huey, L. G., Hanson, D. R., and Howard, C. J.: Reactions of SF_6^- and I^- with atmospheric trace gases, Journal of Physical Chemistry, 99, 5001–5008, 1995.

Huey, L. G., Villalta, P. W., Dunlea, E. J., Hanson, D. R., and Howard, C. J.: Reactions of CF_3O^- with atmospheric trace gases, Journal of Physical Chemistry, 100, 190–194, 1996.

Jacob, D. J.: Introduction to Atmospheric Chemistry, Princeton University Press, 1999.

Jaegle, L., Jacob, D. J., Brune, W. H., Faloona, I., Tan, D., Heikes, B. G., Kondo, Y., Sachse, G. W., Anderson, B., Gregory, G. L., Singh, H. B., Pueschel, R., Ferry, G., Blake, D. R., and Shetter, R. E.: Photochemistry of HO_x in the upper troposphere at northern midlatitudes, Journal of Geophysical Research—Atmospheres, 105, 3877–3892, 2000.

Jimenez, E., Gierczak, T., Stark, H., Burkholder, J. B., and Ravishankara, A. R.: Reaction of OH with HO_2NO_2 (Peroxynitric Acid): Rate Coefficients between 218 and 335 K and Product Yields at 298 K, Journal of Physical Chemistry A, 108, 1139–1149, 2004.

Kanaya, Y., Cao, R. Q., Akimoto, H., Fukuda, M., Komazaki, Y., Yokouchi, Y., Koike, M., Tanimoto, H., Takegawa, N., and Kondo, Y.: Urban photochemistry in central Tokyo: 1. Observed and modeled OH and HO_2 radical concentrations during the winter and summer of 2004, Journal of Geophysical Research—Atmospheres, 112, D21312, doi:10.1029/2007JD008670, 2007.

Kim, S., Huey, L. G., Stickel, R. E., Tanner, D. J., Crawford, J. H., Olson, J. R., Chen, G., Brune, W. H., Ren, X., Lesher, R., Wooldridge, P. J., Bertram, T. H., Perring, A., Cohen, R. C., Lefer, B. L., Shetter, R. E., Avery, M., Diskin, G., and Sokolik, I.: Measurement of HO_2NO_2 in the free troposphere during the intercontinental chemical transport experiment—North America 2004, Journal of Geophysical Research—Atmospheres, 112, D12S01, doi:10.1029/2006JD007676, 2007.

Knight, G., Ravishankara, A. R., and Burkholder, J. B.: UV absorption cross sections of HO_2NO_2 between 343 and 273 K, Physical Chemistry Chemical Physics, 4, 1432–1437, 2002.

Li, S. P., Matthews, J., and Sinha, A.: Atmospheric hydroxyl radical production from electronically excited NO_2 and H_2O, Science, 319, 1657–1660, 2008.

Lurmann, F. W., Lloyd, A. C., and Atkinson, R.: A Chemical Mechanism for Use in Long-Range Transport Acid Deposition Computer Modeling, Journal of Geophysical Research—Atmospheres, 91, 10905–10936, 1986.

Macleod, H., Smith, G. P., and Golden, D. M.: Photodissociation of Pernitric Acid (HO_2NO_2) at 248 nm, Journal of Geophysical Research—Atmospheres, 93, 3813–3823, 1988.

Madronich, S., and Flocke, S.: The role of solar radiation in atmospheric chemistry, in Handbook of Environmental Chemistry, edited by Boule, P., Springer, 1–26, 1998.

Martinez, M., Harder, H., Kovacs, T. A., Simpas, J. B., Bassis, J., Lesher, R., Brune, W. H., Frost, G. J., Williams, E. J., Stroud, C. A., Jobson, B. T., Roberts, J. M., Hall, S. R., Shetter, R. E., Wert, B., Fried, A., Alicke, B., Stutz, J., Young, V. L., White, A. B., and Zamora, R. J.: OH and HO_2 concentrations, sources, and loss rates during the Southern Oxidants Study in Nashville, Tennessee, Summer 1999, Journal of Geophysical Research—Atmospheres, 108, D194617, doi:10.1029/2003JD003551, 2003.

Miller, E. R., and Friesen, R. B.: Standard output data products from the NCAR Research Aviation Facility, NCAR RAF Bulletin 9, 1985. http://www.eol.ucar.edu/raf/Bulletins/bulletin9.html.

Murphy, J. G., Thornton, J. A., Wooldridge, P. J., Day, D. A., Rosen, R. S., Cantrell, C., Shetter, R. E., Lefer, B., and Cohen, R. C.: Measurements of the sum of HO_2NO_2 and $CH_3O_2NO_2$ in the remote troposphere, Atmospheric Chemistry and Physics, 4, 377–384, 2004.

Niki, H., Maker, P. D., Savage, C. M., and Breitenbach, L. P.: Fourier transform IR spectroscopic observation of pernitric acid formed via $HOO + NO_2 \rightarrow HOONO_2$, Chemical Physics Letters, 45, 564–566, 1977.

Olson, J. R., Crawford, J. H., Chen, G., Brune, W. H., Faloona, I. C., Tan, D., Harder, H., and Martinez, M.: A reevaluation of airborne HO_x observations from NASA field campaigns, Journal of Geophysical Research—Atmospheres, 111, D10301, doi:10.1029/2005JD006617, 2006.

Olson, J. R., Crawford, J. H., Chen, G., Fried, A., Evans, M. J., Jordan, C. E., Sandholm, S. T., Davis, D. D., Anderson, B. E., Avery, M. A., Barrick, J. D., Blake, D. R., Brune, W. H., Eisele, F. L., Flocke, F., Harder, H., Jacob, D. J., Kondo, Y., Lefer, B. L., Martinez, M., Mauldin, R. L., Sachse, G. W., Shetter, R. E., Singh, H. B., Talbot, R. W., and Tan, D.: Testing fast photochemical theory during TRACE-P based on measurements of OH, HO_2, and CH_2O, Journal of Geophysical Research—Atmospheres, 109, D15S10, doi:10.1029/2003JD004278, 2004.

Okumura, M., and Sander, S. P: Gas-Phase Formation Rates of Nitric Acid and its Isomers under Urban Conditions, State of California Air Resources Board, 2005.

Ravishankara, A. R., Dunlea, E. J., Blitz, M. A., Dillon, T. J., Heard, D. E., Pilling, M. J., Strekowski, R. S., Nicovich, J. M., and Wine, P. H.: Redetermination of the rate coefficient for the reaction of $O(^1D)$ with N_2, Geophysical Research Letters, 29, 1745, doi:10.1029/2002GL014850, 2002.

Ren, X. R., Brune, W. H., Mao, J. Q., Mitchell, M. J., Lesher, R. L., Simpas, J. B., Metcalf, A. R., Schwab, J. J., Cai, C. X., Li, Y. Q., Demerjian, K. L., Felton, H. D., Boynton, G., Adams, A., Perry, J., He, Y., Zhou, X. L., and Hou, J.: Behavior of OH and HO_2 in the winter atmosphere in New York City, Atmospheric Environment, 40, S252–S263, 2006.

Ren, X. R., Harder, H., Martinez, M., Lesher, R. L., Oliger, A., Simpas, J. B., Brune, W. H., Schwab, J. J., Demerjian, K. L., He, Y., Zhou, X. L., and Gao, H. G.: OH and HO_2 chemistry in the urban atmosphere of New York City, Atmospheric Environment, 37, 3639–3651, 2003.

Ren, X. R., Olson, J. R., Crawford, J. H., Brune, W. H., Mao, J. Q., Long, R. B., Chen, Z., Chen, G., Avery, M. A., Sachse, G. W., Barrick, J. D., Diskin, G. S., Huey, L. G., Fried, A., Cohen, R. C., Heikes, B., Wennberg, P. O., Singh, H. B., Blake, D. R., and Shetter, R. E.: HO_x chemistry

during INTEX-A 2004: Observation, model calculation, and comparison with previous studies, Journal of Geophysical Research—Atmospheres, 113, D05310, doi:10.1029/2007JD009166, 2008.

Roehl, C. M., Nizkorodov, S. A., Zhang, H., Blake, G. A., and Wennberg, P. O.: Photodissociation of Peroxynitric Acid in the Near-IR, Journal of Physical Chemistry A, 106, 3766–3772, 2002.

Rothman, L. S., Jacquemart, D., Barbe, A., Benner, D. C., Birk, M., Brown, L. R., Carleer, M. R., Chackerian, C., Chance, K., Coudert, L. H., Dana, V., Devi, V. M., Flaud, J. M., Gamache, R. R., Goldman, A., Hartmann, J. M., Jucks, K. W., Maki, A. G., Mandin, J. Y., Massie, S. T., Orphal, J., Perrin, A., Rinsland, C. P., Smith, M. A. H., Tennyson, J., Tolchenov, R. N., Toth, R. A., Vander Auwera, J., Varanasi, P., and Wagner, G.: The HITRAN 2004 molecular spectroscopic database, Journal of Quantitative Spectroscopy & Radiative Transfer, 96, 139–204, 2005.

Sander, S. P., Friedl, R. R., DeMore, W. B., Golden, D. M., Kurylo, M. J., Hampson, R. F., Huie, R. E., Moortgat, G. K., Ravishankara, A. R., Kolb, C. E., and Molina, M. J.: Chemical Kinetics and Photochemical Data for Use in Stratospheric Modeling Supplement to Evaluation 12: Update of Key Reactions, JPL Publication 00-3, NASA Jet Propulsion Laboratory, California Institute of Technology, Pasadena, CA 2000.

Sander, S. P., Friedl, R. R., Golden, D. M., Kurylo, M. J., Huie, R. E., Orkin, V. L., Moortgat, G. K., Ravishankara, A. R., Kolb, C. E., Molina, M. J., and Finlayson-Pitts, B. J.: Chemical Kinetics and Photochemical Data for Use in Atmospheric Studies, Evaluation Number 14 JPL Publication 02-25, NASA Jet Propulsion Laboratory, California Institute of Technology, Pasadena, CA 2003.

Sander, S. P., Friedl, R. R., Golden, D. M., Kurylo, M. J., Moortgat, G. K., Keller-Rudek, H., Wine, P. H., Ravishankara, A. R., Kolb, C. E., Molina, M. J., Finlayson-Pitts, B. J., Huie, R. E., and Orkin, V. L.: Chemical Kinetics and Photochemical Data for Use in Atmospheric Studies, Evaluation Number 15 JPL Publication 06-2, NASA Jet Propulsion Laboratory, California Institute of Technology, Pasadena, CA 2006.

Seinfeld, J. H., and Pandis, S. N.: Atmospheric Chemistry and Physics, 2nd ed., John Wiley & Sons, 2006.

Shetter, R. E., and Muller, M.: Photolysis frequency measurements using actinic flux spectroradiometry during the PEM-Tropics mission: Instrumentation description and some results, Journal of Geophysical Research—Atmospheres, 104, 5647–5661, 1999.

Shirley, T. R., Brune, W. H., Ren, X., Mao, J., Lesher, R., Cardenas, B., Volkamer, R., Molina, L. T., Molina, M. J., Lamb, B., Velasco, E., Jobson, T., and Alexander, M.: Atmospheric oxidation in the Mexico City Metropolitan Area (MCMA) during April 2003, Atmospheric Chemistry and Physics, 6, 2753–2765, 2006.

Slusher, D. L., Pitteri, S. J., Haman, B. J., Tanner, D. J., and Huey, L. G.: A chemical ionization technique for measurement of pernitric acid in the upper troposphere and the polar boundary layer, Geophysical Research Letters, 28, 3875–3878, 2001.

Smith, C. A., Molina, L. T., Lamb, J. J., and Molina, M. J.: Kinetics of the Reaction of OH with Pernitric and Nitric-Acids, International Journal of Chemical Kinetics, 16, 41–55, 1984.

Street, J. O., Carroll, R. J., and Ruppert, D.: A Note on Computing Robust Regression Estimates via Iteratively Reweighted Least Squares, The American Statistician, 42, 152–154, 1988.

Trevor, P. L., Black, G., and Barker, J. R.: Reaction Rate Constant for OH + $HOONO_2$ $\rightarrow$ Products over the Temperature Range 246 to 324K, Journal of Physical Chemistry, 86, 1661–1669, 1982.

Weinheimer, A. J., Montzka, D. D., Campos, T. L., Walega, J. G., Ridley, B. A., Donnelly, S. G., Keim, E. R., Del Negro, L. A., Proffitt, M. H., Margitan, J. J., Boering, K. A., Andrews, A. E., Daube, B. C., Wofsy, S. C., Anderson, B. E., Collins, J. E., Sachse, G. W., Vay, S. A., Elkins, J. W., Wamsley, P. R., Atlas, E. L., Flocke, F., Schauffler, S., Webster, C. R., May, R. D., Loewenstein, M., Podolske, J. R., Bui, T. P., Chan, K. R., Bowen, S. W., Schoeberl, M. R., Lait, L. R., and Newman, P. A.: Comparison between DC-8 and ER-2 species measurements in the tropical middle troposphere: NO, NO_y, O_3, CO_2, CH_4, and N_2O, Journal of Geophysical Research—Atmospheres, 103, 22087–22096, 1998.

Wennberg, P. O., and Dabdub, D.: Atmospheric chemistry—Rethinking ozone production, Science, 319, 1624–1625, 2008.

Wert, B. P., Fried, A., Rauenbuehler, S., Walega, J., and Henry, B.: Design and performance of a tunable diode laser absorption spectrometer for airborne formaldehyde measurements, Journal of Geophysical Research—Atmospheres, 108, 4350, doi:10.1029/2002JD002872, 2003.

Zabel, F.: Unimolecular Decomposition of Peroxynitrates, Zeitschrift Fur Physikalische Chemie-International Journal of Research in Physical Chemistry & Chemical Physics, 188, 119–142, 1995.

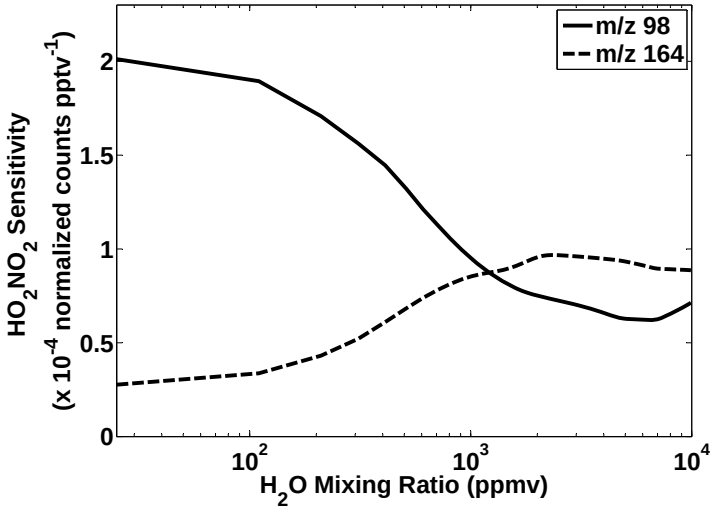

Figure 2.1: Sensitivity curves for m/z 98 (solid) and m/z 164 (dash) as a function of H_2O mixing ratio in the flow tube. The sensitivity curves are used to calculate the final mixing ratios of HO_2NO_2.

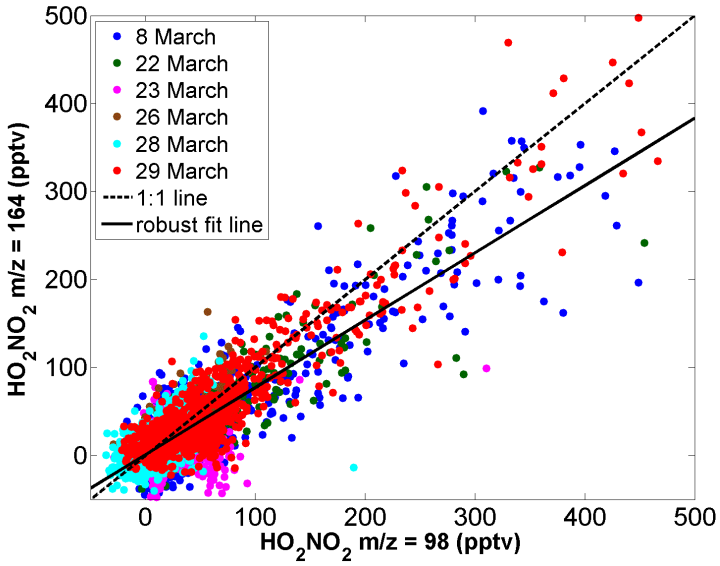

Figure 2.2: HO_2NO_2 is measured with two ions: products of fluoride transfer (m/z = 98) and clustering (m/z = 164). The data are colored by flight date. The data shown are observations obtained when the measured NO_y differs by less than 10% between m/z 98 and m/z 164 sampling times. The slope of the robust fit line is 0.76, and the intercept is 0.90 pptv. $R^2 = 0.94$. Independent measurements of HO_2NO_2 from these two ions agree very well, indicating that these masses are selective to HO_2NO_2.

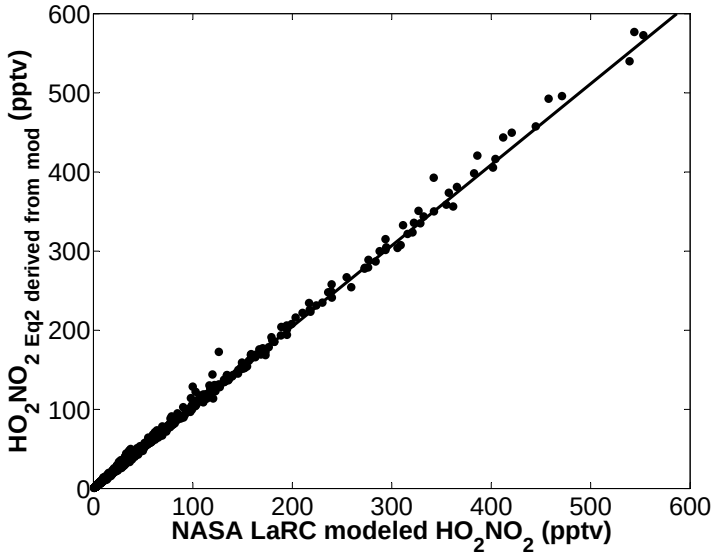

Figure 2.3: $[HO_2NO_2]_{ss}$, calculated from Eq. 2.2, using modeled values of HO_2 and NO_2 versus HO_2NO_2 predicted by the NASA LaRC box model. The slope of the robust fit line is 1.02, and the intercept is 0.10 pptv. $R^2 = 0.99$, demonstrating that Eq. 2.2 is a valid simplification under MILAGRO conditions.

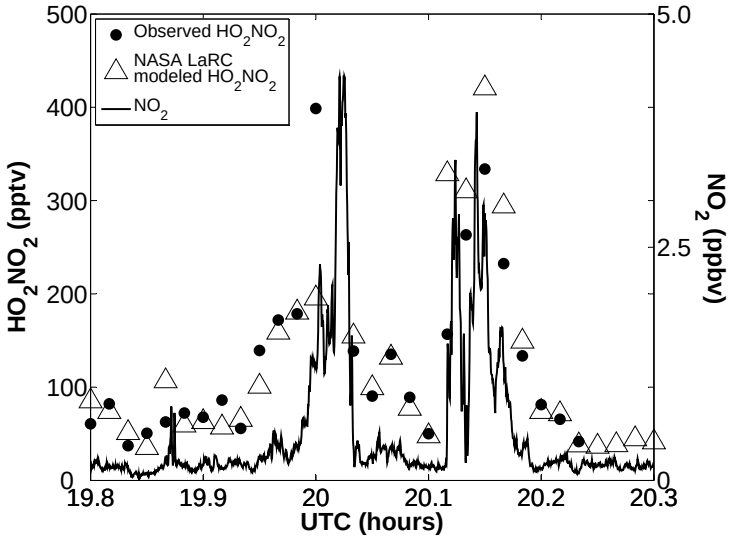

Figure 2.4: Mixing ratios of HO_2NO_2 and NO_2 during the 29 March 2006 flight in an airmass heavily impacted by pollution. Dots are CIMS measurements of HO_2NO_2. Triangles are NASA LaRC box model values of HO_2NO_2. The solid line is observed NO_2 mixing ratio. Variations in the observed and modeled HO_2NO_2 mixing ratios closely follow variations in NO_2.

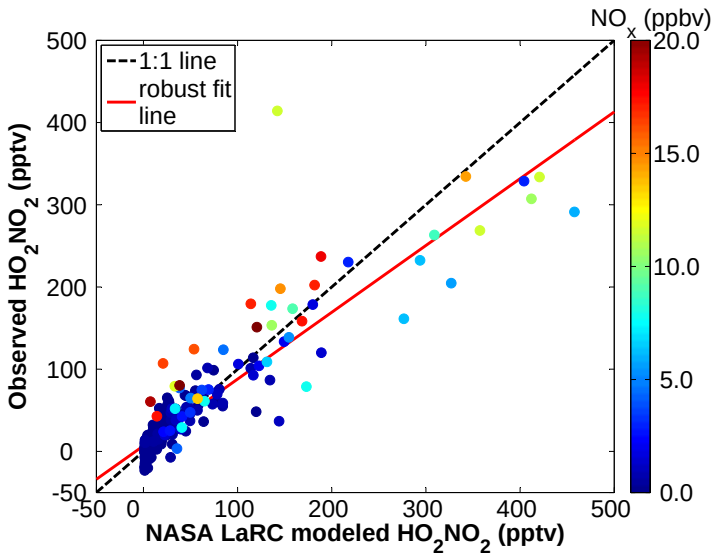

Figure 2.5: Observed HO_2NO_2 versus NASA LaRC box model values of HO_2NO_2. The data presented are observed and modeled values at times when the model was constrained by NMHC observations. The slope of the robust fit line is 0.81, and the intercept is 6.74 pptv. $R^2 = 0.82$.

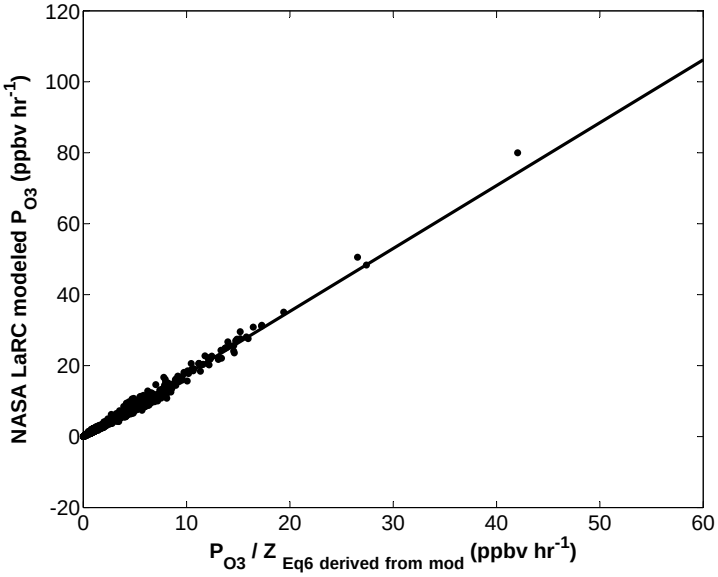

Figure 2.6: The rate of ozone production calculated using Eq. 2.6 and modeled values of HO_2NO_2, NO, and NO_2 is compared to the ozone production rate predicted by the NASA LaRC box model. The slope of the best-fit line, Z, is 1.77. $R^2 = 0.99$.

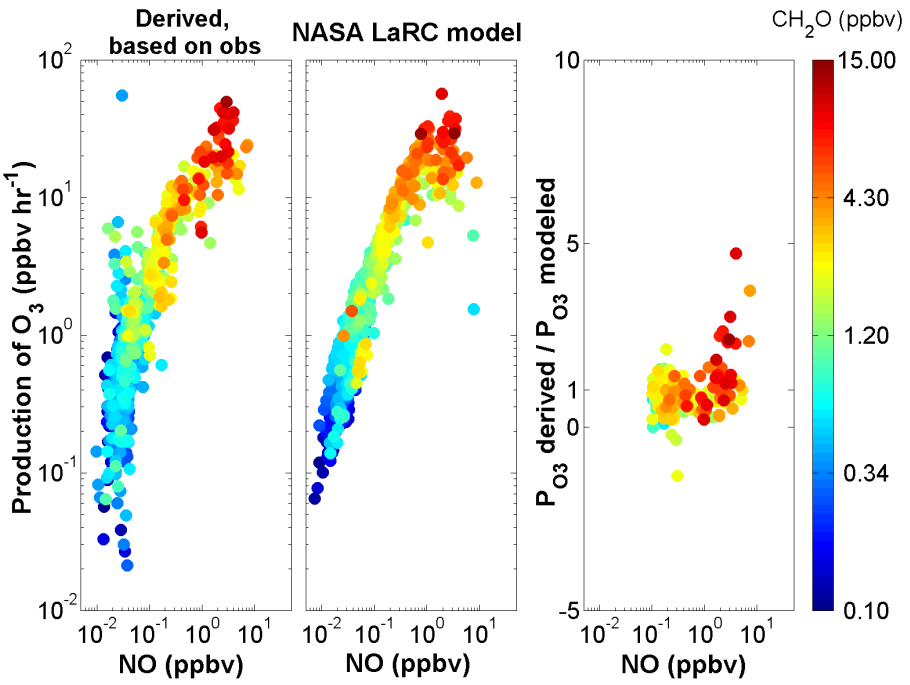

Figure 2.7: P_{O3} derived from Eq. 2.6 and based on measurements of HO_2NO_2 and NO_x versus observed NO, colored by observed CH_2O are shown in the left panel. NASA LaRC box model predictions of P_{O3} versus modeled NO, colored by modeled CH_2O are shown in the center panel. The ratio of derived P_{O3}, based on measurements to NASA LaRC box model predictions of P_{O3} for observed NO greater than 100 pptv, colored by observed CH_2O are shown in the right panel.

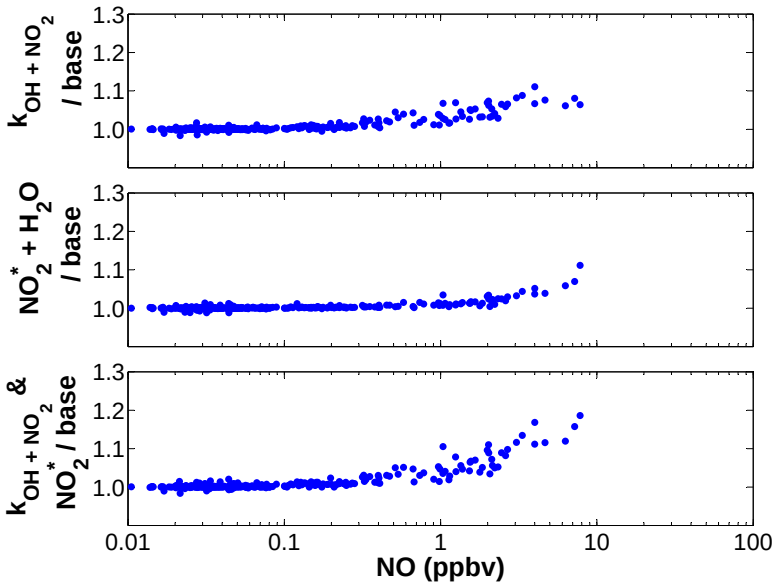

Figure 2.8: Three different variations of the base model were investigated. The mixing ratio of HO_2NO_2 was calculated 1. using the 2000 JPL recommended rate constant for $OH + NO_2$ (top panel), 2. including the reaction $NO_2^* + H_2O \rightarrow OH + HONO$ (center panel), and 3. using both the 2000 JPL recommended rate constant and the NO_2^* reaction (bottom panel). The y-axis is the ratio of HO_2NO_2 mixing ratio as calculated using a model variation to that calculated using the base model. Use of the 2000 JPL recommended rate constant for $OH + NO_2$ and inclusion of the $NO_2^* + H_2O$ reaction result in higher HO_2NO_2 mixing ratios than calculated by the base model. This leads to better agreement between measured and calculated HO_2NO_2.

Chapter 3

Trends in Atmospheric Sulfur in Los Angeles

3.1 Abstract

SO_2 and sulfate are important components of air pollution in the Los Angeles basin. Comparison of aircraft observations from 2002 and 2008 indicate a large decrease in SO_2 concentration and a change in its spatial distribution. The effects of meteorological differences and different measurement techniques are evaluated. These factors do not entirely explain the differences between the 2002 and 2008 observations. Aircraft observations indicate an increase in sulfate concentrations in the Los Angeles basin between 2002 and 2008 while ground-based measurements indicate a modest reduction. Possible explanations of the difference in SO_2 and sulfate trends, such as changes in concentrations of other chemical species and changes in upwind sources, are discussed.

3.2 Introduction

Anthropogenic activities account for ∼75% of total global sulfur emissions into the atmosphere (Forster et al., IPCC, 2007). SO_2 is emitted as a by-product of burning fossil fuels, such as coal and petroleum, that contain sulfur and is removed from the atmosphere by oxidation to sulfate and subsequent dry and wet deposition. Gas-phase oxidation of SO_2 in the troposphere is dominated by reaction with OH radicals (R3.1–R3.3) (Stockwell and Calvert, 1983):

$$SO_2 + OH + M \rightarrow HOSO_2 + M, \tag{R3.1}$$

$$HOSO_2 + O_2 \rightarrow HO_2 + SO_3, \tag{R3.2}$$

$$SO_3 + 2H_2O \rightarrow H_2SO_4 + H_2O, \tag{R3.3}$$

where M represents a third body such as O_2 and N_2, and R3.3 most likely proceeds via reaction of an $H_2O{-}SO_3$ complex with a second water molecule (Morokuma and Muguruma, 1994; Jayne et al., 1997). Because of its low vapor pressure, gas-phase H_2SO_4 rapidly enters the particulate phase

by nucleation or condensation on existing aerosols (Davis et al., 1979).

In addition to gas-phase production, sulfate can be formed by the uptake of SO_2 into liquid cloud or aerosol droplets followed by aqueous-phase oxidation by H_2O_2, O_3, and O_2 when catalyzed by Fe(III) or Mn(II) (Calvert et al., 1985; Hoffmann and Edwards, 1975; Erickson et al., 1977; Huss et al., 1982; Brimblecombe and Spedding, 1974). The rate and importance of each of these heterogeneous oxidation pathways depends on the pH of the droplet, the solubility of the oxidant, and the concentration of the oxidant in the atmosphere. SO_2 conversion to sulfate is driven by gas-phase reaction with OH under clear-sky daylight conditions (Eatough et al., 1994) and aqueous-phase reaction with H_2O_2, O_3, and O_2 catalyzed by iron or manganese under nighttime or cloudy, foggy conditions (Eatough et al., 1984; Penkett et al., 2007; Ibusuki and Barnes, 1984).

A third, less well-understood route for the oxidation of SO_2 may be heterogeneous oxidation on the surface of solid aerosols such as soot and graphite (Chang et al., 1981). The importance of these solid aerosol reactions depends on available surface area and the amount of water adsorbed to the particle surface. Finally, direct emissions of sulfate may be important as primary sulfate emissions are suggested to be 2%–7% of total sulfur emissions from combustion sources (Dominguez et al., 2008).

Health risks and environmental issues are associated with elevated levels of sulfate. Sulfate is a substantial component of particulate matter (PM) in Southern California, accounting for 9%–18% of aerosol mass (Kim et al., 2000). Particulate matter can cause eye, nose, and throat irritation. Due to their ability to become lodged in the lungs, particles with diameters less than 2.5 µm ($PM_{2.5}$) are associated with increased incidents of asthma, lung cancer, and cardiopulmonary mortality (Pope et al., 2002). Aerosols also significantly reduce visibility (Cass, 1979; Eldering et al., 1996) and affect Earth's radiative budget (Ramanathan et al., 2001; Forster et al., IPCC, 2007). Because most SO_2 is oxidized to sulfate, an increase in SO_2 concentration leads to additional atmospheric aerosol loading, if not locally, then downwind of the sources.

In Southern California, there are many sources of SO_2, primary sulfate, and secondary sulfate. These include petroleum refining operations, combustion of fuel used by marine vessels entering and

exiting the Los Angeles–Long Beach Port Complex, and on-road fuel combustion. Large emissions of SO_2, NO_x ($NO_x = NO + NO_2$), and volatile organic compounds coupled with the unique topography and meteorology of the Los Angeles basin often result in a buildup of basin and offshore emissions and their resultant oxidation products. The Environmental Protection Agency (EPA) sets National Ambient Air Quality Standards (NAAQS) for 24-hour and annual exposure to $PM_{2.5}$. In September 2006, the EPA strengthened the 24-hour standard from the 1997 level of 65 µg m^{-3} to 35 µg m^{-3}. The 24-hour standard (65 µg m^{-3} in 2002 and 35 µg m^{-3} in 2008) was exceeded an estimated 93 days in Southern California during 2002 and 19 days during 2008 (CARB, 2008a).

The focus of this work is to compare historical and recent measurements of SO_2 and sulfate in the South Coast Air Basin (SCB). The SCB is defined here as the region between 33° and 35° N latitude and 117° and 119° W longitude (shown in Fig. 3.1). We present in situ measurements of SO_2 and sulfate conducted in the SCB collected in May 2002 and June 2008. The 2002 and 2008 measurements were made from the NOAA WP-3D aircraft during the Intercontinental Transport and Chemical Transformation (ITCT) 2K2 field campaign and the NASA DC-8 aircraft during the California portion of the Arctic Research of the Composition of the Troposphere from Aircraft and Satellites (ARCTAS-CARB) field campaign, respectively. This study includes available data from five 2008 flights (18, 20, 22, 24, and 26 June) and one 2002 flight (13 May) in the SCB. Two additional flights flew over the SCB during the ITCT 2K2 campaign; these flights did not, however, sample in the boundary layer. All flights were conducted during daytime hours. Ground-based measurements of sulfate conducted at Interagency Monitoring of Protected Visual Environments (IMPROVE) network sites in the SCB are presented and observed trends are discussed. We use the EPA Community Multiscale Air Quality (CMAQ) model to investigate the effects of meteorology on observed sulfur concentrations and to evaluate possible explanations of the trends in SO_2 and sulfate observed between 2002 and 2008.

3.3 Methodology

3.3.1 Aircraft Instrumentation

During the 2002 ITCT 2K2 campaign, SO_2 mixing ratios were measured using a modified, commercial UV pulsed-fluorescence instrument (Ryerson et al., 1998) with an uncertainty of ±(20% of the mixing ratio + 0.35 ppbv). Sulfate concentrations were measured with a particle-into-liquid sampler/ion chromatography system (PILS-IC) with an uncertainty of ±20% (Orsini et al., 2003; Weber et al., 2001). CO_2 mixing ratios were measured using a commercial dual cell, nondispersive infrared absorption instrument with an uncertainty of ±(7% of the difference between 380 ppmv and higher measured mixing ratios + 0.4 ppmv) (Parrish et al., 2004b). Further details on the instruments aboard the WP-3D aircraft platform during the ITCT 2K2 campaign are given in Parrish et al. (2004a).

During the 2008 ARCTAS-CARB campaign, CO mixing ratios were measured by tunable diode laser spectroscopy with an uncertainty of ±2% (Sachse et al., 1987). CO_2 mixing ratios were measured with a modified nondispersive infrared gas analyzer with an uncertainty of ±0.25 ppmv (Vay et al., 2003). Further details of measurements made from the NASA DC-8 aircraft platform during the ARCTAS-CARB campaign can be found in Jacob et al. (2009).

Independent measurements of sulfate were made using the University of Colorado–Boulder high-resolution time-of-flight aerosol mass spectrometer (HR-AMS) (DeCarlo et al., 2006) and the University of New Hampshire mist chamber / ion chromatography system (MC/IC) (Scheuer et al., 2003). HR-AMS sulfate measurements are used in this analysis as they provide greater temporal resolution than MC/IC measurements. The uncertainty of the HR-AMS sulfate measurements is ±35%. The two independent measurements of sulfate agree within 35%, with the MC/IC measurements higher on average than the HR-AMS measurements.

Two independent measurements of SO_2 were made using Georgia Institute of Technology (Georgia Tech) and California Institute of Technology (Caltech) chemical ionization mass spectrometry (CIMS) instruments. The Georgia Tech CIMS instrument uses SF_6^- as a reagent ion and has been

described previously by Huey et al. (2004). The Caltech CIMS instrument has been described previously by Crounse et al. (2006), but its use for measurement of SO_2 has not been detailed.

Negative ion chemistry of CF_3O^- has been shown to provide sensitive detection of many atmospheric trace gases (Huey et al., 1996; Amelynck et al., 2000; Crounse et al., 2006; Spencer et al., 2009; Paulot et al., 2009) and is exploited in this work to detect SO_2. The Caltech CIMS instrument consists of a flow tube in which a reagent ion, CF_3O^-, interacts with ambient air diluted 1:4 with ultra high purity nitrogen. The flow tube is controlled at 35 mbar total pressure. Ions are sampled from the flow tube into a quadrupole mass filter and detected with a channel electron multipler. The reaction of CF_3O^- with SO_2 proceeds via fluoride ion transfer through R3.4 (Huey et al., 1996). Water clustering of $SO_2 \cdot F^-$ also occurs through R3.5. Ion signals at m/z 83 and m/z 101 are used to calculate SO_2 concentration. Each mass-to-charge ratio is observed for ∼0.5 seconds. SO_2 masses are monitored every ∼15 seconds.

$$CF_3O^- + SO_2 \rightarrow SO_2 \cdot F^- \ (m/z\ 83) + CF_2O \tag{R3.4}$$

$$SO_2 \cdot F^- \ (m/z\ 83) + H_2O + M \rightleftharpoons SO_2 \cdot F^- \cdot H_2O \ (m/z\ 101) + M \tag{R3.5}$$

3.3.1.1 Sensitivity and Calibration of the Caltech SO_2 Measurement

The sensitivity of the Caltech CIMS instrument to SO_2 and the dependence of the sensitivity and ion products on the mixing ratio of water vapor in the flow tube were quantified in the laboratory. A small quantity of SO_2 was introduced into the flow tube by flowing a known amount of dry N_2 over an SO_2 permeation tube. The permeation rate was determined by mass loss. The concentration of SO_2 that entered the instrument flow tube was verified with FTIR spectroscopy using HITRAN line lists (Rothman et al., 2005) and the nonlinear NLM4 software developed by Griffith (1996). The flow tube humidity was controlled using mass flow controllers to adjust the ratio of N_2 saturated with water vapor to dry N_2. Humidity was quantified by Fourier Transform Infrared (FTIR) spectroscopy using HITRAN line lists (Rothman et al., 2005). Instrument sensitivity to the fluoride ion transfer product

(m/z 83) and the water cluster of the fluoride ion transfer product (m/z 101) (R3.4 and R3.5) was determined as a function of humidity to obtain water-dependent sensitivity curves. These sensitivity curves are presented in Fig. 3.2. Sensitivity is expressed in ion counts, normalized by the ion counts of the ^{13}C isotope of the reagent ion and its one-water cluster ($^{13}CF_3O^-$ and $^{13}CF_3O^- \cdot H_2O$), per pptv of SO_2. Pre- and postmission laboratory calibrations for SO_2 were conducted. During flight, isotopically labeled HNO_3 as well as other calibration gases (formic acid, acetic acid, and H_2O_2) were periodically added to the flow tube to monitor the stability of the instrument sensitivity. Sensitivity of the instrument to HNO_3 was consistent between laboratory and flight. Similarly, calibrations for H_2O_2 and organic acids were found to be consistent between preflight, in-flight, and postflight calibrations lending confidence that the sensitivity of the instrument to SO_2 was also consistent.

In the absence of SO_2, ion signals at m/z 83 and m/z 101 are nonzero, and these background signals must be accounted for in the data analysis. Background signals were measured during flight by periodically passing ambient air through a filter consisting of alumina pellets coated with palladium followed by nylon wool coated with sodium bicarbonate, quantitatively removing SO_2. This technique is described further in Crounse et al. (2006).

3.3.1.2 Ambient SO_2 concentration

Caltech CIMS SO_2 concentrations are calculated from the ion signals observed at m/z 83 and m/z 101 after normalization by the amount of reagent ion signal, subtraction of signals due to known interferences, subtraction of background signals, and application of the appropriate sensitivity factor.

Formic acid is a known interference in the m/z 83 ion signal and is detected by the Caltech CIMS instrument as a fluoride transfer product ($HF \cdot HC(O)O^-$, m/z 65) or as a one-water cluster of the fluoride transfer product ($HF \cdot HC(O)O^- \cdot H_2O$, m/z 83). Isotopically labeled formic acid ($H^{13}C(O)OH$) was used during in-flight calibrations, and the ratio of $HF \cdot H^{13}C(O)O^- \cdot H_2O$ to $HF \cdot H^{13}C(O)O^-$ as a function of water vapor was determined. This ratio and the formic acid m/z 65 ion signal were combined to estimate the contribution of formic acid to the m/z 83 ion signal. The formic acid isobaric interference produced a signal equivalent to 50–350 pptv SO_2

during the ARCTAS-CARB campaign. Background signals due to impurities in the ion source were measured (as described above) every 15 minutes and were used to correct the data for instrumental backgrounds. These backgrounds are generally small (equivalent to <250 pptv SO_2) and stable.

After normalizing by the amount of reagent ion signal and correcting for background and interference signals, the corrected ion signals at m/z 83 and m/z 101 were combined, and the corresponding sensitivity factor (solid line in Fig. 3.2) was applied to yield ambient SO_2 concentration.

The relationship between the two independent measurements of SO_2 during the ARCTAS-CARB campaign is linear; however, the Caltech CIMS measurement is, on average, 43% higher than the Georgia Tech CIMS measurement (Fig. 3.3). The reason for the bias is not known. The uncertainty in the Georgia Tech SO_2 measurements is ±20%. The uncertainty in the Caltech SO_2 measurements is ±(30% of the mixing ratio + 100 pptv). The uncertainty in the Caltech measurements reflects the sum of the precision of the data determined by the counting statistics of the ions, the variability of the background signal, and the uncertainty in the sensitivities shown in Fig. 3.2. The concentration of SO_2 used in the subsequent analysis is the mean of the concentrations determined by the two independent measurements.

The NOAA UV pulsed-fluorescence instrument and the Caltech CIMS instrument both flew on the NSF C-130 during the 2006 NASA INTEX-B/MILAGRO campaign. Using the same data analysis procedure described above and postflight calibration of the CIMS instrument (preflight calibrations were not performed for SO_2), SO_2 concentrations determined using the Caltech CIMS instrument were 10% higher than those determined by the NOAA UV pulsed-fluorescence instrument.

3.3.2 IMPROVE Sites

The IMPROVE monitoring program is an extensive effort to monitor visibility and fine particle concentrations at over 100 sites nationwide, focusing on national parks and wilderness areas (http://vista.circa.colostate.edu/improve/). There are three IMPROVE sites in the SCB. The Agua Tibia site is located at 33.46° N latitude and 116.97° W longitude at an elevation of 507 m. The

San Gabriel site is located at 34.30° N latitude and 118.03° W longitude at an elevation of 1791 m. The San Gorgonio Wilderness site is located at 34.19° N latitude and 116.91° W longitude at an elevation of 1726 m (locations shown in Fig. 3.1). Aerosol samples are collected for 24 hours every third day. IMPROVE samplers consist of four independent modules each with a separate inlet, filter pack, and pump assembly (DeBell et al., 2006) and are described in detail in Malm et al. (1989, 2000). For sulfate quantification, aerosol particles of diameters less than 2.5 µm are collected on nylon filters. The collected material is extracted ultrasonically in an aqueous solution and analyzed by ion chromatography (DeBell et al., 2006).

3.3.3 EPA CMAQ Model

The EPA Community Multiscale Air Quality (CMAQ) model version 4.6 (Byun and Ching, 1998) was used to perform simulations of 2002 and 2008 air quality in the SCB. The model domain was the state of California at a resolution of 4 x 4 km. The SAPRC 99 mechanism was used to represent gas-phase chemistry (Carter, 2000). Meteorology of both 2002 and 2008 was computed using MM5 (Grell et al., 1994). Gridded emissions were used to estimate anthropogenic and biogenic emissions. 2008 emissions were obtained from the CARB 2008 emissions inventory; however, no 2002 inventory was available. Instead the 2000 inventory was used (CARB, 2008b). The resultant simulated SO_2 concentrations were much lower than observed during the 2002 ITCT campaign. Based on the observed spatial distribution of SO_2 in 2002 (discussed below), the missing sulfur appears to originate from a diffuse source.

To obtain simulated SO_2 concentrations that are consistent with 2002 aircraft observations, a diffuse source of SO_2 was added to the emissions inventory. Inventory sources of SO_2 were divided into three categories: ocean, stationary, and on-road. Ocean sources were defined as ocean-going vessels, commercial harbor craft, and recreational boats. Stationary sources were defined as all stationary sources and off-road equipment (e.g., mining, construction, and airport equipment). On-road sources were defined as all on-road motor vehicles and trains. NO_x sources were also divided into mobile and stationary sources. The former were used as a marker for emissions due to a diffuse

source, such as traffic. Additional SO_2 emissions corresponding to the spatial and temporal pattern of the NO traffic marker were added to provide a diffuse source of sulfur to the basin.

3.4 Observations

2002 aircraft observations indicate a broad, regional distribution of SO_2. Low altitude (<2 km pressure altitude) 2002 WP-3D flight tracks over the Pacific Ocean and the SCB colored by observed SO_2 mixing ratios are shown in Fig. 3.4A. Inland SO_2 concentrations are at least comparable to if not greater than those observed offshore and along the coast.

In contrast, in 2008, elevated SO_2 concentrations are localized offshore and along the coast. Low altitude (<2 km pressure altitude) 2008 DC-8 flight tracks colored by observed SO_2 mixing ratios are shown in Fig. 3.4B. Inland SO_2 concentrations are much lower than those observed in 2002. Measured DMS mixing ratios were less than 15 pptv in both 2002 and 2008, implying the contribution of DMS to reactive sulfur in the SCB was negligible.

3.5 Results and Discussion

For an atmospheric compound with a lifetime longer than a few hours, it is impossible to directly infer source distribution and strength from sparse measurements of its concentration. Chemical transport models can help, but, for observations obtained over a heterogeneous city such as Los Angeles, such models do not generally have sufficient resolution and transport accuracy to undertake a point-by-point comparison. Tracer-tracer correlations offer the advantage of accounting for some aspects of the transport error and are used here to compare the simulations and observations.

Offshore and near-shore sources were explicitly targeted during the 2008 ARCTAS-CARB campaign. To avoid oversampling the emissions on the west side of the basin relative to the basin-wide emissions in the analysis, an inland region of the SCB is defined using tracer-tracer correlations. This subset of the SCB, which is removed from the Los Angeles–Long Beach port complex and the neighboring refineries, is demarcated in yellow in Fig. 3.1. The strong correlation between pollutants

CO and CO_2 in the inland region of the SCB is shown in Fig. 3.5 ($R^2 = 0.87$). Linear regression, using the York et al. (2004) method that takes into account errors in both the abscissa and ordinate values, gives a slope of 1.2 x 10^{-2} moles of CO to ΔCO_2, where ΔCO_2 equals the mixing ratio of ambient CO_2 minus the mixing ratio of background CO_2. Background CO_2 in the SCB was 385 ppmv in 2008. This is consistent with the basin-wide ratio of emissions of these gases (Wunch et al., 2009), indicating the subset of the SCB is representative of the basin. The effects of the explicit targeting of marine vessels and refinery emissions in 2008 are expected to be minimal when comparing 2002 and 2008 observations obtained in this inland SCB region.

In the inland region, SO_2 and sulfate concentrations are correlated with the regional-scale pollution tracers CO and CO_2. This does not necessarily imply that the sources of CO_2 and SO_2 are colocated but simply that, over the inland area, boundary layer mixing is sufficiently fast to mix these emissions. The slopes of the correlations of SO_2 and sulfate with ΔCO_2 and ΔCO are shown in Table 3.1. Background CO_2 in the SCB was 375 ppmv in 2002 and 385 ppmv in 2008. Background CO in the SCB was 85 ppbv in 2002 and 65 ppbv in 2008. As shown in Fig. 3.6, the observed ratio of moles of SO_2 to ΔCO_2 is 1.9 x 10^{-4} and 4.4 x 10^{-5} in 2002 and 2008, respectively. The range of ΔCO_2 observed during the two campaigns is similar, suggesting the aircraft sampled a similar range of polluted air. The ratio of SO_2 to ΔCO_2 observed in 2008 is 4.3 times less than that observed in 2002.

SO_2 concentrations in the SCB are partially dependent on wind direction and speed, and variations in these factors may affect measured SO_2 concentrations. We employ the CMAQ model, coupled with tracer analysis of aircraft data, to assess the impact of meteorological differences on the 2002 and 2008 aircraft observations. Two scenarios are investigated. The 2008 CARB emissions inventory is used in both scenarios while the meteorology is varied. The 2002 meteorology and the 2008 meteorology are used in the first and second scenarios, respectively. The model output of both scenarios is sampled along the 2008 inland SCB flight tracks. The ratio of moles of SO_2 to moles of CO for the first and second scenario is 4.2 x 10^{-3} and 2.4 x 10^{-3}, respectively (Table 3.2). These ratios suggest that the 2002 meteorological conditions would result in SO_2 to CO_2 ratios 1.75 times

greater than those observed under the 2008 meteorological conditions. Thus, meteorology alone may explain 40% (1.75/4.3) of the difference between observed 2002 and 2008 SO_2 and CO_2 correlations.

Meteorology is not the only factor in the observed reduction in SO_2 concentration. As described in Section 3.3.1.2, there is a bias of 43% between the independent measurements of SO_2 in 2008 (Fig. 3.3). SO_2 concentrations measured by the Caltech CIMS instrument are, on average, 22% greater than those used in this analysis and yield an inland ratio of 5.4 x 10^{-5} moles of SO_2 to ΔCO_2. Using this ratio, the 2008 correlation is 3.5, not 4.3, times smaller than the 2002 correlation. Thus, differences in analytical methods may explain a factor of 0.8 $(4.3 - 3.5)$ difference between SO_2 and CO_2 correlations observed in 2002 and 2008.

Together meteorology and analytical uncertainty may account for as much as 60% [(1.75 + 0.8) / 4.3] of the difference between observed 2002 and 2008 SO_2 and CO_2 correlations. At least 40% of the difference, corresponding to a factor of 1.75, remains unexplained. Based on the change in spatial source distribution between 2002 and 2008, the reduction in SO_2 concentrations appears to be the result of a change in a diffuse source.

There are several such diffuse sources in the SCB, such as natural gas and transportation fuel. Natural gas, however, is not expected to be a large source of atmospheric sulfur in the SCB as natural gas in California pipelines contains no more than 17 ppm total sulfur by mass (PGE, 2009). A change in transportation fuel also appears to be an unlikely cause of the observed change in SO_2. As discussed below, ground-based measurements indicate a modest ($\leq$25%) reduction in particulate sulfate concentration. If the observed reduction in SO_2 concentration is due to a change in transportation fuel, a comparable reduction in sulfate would be expected.

Given the large reduction in measured SO_2 concentration, a similarly large decrease in sulfate concentration is expected. However, this is not seen in aircraft or ground-based measurements. In fact, aircraft observations indicate an increase in the ratio of moles of sulfate to ΔCO_2 between 2002 and 2008 from 6.6 x 10^{-6} to 2.0 x 10^{-5} (Fig. 3.7). Measurements conducted at the three IMPROVE ground sites in the SCB indicate a modest reduction in sulfate concentration between 2002 and 2008. Monthly averages of fine sulfate concentration are used to calculate annual mean

concentrations (shown in Fig. 3.8) at each of the sites as the number of measurements per month varies and day-to-day variability in sulfate concentration is smaller than monthly variability. An annual average is not included if more than two months of data are unavailable during that year (i.e., Agua Tibia site in 2006). Sulfate concentrations at the Agua Tibia site decreased 25% between 2002 and 2008 with smaller reductions (16% and 12%, respectively) at the San Gabriel and San Gorgonio Wilderness sites.

After accounting for differences in meteorology and analytical techniques, SO_2 concentrations in the SCB appear to have decreased by 40% while sulfate concentrations have not. There are several possible explanations for the modest reduction in sulfate measured at the IMPROVE sites compared to the reduction in SO_2 as measured from aircraft observations. One intriguing possibility is that there has been a substantial increase in the efficiency of conversion of SO_2 to sulfate. Possibly, changes in concentrations of other chemical species may have contributed to a change in the oxidation efficiency of SO_2 in the SCB.

Both aircraft measurements and CMAQ model simulations imply an increase in oxidation efficiency in the SCB between 2002 and 2008. Assuming all sulfur is emitted as SO_2, the percentage of SO_2 oxidized to sulfate in the SCB is calculated by dividing the ratio of sulfate to ΔCO_2 by the sum of the ratios of SO_2 and sulfate to ΔCO_2. The aircraft-observed ratios indicate 3.3% and 31% of SO_2 was oxidized in the SCB in 2002 and 2008, respectively. Results of CMAQ model simulations of seven SCB locations show a similar pattern but a smaller effect (Table 3.3). Although SO_2 concentrations decreased substantially between 2002 and 2008, an increase in the efficiency of SO_2 oxidation to sulfate may result in a smaller reduction in sulfate concentration. SO_2 that previously would have been converted to sulfate downwind of the SCB may now contribute to sulfate concentrations in the SCB.

Changes in concentrations of species such as OH, H_2O_2, and SO_2 itself may have altered the oxidation efficiency within the SCB. Between 2002 and 2008, NO_x concentration in the SCB decreased by 25%. Due to the coupling of the HO_x and NO_x cycles, this decrease is expected to result in an increase in OH and H_2O_2 concentrations. Gas-phase reaction with OH and aqueous-phase

reaction with H_2O_2, both dependent on the concentration of OH radical present in the atmosphere, are important SO_2 oxidation pathways in the SCB. Therefore, as OH concentration increases, more SO_2 is converted to sulfate. Additionally, a reduction in atmospheric SO_2 may have altered the rate of aqueous-phase sulfur oxidation by increasing the pH of cloud droplets. On dissolution, gas-phase SO_2 hydrolyzes and participates in several equilibrium reactions (Seinfeld and Pandis, 2006).

$$SO_{2\ (g)} + H_2O \rightleftharpoons SO_2 \cdot H_2O \tag{R3.6}$$

$$SO_2 \cdot H_2O \rightleftharpoons H^+ + HSO_3^- \tag{R3.7}$$

$$HSO_3^- \rightleftharpoons H^+ + SO_3^{2-} \tag{R3.8}$$

If the concentration of gas-phase SO_2 decreased, the equilibrium would shift such that H^+ concentration in the cloud droplets decreased. For a constant atmospheric concentration of oxidant, the rate of sulfur oxidation can vary by three orders of magnitude if pH changes by two units and increases with increasing pH (Martin, 1984; Martin et al., 1991).

Changes in upwind sources, such as ships, may have also affected inland sulfate concentrations. The Los Angeles–Long Beach port complex is the fifth busiest port in the world in terms of container volume (BST Associates, 2007). The worldwide average of sulfur content in marine fuels is 2.7% (27,000 ppm) by mass (Entec, 2002). Vutukuru and Dabdub (2008) performed air quality simulations of the SCB for a base year (2002) and a future year (2020). They estimated that 24.1% of total basin-wide emissions of SO_x were attributable to emissions from ocean-going vessels in 2002. In the 2020 future case, 40.5% of total basin-wide emissions were estimated to come from ocean-going vessels. The increased percentage of SO_x attributed to ships between 2002 and 2020 was due to both an anticipated increase in SO_x emissions from an increased number of ships and a decrease in SO_x emissions from land-based sources. If upwind emissions of SO_2 increase, larger sulfate concentrations can be expected downwind.

3.6 Conclusions

Ambient measurements of atmospheric SO_2 and sulfate concentrations were conducted in the Los Angeles basin in 2008. Comparison of these observations with measurements taken in 2002 indicates a large decrease in SO_2 concentration and a change in spatial distribution. Based on simulations comparing the 2002 and 2008 meteorology, meteorological differences can explain 40% of the observed difference in SO_2 concentration between the two years. Differences in analytical techniques can potentially account for up to 20% of the observed difference. Although aircraft observations indicate an increase in sulfate concentration during this time, a modest reduction is observed at IMPROVE sites in the SCB. A change in SO_2 oxidation efficiency is expected to be at least partially responsible for the difference in SO_2 and sulfate trends. Changes in sources upwind of the SCB, such as the Los Angeles–Long Beach port complex, may also be important in explaining the relatively small reduction in sulfate compared to the substantial reduction in SO_2.

3.7 Acknowledgements

K. M. S. thanks Kemal Gurer for providing meteorological inputs for CMAQ. F. P. thanks California Air Resources Board for providing meteorological and emissions inputs for CMAQ, Ying Xie, Rob Pinder, and Christopher Nolte for helpful discussions, and Naveed Near-Ansari for assistance installing CMAQ on the Caltech cluster. The numerical simulations for this research were performed on Caltech's Division of Geological and Planetary Sciences Dell cluster. The authors also wish to thank the DC-8 crew and support team. The Caltech CIMS SO_2 measurements and their interpretation were made possible with the financial support of NASA (NAG: NNX08AD29G). J. D. C. acknowledges financial support from the EPA-STAR Fellowship Program (FP916334012). A. K. acknowledges financial support from the German Research Foundation (/DFG/-Forschungsstipendium KU 2539/1-1/). M. J. C. and J. L. J. acknowledge NASA (NAG: NNX08AD39G). This work has not been formally reviewed by the EPA. The views expressed in this document are solely those of the authors and the EPA does not endorse any products or commercial services mentioned in this

publication.

Bibliography

Amelynck, C., Schoon, N., and Arijs, E.: Gas phase reactions of CF_3O^- and $CF_3O^- \cdot H_2O$ with nitric, formic, and acetic acid, International Journal of Mass Spectrometry, 203, 165–175, 2000.

Brimblecombe, P., and Spedding, D. J.: The catalytic oxidation of micromolar aqueous sulfur dioxide. 1. Oxidation in dilute solutions containing iron (III), Atmospheric Environment, 8, 937–945, 1974.

BST Associates: Trade impacts study. Prepared for Port of Los Angeles, Port of Long Beach and Almeda Corridor Transportation Authority, 2007. (Available at http://www.portoflosangeles.org/DOC/REPORT_ACTA_Trade_Impact_Study.pdf)

Byun, D. W., and Ching, J. K. S.: Science algorithms of the EPA Models-3 Community Multiscale Air Quality (CMAQ) modeling system, U.S. Environmental Protection Agency, Washington, D.C., EPA/600/R-99/030, 1998.

California Air Resources Board (CARB): Air Quality Data Statistics—1973 to 2008, 2008a. (Available at http://www.arb.ca.gov/adam)

California Air Resources Board (CARB): California Emission Inventory Data Almanac, technical report, 2008b. (Available at http://www.arb.ca.gov/app/emsinv/emssumcat.php)

Calvert, J. G., Lazrus, A., Kok, G. L., Heikes, B. G., Walega, J. G., Lind, J., and Cantrell, C. A.: Chemical mechanisms of acid generation in the troposphere, Nature, 317, 27–35, 1985.

Carter, W. P. L: The SAPRC-99 chemical mechanism and updated VOC reactivity scales, Final Report, California Air Resources Board Contracts, 92-329, 2000.

Cass, G. R.: On the relationship between sulfate air quality and visibility with examples in Los Angeles, Atmospheric Environment, 13, 1069–1084, 1979.

Chang, S. G., Toossi, R., and Novakov, T.: The importance of soot particles and nitrous acid in oxidizing SO_2 in atmospheric aqueous droplets, Atmospheric Environment, 15, 1287–1292, 1981.

Crounse, J. D., McKinney, K. A., Kwan, A. J., and Wennberg, P. O.: Measurement of gas-phase hydroperoxides by chemical ionization mass spectrometry, Analytical Chemistry, 78, 6726–6732, 2006.

Davis, D. D., Ravishankara, A. R., and Fischer, S.: SO_2 oxidation via the hydroxyl radical: Atmospheric fate of HSO_x radicals, Geophysical Research Letters, 6, 113–116, 1979.

DeBell, L. J., Gebhart, K. A., Hand, J. L., Malm, W. C., Pitchford, M. L., Schichtel, B. A., and White, W. H.: Spatial and seasonal patterns and temporal variability of haze and its constituents in the United States Report IV, Interagency Monitoring of Protected Visual Environments Report, 2006.

DeCarlo, P. F., Kimmel, J. R., Trimborn, A., Northway, M. J., Jayne, J. T., Aiken, A. C., Gonin, M., Fuhrer, K., Horvath, T., Docherty, K. S., Worsnop, D. R., and Jimenez, J. L.: Field-deployable, high-resolution, time-of-flight aerosol mass spectrometer, Analytical Chemistry, 78, 8281–8289, doi:10.1021/AC061249N, 2006.

Dominguez, G., Jackson, T., Brothers, L., Barnett, B., Nguyen, B., and Thiemens, M. H.: Discovery and measurement of an isotopically distinct source of sulfate in Earth's atmosphere, Proceedings of the National Academy of Sciences of the United States of America, 105, 12769–12773, doi:10.1073/PNAS.0805255105, 2008.

Eatough, D. J., Arthur, R. J., Eatough, N. L., Hill, M. W., Mangelson, N. F., Richter, B. E., Hansen, L. D., and Cooper, J. A.: Rapid conversion of SO_2(g) to sulfate in a fog bank, Environmental Science & Technology, 18, 855–859, 1984.

Eatough, D. J., Caka, F. M., and Farber, R. J.: The conversion of SO_2 to sulfate in the atmosphere, Israel Journal of Chemistry, 34, 301–314, 1994.

Eldering, A., and Cass, G. R.: Source-oriented model for air pollutant effects on visibility, Journal of Geophysical Research—Atmospheres, 101, 19343–19369, 1996.

Entec UK Limited: European Commission: Quantification of emissions from ships associated with ship movements between ports in the European Community. Final Report, London, UK, 2002.

Erickson, R. E., Yates, L. M., Clark, R. L., and McEwen, D.: Reaction of sulfur dioxide with ozone in water and its possible atmospheric significance, Atmospheric Environment, 11, 813–817, 1977.

Forster, P., Ramaswamy, V., Artaxo, P., Berntsen, T., Betts, R., Fahey, D. W., Haywood, J., Lean, J., Lowe, D. C., Myhre, G., Nganga, J., Prinn, R., Raga, G., Schulz, M., and Van Dorland, R.: Changes in atmospheric constituents and in radiative forcing, in Climate Change 2007: The Physical Science Basis. Contribution of Working Group I to the Fourth Assessment Report of the Intergovernmental Panel on Climate Change, edited by Solomon, S., Qin, D., Manning, M., Chen, Z., Marquis, M., Averyt, K. B., Tignor, M., and Miller, H.L., Cambridge University Press, Cambridge, United Kingdom and New York, NY, USA, 2007.

Grell, G. A., Dudhia, J., and Stauffer, D. R.: A description of the fifth-generation Penn State/NCAR Mesoscale Model (MM5), NCAR Technical Note, 398, 122, 1994.

Griffith, D. W. T.: Synthetic calibration and quantitative analysis of gas-phase FT-IR spectra, Applied Spectroscopy, 50, 59–70, 1996.

Hoffmann, M. R., and Edwards, J. O.: Kinetics of oxidation of sulfite by hydrogen peroxide in acidic solution, Journal of Physical Chemistry, 79, 2096–2098, 1975.

Huey, L. G., Tanner, D. J., Slusher, D. L., Dibb, J. E., Arimoto, R., Chen, G., Davis, D., Buhr, M. P., Nowak, J. B., Mauldin, R. L., Eisele, F. L., and Kosciuch, E.: CIMS measurements of HNO_3 and SO_2 at the South Pole during ISCAT 2000, Atmospheric Environment, 38, 5411–5421, doi:10.1016/J.ATMOSENV.2004.04.037, 2004.

Huey, L. G., Villalta, P. W., Dunlea, E. J., Hanson, D. R., and Howard, C. J.: Reactions of CF_3O^- with atmospheric trace gases, Journal of Physical Chemistry, 100, 190–194, 1996.

Huss, A., Lim, P. K., and Eckert, C. A.: Oxidation of aqueous sulfur dioxide. 1. Homogeneous manganese(II) and iron(III) catalysis at low pH, Journal of Physical Chemistry, 86, 4224–4228, 1982.

Ibusuki, T., and Barnes, H. M.: Manganese(II) catalyzed sulfur dioxide oxidation in aqueous solution at environmental concentrations, Atmospheric Environment, 18, 145–151, 1984.

Jacob, D. J., Crawford, J. H., Maring, H., Clarke, A. D., Dibb, J. E., Ferrare, R. A., Hostetler, C. A., Russell, P. B., Singh, H. B., Thompson, A. M., Shaw, G. E., McCauley, E., Pederson, J. R., and Fisher, J. A.: The ARCTAS aircraft mission: design and execution, Atmospheric Chemistry and Physics Discussions, 9, 17073–17123, 2009

Jayne, J. T., Poschl, U., Chen, Y. M., Dai, D., Molina, L. T., Worsnop, D. R., Kolb, C. E., and Molina, M. J.: Pressure and temperature dependence of the gas-phase reaction of SO_3 with H_2O and the heterogeneous reaction of SO_3 with H_2O/H_2SO_4 surfaces, Journal of Physical Chemistry A, 101, 10000–10011, 1997.

Kim, B. M., Teffera, S., and Zeldin, M. D.: Characterization of $PM_{2.5}$ and PM_{10} in the South Coast Air Basin of Southern California: Part 1—Spatial variations, Journal of the Air & Waste Management Association, 50, 2034–2044, 2000.

Malm, W. C., Gebhart, K. A., Latimer, D. A., Cahill, T. A., Eldred, R. A., Pielke, R., Stocker, R., and Watson, J.: National Park Service Report on the Winter Haze Intensive Tracer Experiment, Final Report, 1989.

Malm, W. C., Sisler, J. F., Pitchford, M. L., Scruggs, M., Ames, R., Copeland, S., Gebhart, K. A., and Day, D. E.: IMPROVE (Interagency Monitoring of Protected Visual Environments): Spatial and seasonal patterns and temporal variability of haze and its constituents in the United States: Report III, CIRA Report ISSN: 0737-5352-47, Colorado State University, Fort Collins, 2000.

Martin, L. R., Kinetic studies of sulfite oxidation in aqueous solutions, in: SO_2, NO, and NO_2

Oxidation Mechanisms: Atmospheric Consideration, Acid Precipitation Series, edited by Teasley, J. I., Butterworth, Stoneham, MA, 1984.

Martin, L. R., Hill, M. W., Tai, A. F., and Good, T. W.: The iron catalyzed oxidation of sulfur(IV) in aqueous solution: Differing effects of organics at high and low pH, Journal of Geophysical Research—Atmospheres, 96, 3085–3097, 1991.

Morokuma, K., and Muguruma, C.: Ab-Initio molecular orbital study of the mechanism of the gas phase reaction $SO_3 + H_2O$: Importance of the second water molecule, Journal of the American Chemical Society, 116, 10316–10317, 1994.

Orsini, D. A., Ma, Y. L., Sullivan, A., Sierau, B., Baumann, K., and Weber, R. J.: Refinements to the particle-into-liquid sampler (PILS) for ground and airborne measurements of water soluble aerosol composition, Atmospheric Environment, 37, 1243–1259, doi:10.1016/S1352-2310(02)010150-4, 2003.

Pacific Gas and Electric Company (PGE): Gas Rule No. 21, Section C, PGE Tariff Book, 2009. (Available at http://www.pge.com/tariffs/tm2/pdf/GAS_RULES_21.pdf)

Parrish, D. D., Kondo, Y., Cooper, O. R., Brock, C. A., Jaffe, D. A., Trainer, M., Ogawa, T., Hubler, G., and Fehsenfeld, F. C.: Intercontinental Transport and Chemical Transformation 2002 (ITCT 2K2) and Pacific Exploration of Asian Continental Emission (PEACE) experiments: An overview of the 2002 winter and spring intensives, Journal of Geophysical Research—Atmospheres, 109, 13, D23S01, doi:10.1029/2004JD004980, 2004a.

Parrish, D. D., Ryerson, T. B., Holloway, J. S., Neuman, J. A., Roberts, J. M., Williams, J., Stroud, C. A., Frost, G. J., Trainer, M., Hubler, G., Fehsenfeld, F. C., Flocke, F., and Weinheimer, A. J.: Fraction and composition of NO_y transported in air masses lofted from the North American continental boundary layer, Journal of Geophysical Research—Atmospheres, 109, D09302, doi:10.1029/2003JD004226, 2004b.

Paulot, F., Crounse, J. D., Kjaergaard, H. G., Kroll, J. H., Seinfeld, J. H., and Wennberg, P.

O.: Isoprene photooxidation: New insights into the production of acids and organic nitrates, Atmospheric Chemistry and Physics, 9, 1479–1501, 2009.

Penkett, S. A., Jones, B. M. R., Brice, K. A., and Eggleton, A. E. J.: The importance of atmospheric ozone and hydrogen peroxide in oxidising sulphur dioxide in cloud and rainwater, Atmospheric Environment, 41, 154–168, 2007.

Pope, C. A., Burnett, R. T., Thun, M. J., Calle, E. E., Krewski, D., Ito, K., and Thurston, G. D.: Lung cancer, cardiopulmonary mortality, and long-term exposure to fine particulate air pollution, Journal of the American Medical Association, 287, 1132–1141, 2002.

Ramanathan, V., Crutzen, P. J., Kiehl, J. T., and Rosenfeld, D.: Atmosphere—Aerosols, climate, and the hydrological cycle, Science, 294, 2119–2124, 2001.

Rothman, L. S., Jacquemart, D., Barbe, A., Benner, D. C., Birk, M., Brown, L. R., Carleer, M. R., Chackerian, C., Chance, K., Coudert, L. H., Dana, V., Devi, V. M., Flaud, J. M., Gamache, R. R., Goldman, A., Hartmann, J. M., Jucks, K. W., Maki, A. G., Mandin, J. Y., Massie, S. T., Orphal, J., Perrin, A., Rinsland, C. P., Smith, M. A. H., Tennyson, J., Tolchenov, R. N., Toth, R. A., Vander Auwera, J., Varanasi, P., and Wagner, G.: The HITRAN 2004 molecular spectroscopic database, Journal of Quantitative Spectroscopy & Radiative Transfer, 96, 139–204, 2005.

Ryerson, T. B., Buhr, M. P., Frost, G. J., Goldan, P. D., Holloway, J. S., Hubler, G., Jobson, B. T., Kuster, W. C., McKeen, S. A., Parrish, D. D., Roberts, J. M., Sueper, D. T., Trainer, M., Williams, J., and Fehsenfeld, F. C.: Emissions lifetimes and ozone formation in power plant plumes, Journal of Geophysical Research—Atmospheres, 103, 22569–22583, 1998.

Sachse, G. W., Hill, G. F., Wade, L. O., and Perry, M. G.: Fast-response, high-precision Carbon Monoxide Sensor using a tunable diode laser absorption technique, Journal of Geophysical Research—Atmospheres, 92, 2071–2081, 1987.

Scheuer, E., Talbot, R. W., Dibb, J. E., Seid, G. K., DeBell, L., and Lefer, B.: Seasonal distributions

of fine aerosol sulfate in the North American Arctic basin during TOPSE, Journal of Geophysical Research—Atmospheres, 108, 8370, doi:10.1029/2001JD001364, 2003.

Seinfeld, J. H., and Pandis, S. N.: Atmospheric Chemistry and Physics, 2nd ed., John Wiley & Sons, 2006.

Spencer, K. M., McCabe, D. C., Crounse, J. D., Olson, J. R., Crawford, J. H., Weinheimer, A. J., Knapp, D. J., Montzka, D. D., Cantrell, C. A., Hornbrook, R. S., Mauldin, R. L., and Wennberg, P. O.: Inferring ozone production in an urban atmosphere using measurements of peroxynitric acid, Atmospheric Chemistry and Physics, 9, 3697–3707, 2009.

Stockwell, W. R., and Calvert, J. G.: The Mechanism of the HO$-$$SO_2$ Reaction, Atmospheric Environment, 17, 2231–2235, 1983.

Vay, S. A., Woo, J. H., Anderson, B. E., Thornhill, K. L., Blake, D. R., Westberg, D. J., Kiley, C. M., Avery, M. A., Sachse, G. W., Streets, D. G., Tsutsumi, Y., and Nolf, S. R.: Influence of regional-scale anthropogenic emissions on CO_2 distributions over the western North Pacific, Journal of Geophysical Research—Atmospheres, 108, 8801, doi:10.1029/2002JD003094, 2003.

Vutukuru, S., and Dabdub, D.: Modeling the effects of ship emissions on coastal air quality: A case study of southern California, Atmospheric Environment, 42, 3751–3764, doi:10.1016/J.ATMOSENV.2007.12.073, 2008.

Weber, R. J., Orsini, D., Daun, Y., Lee, Y. N., Klotz, P., and Brechtel, F.: A particle-into-liquid collector for rapid measurements of aerosol chemical composition, Aerosol Sci. Tech., 35, 718–727, 2001.

Wunch, D., Wennberg, P. O., Toon, G. C., Keppel-Aleks, G., and Yavin, Y. G.: Emissions of greenhouse gases from a North American megacity, Geophysical Research Letters, 36, L15810, doi:10.1029/2009GL039825, 2009.

York, D., Evensen, N. M., Martinez, M. L., and Delgado, J. D.: Unified equations for the slope,

intercept, and standard errors of the best straight line, American Journal of Physics, 72, 367–375, doi:10.1119/1.1632486, 2004.

	SO_2		Sulfate	
	Slope	R^2	Slope	R^2
2002				
ΔCO	9.3 x 10^{-3}	0.72	3.5 x 10^{-4}	0.63
ΔCO_2	1.9 x 10^{-4}	0.80	6.6 x 10^{-6}	0.67
2008				
ΔCO	3.1 x 10^{-3}	0.78	1.5 x 10^{-3}	0.65
ΔCO_2	4.4 x 10^{-5}	0.72	2.2 x 10^{-5}	0.76

Table 3.1: Slopes of correlations and R^2 values of SO_2 and sulfate with regional-scale pollution tracers CO and CO_2 as observed in 2002 and 2008.

Meteorology / Emissions	SO_2 / CO (mol / mol)
2002 / 2008	4.2 x 10^{-3}
2008 / 2008	2.4 x 10^{-3}

Table 3.2: Slopes of correlations between SO_2 and regional-scale pollution tracer CO as predicted using the EPA CMAQ model.

	% decrease from 2002 to 2008		% of SO_2 oxidized to sulfate	
	SO_2	Sulfate[a]	2002	2008
Agua Tibia	77	47	41	62
Anaheim	71	27	13	27
Long Beach	26	14	10	11
Los Angeles	83	31	10	30
Riverside	79	50	20	37
San Gabriel	84	43	15	39
San Gorgonio	69	35	30	47

[a]Excluding primary sulfate emissions.

Table 3.3: Results of CMAQ simulations of 2000 and 2008 SO_2 and sulfate concentrations at seven locations in the SCB. Average 2002 and 2008 SO_2 and sulfate concentrations between 09:00 and 17:00 were calculated. The percentage of SO_2 oxidized to sulfate ([sulfate / sum of SO_2 and sulfate] x 100, excluding primary sulfate emissions) in 2002 and in 2008 are shown. Simulated SO_2 concentrations decreased substantially between 2002 and 2008. However, a larger percentage of SO_2 was oxidized to sulfate in the SCB in 2008 compared to 2002.

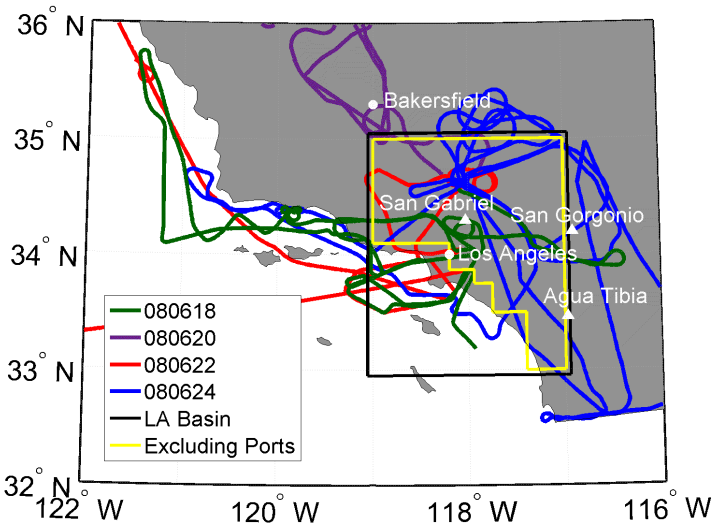

Figure 3.1: 2008 DC-8 flight tracks of the ARCTAS-CARB flights. The South Coast Air Basin (SCB) is demarcated in black. To avoid oversampling the emissions on the west side of the basin relative to the basin-wide emissions in the analysis, a subregion within the SCB was selected that excludes industrial ports. This region is outlined in yellow. The Agua Tibia, San Gabriel, and San Gorgonio Wilderness IMPROVE sites are marked by triangles.

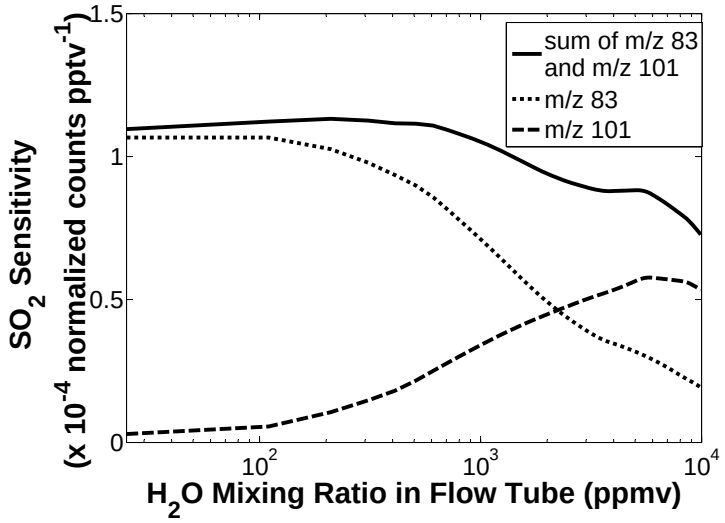

Figure 3.2: Sensitivity curves for m/z 83 (dotted line), m/z 101 (dashed line), and the sum of the two (solid line) as a function of H_2O mixing ratio in the flow tube. The sensitivity curve of the sum of m/z 83 and m/z 101 is used to calculate the concentration of SO_2.

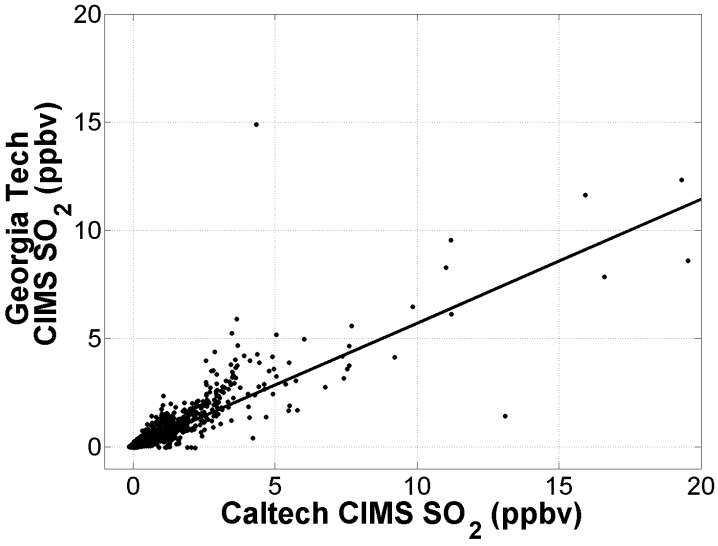

Figure 3.3: Two independent measurements of SO_2 concentration during the ARCTAS-CARB campaign: Georgia Tech CIMS instrument using reagent ion SF_6^- and Caltech CIMS instrument using reagent ion CF_3O^-. The relationship between the two independent measurements is linear, although the Caltech measurement is, on average, 43% higher than the Georgia Tech measurement. The slope of the linear regression is 0.57, and the intercept is 6 pptv. $R^2 = 0.74$. The concentration of SO_2 used in this analysis is the mean of the concentrations determined by the two independent measurements.

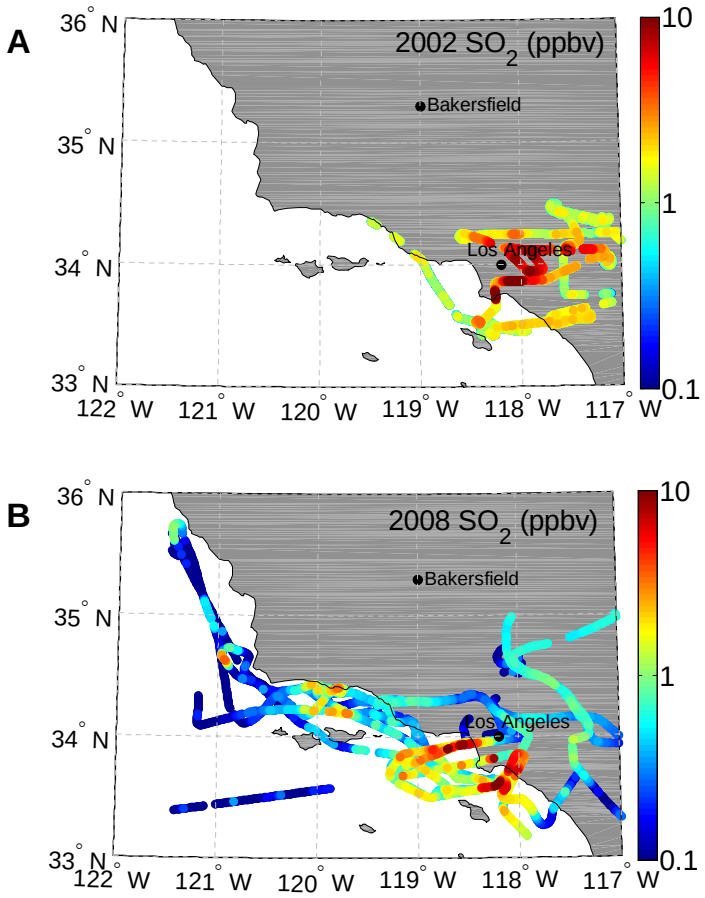

Figure 3.4: 2002 WP-3D (A) and 2008 DC-8 (B) flight tracks over the Pacific Ocean and SCB colored by SO_2. Data presented are those obtained at pressure altitudes less than 2 km. Broad, regional sulfur sources were observed in 2002. In 2008, localized sources were observed offshore and along the coast of the SCB.

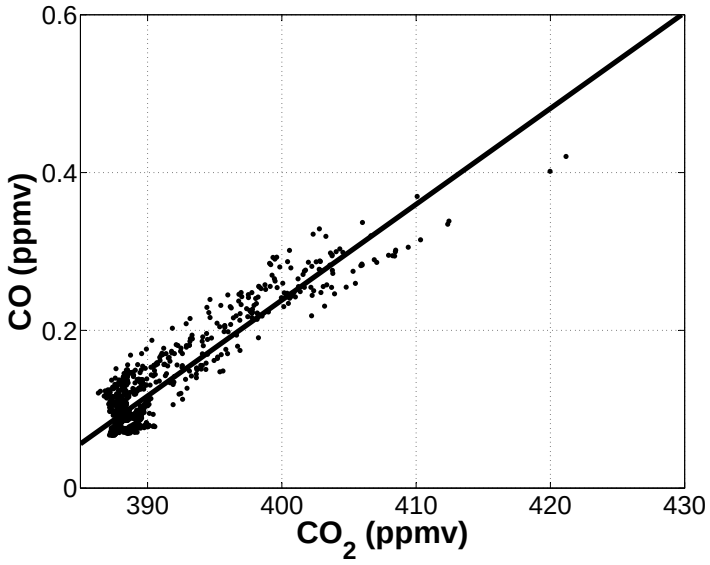

Figure 3.5: Observed CO versus observed CO_2 for points within the inland region of the SCB (Fig. 3.1, yellow box) in 2008. Data influenced by wildfires are excluded. The slope of the linear regression is 0.012. $R^2 = 0.87$. The relationship between CO and CO_2 demonstrates the strong correlation between these pollutants in the inland SCB.

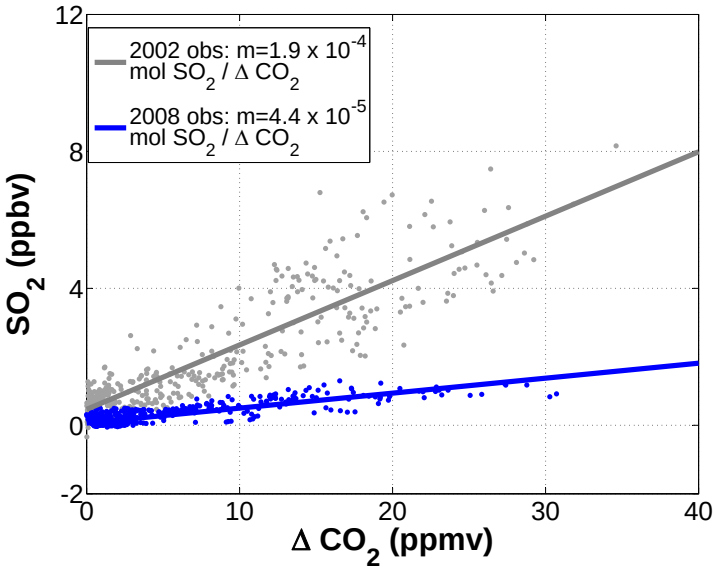

Figure 3.6: Observed moles of SO_2 versus ΔCO_2, where ΔCO_2 equals the mixing ratio of ambient CO_2 minus the mixing ratio of background CO_2. Background CO_2 in the SCB was 375 ppmv in 2002 and 385 ppmv in 2008. Data shown are those in the inland region of the SCB (Fig. 3.1, yellow box). The 2002 observations are shown in gray. The 2008 observations are shown in blue. The observed correlation of SO_2 and ΔCO_2 in 2008 was 4.3 times lower than that observed in 2002.

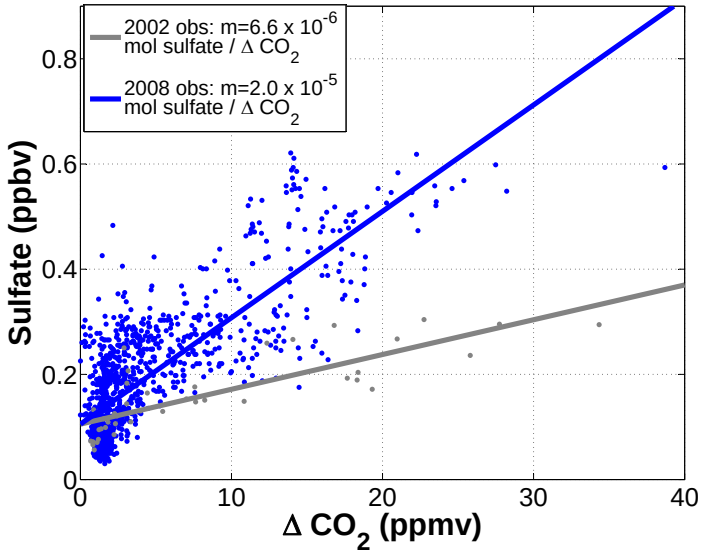

Figure 3.7: Observed moles of sulfate versus ΔCO_2, where ΔCO_2 equals the mixing ratio of ambient CO_2 minus the mixing ratio of background CO_2. Background CO_2 in the SCB was 375 ppmv in 2002 and 385 ppmv in 2008. The data shown are those in the inland region of the SCB (Fig. 3.1, yellow box). The 2002 observations are shown in gray. The 2008 observations are shown in blue.

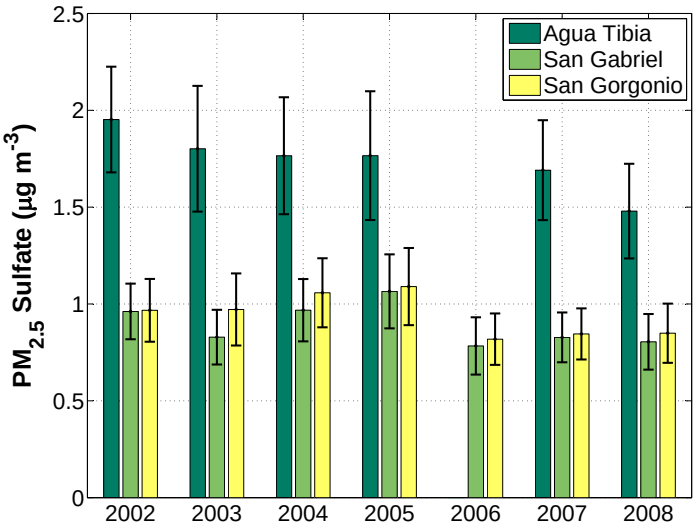

Figure 3.8: Annual averages of $PM_{2.5}$ sulfate concentrations at the Agua Tibia, San Gabriel, and San Gorgonio Wilderness IMPROVE sites. Sulfate concentrations decreased 25%, 16%, and 12%, respectively, between 2002 and 2008. The elevation of the Agua Tibia site is 507 m while the elevation of the San Gabriel and San Gorgonio Wilderness sites is greater than 1700 m. This difference in elevation may partially explain the higher $PM_{2.5}$ sulfate concentrations measured at the Agua Tibia site.

Chapter 4

Quantification of Hydroxyacetone and Glycolaldehyde Using Chemical Ionization Mass Spectrometry

4.1 Abstract

Chemical ionization mass spectrometry (CIMS) enables online, fast, in situ detection and quantification of hydroxyacetone and glycolaldehyde. Two different CIMS approaches are demonstrated employing the strengths of single quadrupole mass spectrometry and triple quadrupole (tandem) mass spectrometry. Both methods are capable of the measurement of hydroxyacetone, an analyte with minimal known isobaric interferences. Tandem mass spectrometry provides direct separation of the isobaric compounds glycolaldehyde and acetic acid using distinct, collision-induced dissociation daughter ions. Measurement of hydroxyacetone and glycolaldehyde by these methods was demonstrated during the ARCTAS-CARB 2008 campaign and the BEARPEX 2009 campaign. Enhancement ratios of these compounds in ambient biomass burning plumes are reported for the ARCTAS-CARB campaign. BEARPEX observations are compared to simple box model predictions of biogenic volatile organic compound oxidation at the site.

4.2 Introduction

Because of their reactivity, carbonyl compounds make a large contribution to the production of free radicals and photooxidants in the atmosphere. Hydroxyacetone ($H_3CC(O)CH_2OH$) and glycolaldehyde ($HC(O)CH_2OH$) have both biogenic and biomass burning sources. Both species are important oxidation products of isoprene (2-methyl-1,3-butadiene), and glycolaldehyde is also produced during the oxidation of 2-methyl-3-buten-2-ol (MBO). Isoprene is produced by deciduous plants and is the single largest source of nonmethane hydrocarbon in the atmosphere (Guenther et al., 1995) while MBO is emitted in large quantities from several species of pine (Goldan et al., 1993; Harley et al., 1998). Isoprene undergoes photooxidation to produce methyl vinyl ketone (MVK) and methacrolein (MACR) (Tuazon and Atkinson, 1990a; Paulson et al., 1992). MVK and MACR are further photooxidized to produce second-generation isoprene photooxidation products glycolaldehyde, hydroxyacetone, methylglyoxal ($H_3CC(O)CH(O)$), and formaldehyde (CH_2O) (Tuazon and Atkinson, 1989, 1990b). Recent studies also suggest additional prompt sources of hydroxyacetone

and glycolaldehyde during the isomerization of alkoxyradicals formed from isoprene photooxidation (Dibble, 2004a,b; Paulot et al., 2009a; Galloway et al., 2011). Hydroxyacetone and glycolaldehyde are also emitted during biomass burning. Christian et al. (2003) quantified hydroxyacetone and glycolaldehyde in laboratory fires of Indonesian and African fuels, and Bertschi et al. (2003) observed glycolaldehyde in emissions of laboratory fires of downed logs, duff, and organic soils.

Hydroxyacetone and glycolaldehyde are precursors of other atmospherically relevant species. Major products of hydroxyacetone and glycolaldehyde photooxidation are methylglyoxal and glyoxal (OCHCHO), respectively (Grosjean et al., 1993; Niki et al., 1987). Additionally, Butkovskaya et al. (2006a,b) found oxidation of hydroxyacetone and glycolaldehyde by OH yields formic acid while OH oxidation of hydroxyacetone also produces acetic acid. Oxidation products of biogenic volatile organic compounds have been shown to play a significant role in tropospheric ozone production (Chameides et al., 1988; Atkinson and Arey, 2003) and formation of secondary organic aerosol (Kroll et al., 2006).

Previous measurements of hydroxyacetone and glycolaldehyde concentrations have been made using a range of analytical techniques. The most common of these involve ambient sample collection, derivatization with a chemical agent, separation of compounds, and detection by HPLC, GC-MS, or GC-FID (Lee et al., 1993, 1995; Zhou et al., 2009; Moortgat et al., 2002; Spaulding et al., 2003; Matsunaga et al., 2003). Two shortcomings of these techniques are the intensive sample processing required and the time lag between sample collection and concentration measurement. In contrast, both single quadrupole and triple quadrupole (tandem) chemical ionization mass spectrometry enable online, fast, in situ measurements with no sample processing. In these techniques, the ambient sample enters the instrument directly and reaches the detector in less than one second, enabling immediate detection of these compounds. The Caltech single quadrupole and tandem chemical ionization mass spectrometers are equally capable of quantifying hydroxyacetone, an analyte with minimal known isobaric interferences. The Caltech tandem chemical ionization mass spectrometer enables direct separation of mass analogues glycolaldehyde and acetic acid.

We present in situ measurements of hydroxyacetone and glycolaldehyde in the boundary layer

of California and at a tower site approximately 80 km northeast of Sacramento, CA. The first set of measurements was made in June of 2008 from the NASA DC-8 aircraft platform using the Caltech single quadrupole chemical ionization mass spectrometry (CIMS) instrument during the California portion of the NASA-CARB Arctic Research of the Composition of the Troposphere from Aircraft and Satellites (ARCTAS-CARB) field experiment. The four ARCTAS-CARB flights included in this study (18, 20, 22, and 26 June) occurred during daytime hours. Enhancement ratios of hydroxyacetone and glycolaldehyde in biomass burning plumes are presented and compared to literature values for laboratory fire data.

The second set of measurements was made during the Biosphere Effects on Aerosols and Photochemistry Experiment (BEARPEX) 2009 field experiment from 28 June to 20 July using the Caltech tandem CIMS instrument. The site is a ponderosa pine plantation (38°53'42.9" N, 120°37'57.9" W, elevation 1315 m), located near the University of California's Blodgett Forest Research Station, on the western slope of the Sierra Nevada. The site is approximately five hours downwind of Sacramento and has been described in detail previously by Goldstein et al. (2000) and Dreyfus (2002). The measurements presented here were conducted from the top platform of the north tower; the instrument inlet was located 17.8 m above the ground. Concentrations of hydroxyacetone and glycolaldehyde are compared to results from a simple box model used to estimate the contribution of biogenic sources to the budget of glycolaldehyde and hydroxyacetone at the site.

4.3 Instrumentation

4.3.1 Instrument Description

Negative ion chemistry of CF_3O^- has been shown to provide sensitive detection of many atmospheric trace gases (Huey et al., 1996; Amelynck et al., 2000a,b; Crounse et al., 2006; Spencer et al., 2009; Paulot et al., 2009b; St. Clair et al., 2010) and was exploited in this work to detect hydroxyacetone, glycolaldehyde, and acetic acid. The use of CF_3O^- to detect hydroxyacetone and glycolaldehyde was introduced briefly by Paulot et al. (2009a) and Chan et al. (2009) and is described in detail

here. Hydroxyacetone and glycolaldehyde react with CF_3O^- via clustering between the reagent ion and the analyte through reactions R4.1 and R4.2, respectively. Acetic acid reacts with CF_3O^- via fluoride ion transfer through reaction R4.3 and clustering through reaction R4.4, providing two distinct ion signals. Reactions R4.1 – R4.4 are complicated by competing reactions with CF_3O^- water cluster ($CF_3O^- \cdot H_2O$).

$$CF_3O^- + H_3CC(O)CH_2OH \rightarrow CF_3O^- \cdot H_3CC(O)CH_2OH \ (m/z\ 159) \tag{R4.1}$$

$$CF_3O^- + HC(O)CH_2OH \rightarrow CF_3O^- \cdot HC(O)CH_2OH \ \ (m/z\ 145) \tag{R4.2}$$

$$CF_3O^- + H_3CC(O)OH \rightarrow H_3CC(O)O^- \cdot HF \ \ (m/z\ 79) + CF_2O \tag{R4.3}$$

$$CF_3O^- + H_3CC(O)OH \rightarrow CF_3O^- \cdot H_3CC(O)OH \ \ (m/z\ 145) \tag{R4.4}$$

Hydroxyacetone and glycolaldehyde measurements were made using the Caltech single quadrupole CIMS instrument and the Caltech tandem CIMS instrument. The Caltech single quadrupole CIMS instrument consists of a flow tube controlled at 35 hPa total pressure, where a reagent ion, CF_3O^-, interacts with ambient air diluted 1:4 with ultra high purity N_2. Ions are sampled from the flow tube into a quadrupole mass filter and detected with a channel electron multipler. Each mass-to-charge ratio is observed for ∼0.5 seconds. Hydroxyacetone, glycolaldehyde, and acetic acid masses were monitored once every ∼15 seconds. As in the Caltech single quadrupole CIMS instrument, the flow tube of the Caltech tandem CIMS instrument is maintained at 35 hPa total pressure. During the BEARPEX campaign, ambient air was diluted 1:7 with liquid nitrogen boil off. The Caltech tandem CIMS instrument contains three quadrupoles. The first quadrupole filters ions for a specific mass-to-charge ratio. These ions then enter the second quadrupole, which serves as a collision-induced dissociation (CID) chamber. The pressure in this quadrupole is maintained at 2.7 x 10^{-3} hPa N_2.

Ions that reach this chamber collide with N_2 molecules and fragment into daughter ions. The third quadrupole selects for a specific daughter ion. Each mass-to-charge ratio is observed for ∼1 second. Hydroxyacetone, glycolaldehyde, and acetic acid masses were monitored once every ∼25 seconds. Further details on the Caltech single quadrupole and tandem CIMS instruments are given in Crounse et al. (2006) and St. Clair et al. (2010), respectively.

4.3.2 Calibration and Sensitivity

Due to differences in the reactivity of the analyte with CF_3O^- and $CF_3O^- \cdot H_2O$, the sensitivity of the Caltech CIMS instrumentation to the ion products of reactions R4.1–R4.4 varies with the mixing ratio of water vapor present in the flow tube. H_2O can also displace or hydrolyze the analyte anion. The dependence of instrument sensitivity on water vapor mixing ratio was quantified during laboratory calibrations, in which a known quantity of analyte was added to the flow tube. The ion signal was determined as a function of humidity to obtain a water-dependent sensitivity curve. In all calibrations, mass flow controllers were used to control the flow tube humidity by adjusting the ratio of moist N_2 to dry N_2. Humidity was quantified by Fourier Transform Infrared (FTIR) spectroscopy using HITRAN line lists (Rothman et al., 2005) and the nonlinear fitting software NLM4 developed by Griffith (1996). All analyte sensitivities were corrected for background signals.

For calibrations, hydroxyacetone and glycolaldehyde standards were prepared by serial dilution, and an acetic acid permeation tube was used. Gas-phase hydroxyacetone was produced by flowing dry N_2 over commercially available, 95% pure hydroxyacetone (Alfa Aesar) into a 150 L Teflon bag. Additional dry N_2 was added to the bag such that the final concentration of hydroxyacetone was 150 ppmv. Initially, the hydroxyacetone concentration was determined by both FTIR absorption (Orlando et al., 1999) and quantification of the mass loss of the liquid. These methods agreed within 25%; the concentration determined by mass loss was higher than that determined by FTIR absorption. In subsequent calibration experiments, hydroxyacetone concentration was determined by mass loss alone as the FTIR absorption instrument was dedicated to the determination of water vapor concentration. 150 mL from the 150 L bag were quantitatively transferred to a 400 L Teflon

bag. A known quantity of dry N_2 was added such that the concentration of hydroxyacetone was 50 ppbv. Similarly, gas-phase glycolaldehyde was transferred to a 100 L Teflon bag by flowing dry N_2 over commercially available glycolaldehyde dimer (Fluka Analytical) while gently heating the compound. Additional dry N_2 was added to the bag such that the concentration of glycolaldehyde was 100 ppmv. Similarly to hydroxyacetone, the glycolaldehyde concentration was determined by both FTIR absorption (Tuazon and Atkinson, 1989) and quantification of the mass loss of the solid. These methods agreed within 45%; the concentration determined by mass loss was higher than that determined by FTIR absorption. Glycolaldehyde concentration in subsequent experiments was determined by mass loss alone. 300 mL from the 100 L bag were quantitatively transferred to a 400 L Teflon bag. A known quantity of dry N_2 was added such that the concentration of glycolaldehyde was 75 ppbv. A ^{13}C isotopically labeled acetic acid standard was used. The acetic acid evolved from a permeation tube held at a constant temperature (Washenfelder et al., 2003), and the permeation rate was determined by mass loss.

Calibrations of hydroxyacetone, glycolaldehyde, and acetic acid were conducted separately, but the method was similar for all calibrations. A known quantity of analyte from the standards discussed above was combined with water vapor and N_2 dilution gas in the instrument flow tube. The CIMS instrument signal was monitored as a function of water vapor in the flow tube to develop the instrument sensitivity curve. The sensitivity of the single quadrupole CIMS instrument to the cluster channel of hydroxyacetone (m/z 159), the cluster channel of glycolaldehyde (m/z 145), the fluoride transfer channel of acetic acid (m/z 79), and the cluster channel of acetic acid (m/z 145) is shown in red, green, blue, and black, respectively, in Fig. 4.1. The sensitivity of the tandem CIMS instrument to the hydroxyacetone daughter ion (m159m85), glycolaldehyde daughter ion (m145m85), acetic acid fluoride transfer daughter ion (m79m59), and acetic acid cluster daughter ion (m145m79) is shown in red, green, blue, and black, respectively, in Fig. 4.2. Daughter ions produced in the CID chamber of the Caltech tandem CIMS instrument are discussed below in Section 4.4.2. Sensitivity is expressed in ion counts, normalized by the ion counts of the ^{13}C isotope of the reagent ion and its one-water cluster ($^{13}CF_3O^-$ and $^{13}CF_3O^- \cdot H_2O$), per pptv of analyte. Daughter ions m86m86, m104m86,

and m104m104 of the reagent ions are used in normalization of the tandem CIMS instrument ion counts.

Postmission laboratory calibrations for hydroxyacetone, glycolaldehyde, and acetic acid were conducted for both the single quadrupole CIMS instrument and the tandem CIMS instrument. During the ARCTAS-CARB flights and the BEARPEX experiment, isotopically labeled acetic acid from the permeation tube was periodically added to the flow tube of the CIMS instruments to quantify the instrument sensitivity. The sensitivity of the single quadrupole CIMS instrument to acetic acid during the ARCTAS-CARB campaign was comparable to that of postmission laboratory calibrations. The consistent sensitivity of the tandem CIMS instrument was similarly confirmed during the BEARPEX campaign and postmission laboratory calibrations.

In the absence of hydroxyacetone, glycolaldehyde, and acetic acid, ion signals at m/z 159, m/z 145, and m/z 79 are nonzero, and these background signals must be accounted for in the data analysis. Background signals were measured during flight by periodically passing ambient air through a filter consisting of alumina pellets coated with palladium and nylon wool coated with sodium bicarbonate, quantitatively removing hydroxyacetone, glycolaldehyde, and acetic acid. This technique is described in Crounse et al. (2006). Background signals were monitored approximately every 20 minutes during the ARCTAS-CARB flights and approximately every 45 minutes during the BEARPEX campaign. The measured background signals are used to model background levels during data collection.

4.4 Determination of Analyte Concentration

4.4.1 Single Quadrupole CIMS Instrument

The single quadrupole CIMS instrument was used to conduct ambient measurements in and around California during the ARCTAS-CARB campaign. Determination of the analyte ion signal of hydroxyacetone, glycolaldehyde, and acetic acid is discussed below. Ambient concentrations of these trace gases are calculated from the analyte ion signal after normalization by the amount of reagent

ion signal, subtraction of background signals, and application of the appropriate sensitivity factor.

4.4.1.1 Hydroxyacetone

As discussed above, hydroxyacetone clusters with the reagent ion CF_3O^- and is detected at *m/z* 159. The uncertainty in the single quadrupole hydroxyacetone measurements is approximately ±(30% of the measurement value + 50 pptv). The uncertainty reflects the sum of the precision of the data determined by the counting statistics of the ions, the variability of the background signal, and the uncertainty in the sensitivity factor shown in Fig. 4.1. Propanoic acid is also observed at this mass, but its concentration is low (Yokelson et al., 2009).

4.4.1.2 Glycolaldehyde

The quantification of glycolaldehyde is complicated by a significant interference due to acetic acid, an exact mass analogue of glycolaldehyde. Both species undergo CF_3O^- clustering chemistry and are detected at *m/z* 145. The *m/z* 145 signal due to acetic acid in the form $CF_3O^- \cdot H_3CC(O)OH$ must be accounted for when determining the ambient glycolaldehyde concentration. This is accomplished by estimating the *m/z* 145 acetic acid signal from the acetic acid signal detected at *m/z* 79.

As discussed above, acetic acid also undergoes fluoride ion transfer with the CF_3O^- reagent ion and is detected as $H_3CC(O)O^- \cdot HF$ at *m/z* 79 (R4.3). There are no known interferences at this mass-to-charge ratio. The ratio of fluoride transfer ions (*m/z* 79) to clustering ions (*m/z* 145) for acetic acid is dependent on the amount of water in the instrument flow tube (Fig. 4.1). The ratio is determined experimentally via the laboratory and field calibrations discussed above. The *m/z* 145 signal due to acetic acid is estimated by multiplying the *m/z* 79 acetic acid signal by the water-dependent ratio of the acetic acid *m/z* 145 signal to the acetic acid *m/z* 79 signal. The average acetic acid contribution to the *m/z* 145 signal ranged from 40% to 60% of the total *m/z* 145 signal for the four flights. The contribution of acetic acid and glycolaldehyde to the *m/z* 145 signal are shown for the 18 June 2008 flight in Fig. 4.3.

The *m/z* 145 signal due to glycolaldehyde is calculated by subtracting the *m/z* 145 signal due

to acetic acid from the total m/z 145 signal detected by the single quadrupole CIMS instrument. The corrected glycolaldehyde signal is converted to concentration by application of the laboratory-determined instrument sensitivity factor for glycolaldehyde (Fig. 4.1, green curve). The uncertainty in the single quadrupole glycolaldehyde measurements is approximately ±(60% + 50 pptv). The uncertainty reflects the sum of the precision of the data determined by the counting statistics of the ions, the variability of the background signal, the uncertainty in the sensitivity factor shown in Fig. 4.1, and the uncertainty in acetic acid attribution.

4.4.2 Tandem CIMS Instrument

The tandem CIMS instrument was used to conduct ambient measurements at a tower site about five hours downwind of Sacramento during the BEARPEX 2009 campaign. Determination of the analyte ion signals of hydroxyacetone, glycolaldehyde, and acetic acid is discussed below. Similar to measurements made using the single quadrupole instrument, ambient concentrations of these trace gases are calculated from the ion signals after normalization by the amount of reagent ion signal, subtraction of background signals, and application of the appropriate sensitivity factor. An advantage of tandem CIMS lies in the ability to differentiate between isobaric species provided their fragmentation patterns are sufficiently different.

4.4.2.1 Hydroxyacetone

Tandem mass spectrometry measurement of hydroxyacetone is similar to that of single quadrupole mass spectrometry. The hydroxyacetone daughter ion signal at m/z 85 (m159m85) was used. The uncertainty in the tandem hydroxyacetone measurements is approximately ±(30% + 50 pptv). The uncertainty reflects the sum of the precision of the data determined by the counting statistics of the ions, the variability of the background signal, and the uncertainty in the sensitivity factor shown in Fig. 4.2.

4.4.2.2 Glycolaldehyde

The advantages of tandem mass spectrometry are demonstrated in the separate quantification of isobaric compounds glycolaldehyde and acetic acid. The sequence of quadrupole mass filter, collision-induced dissociation (CID) chamber, and second quadrupole mass filter enables the decomposition of isobaric ions into daughter ion fragments. As discussed above, while operating in tandem MS mode, ions of a selected mass-to-charge ratio pass through the first quadrupole mass filter and into the CID chamber, where they collide with N_2 molecules and fragment into daughter ions. The second quadrupole mass filter selects daughter ions of a certain mass-to-charge ratio.

Glycolaldehyde and acetic acid CF_3O^- cluster ions fragment differently due to differences in the stabilities of their clusters and the resultant daughter fragments. Significant daughter ion signals were observed at m/z 79, m/z 85, and m/z 145 and are denoted m145m79, m145m85, and m145m145, respectively. Figure 4.4 shows the parent ions—glycolaldehyde and acetic acid—and their significant daughter ion fragments. The daughter ion signals are reported relative to the sum of the three significant daughter ion signals for each compound. As shown in Fig. 4.4A, 90% of glycolaldehyde m/z 145 parent ions fragment to m/z 85 daughter ions, and zero percent fragment to m/z 79 daughter ions. The predominate daughter ion of acetic acid m/z 145 parent ions is m/z 79 (72%) (Fig. 4.4B). Ten percent of acetic acid m/z 145 parent ions fragment to m/z 85. 10% of glycolaldehyde and 18% of acetic acid m/z 145 parent ions do not fragment and are detected at m145m145. These percentages are too similar to enable unambiguous determination of the two species using m145m145 daughter ions. Acetic acid also fragments to m145m59, but the ion signal is a factor of ten less than that observed at m145m79.

Based on these fragmentation patterns, ambient signals due to glycolaldehyde and acetic acid can be separated. The m145m85 signal is mainly due to glycolaldehyde, and the small contribution due to acetic acid is accounted for during data analysis. The signal at m145m85 due to acetic acid is calculated by multiplying the acetic acid signal at m145m79 by the laboratory-derived ratio of acetic acid signal at m145m85 to acetic acid signal. The m145m85 signal due to glycolaldehyde is calculated by subtracting the acetic acid m145m85 signal from the total m145m85 signal.

Final glycolaldehyde concentrations are calculated using the corrected glycolaldehyde m145m85 ion signal and the corresponding tandem CIMS instrument sensitivity curve. Final acetic acid concentrations are calculated using both the m79m59 and m145m79 ion signals and their respective sensitivity curves. The uncertainty in the tandem glycolaldehyde measurements is approximately ±(50% + 50 pptv). The uncertainty in the tandem acetic acid measurements is approximately ±(40% + 50 pptv). The uncertainties reflect the sum of the precision of the data determined by the counting statistics of the ions, the variability of the background signal, and the uncertainty in the sensitivity factors shown in Fig. 4.2.

4.5 Observations

Aircraft observations indicate a range of hydroxyacetone and glycolaldehyde concentrations in California. Low altitude (<1.5 km pressure altitude) DC-8 flight tracks over northern and central California colored by observed hydroxyacetone concentrations are shown in Fig. 4.5A. Observed concentrations range from several hundred pptv along the coast to concentrations greater than 2 ppbv further inland, closer to biomass burning and biogenic sources. Flight tracks colored by observed glycolaldehyde concentrations are shown in Fig. 4.5B. Similar to hydroxyacetone concentrations, glycolaldehyde concentrations are low along the coast and much greater (>10 ppbv) closer to biomass burning and biogenic sources.

Ground-based measurements of hydroxyacetone, glycolaldehyde, and acetic acid concentrations during BEARPEX 2009 are shown in Fig. 4.6; ambient temperature is shown also. The average ambient temperature was ∼5 K higher for days after Day of Year (DOY) 195 compared to those prior. This may help explain the increase in observed hydroxyacetone, glycolaldehyde, and acetic acid concentrations after DOY 195 as emissions of isoprene and MBO are light and temperature dependent (Baker et al., 1999; Lamanna et al., 1999; Schade et al., 2000; Schade and Goldstein, 2001; Gray et al., 2005).

4.6 Results and Discussion

4.6.1 ARCTAS-CARB 2008

Hydroxyacetone and glycolaldehyde concentrations are well correlated during the ARCTAS-CARB 2008 campaign. The concentration of glycolaldehyde compared to that of hydroxyacetone colored by hydrogen cyanide (HCN) concentration is shown in Fig. 4.7. Data shown are low altitude measurements (<1.5 km). Linear regression, using the York et al. (2004) method that takes into account errors in both the abscissa and ordinate values, gives a slope of 4.6 and an intercept of −100 pptv. $R^2 = 0.87$. HCN is an atmospheric tracer of biomass burning emissions (e.g., Li et al., 2003) and was also measured during the ARCTAS-CARB campaign using the Caltech single quadrupole CIMS instrument (Crounse et al., 2009). Significant hydroxyacetone and glycolaldehyde occur only in airmasses with elevated HCN (≥250 pptv). In 2003, Christian et al. reported major, previously unobserved hydroxyacetone and glycolaldehyde emissions from combustion of Indonesian and African fuels during laboratory studies.

Emission ratios and enhancement ratios are commonly used to describe biomass burning emissions. An enhancement ratio or normalized excess mixing ratio typically takes the form Δ[X] / Δ[Y], where X and Y are two species present in the smoke plume. Δ[X] is the enhancement of the mixing ratio of X in the plume compared to the mixing ratio of X in background air. ΔY is usually a long-lived plume tracer such as ΔCO or ΔCO_2 (Yokelson et al., 2007). As the plumes analyzed in this work were not nascent plumes (age ranged from several minutes to one day) (Hornbrook et al., 2011), enhancement ratios rather than emission ratios are presented.

Enhancement ratios relative to CO for hydroxyacetone, glycolaldehyde, and HCN were calculated for plumes of biomass burning origin encountered during ARCTAS-CARB and were compared to previous field and laboratory findings. Many previous studies have determined emission or enhancement ratios of HCN from biomass burning; few studies have reported enhancement ratios for hydroxyacetone and glycolaldehyde.

Individual enhancement ratios were calculated for three biomass burning plumes in which hy-

droxyacetone, glycolaldehyde, HCN, and CO were measured. A list of biomass burning plumes encountered by the DC-8 during the ARCTAS campaign can be found in Hornbrook et al. (2011). Possible biomass burning plumes are identified by time periods of elevated biomass burning tracer mixing ratios. Plumes are defined by HCN greater than 400 pptv, acetonitrile (CH_3CN) greater than 200 pptv, and CO greater than 175 ppbv. Elevated mixing ratios of NO_x and toluene, anthropogenic tracers, were used to exclude plumes sampled in urban regions. Multiple samplings of a plume were grouped together and are referred to as a single plume. The plumes analyzed in this work were encountered at UTC 18:27–18:30 and 18:38–18:41 on 18 June, 21:08–21:12 and 21:23–21:44 on 22 June, and 14:32–14:35, 15:34–16:17, and 16:39–16:57 on 26 June. The correlation of the species of interest (hydroxyacetone, glycolaldehyde, or HCN) versus a long-lived plume tracer (CO) was determined by linear regression using the York et al. (2004) method. Calculated enhancement ratios, the associated R^2 values, and plume age of the three plumes are given in Table 4.1.

There is substantial variability in previous measurements of HCN enhancement ratios with respect to CO. Using a total least-squares analysis method, Crounse et al. (2009) calculated an emission ratio of 9.6 HCN to CO (pptv / ppbv) in Mexico City. This is consistent with the median emission ratio value of 8.5 determined by Yokelson et al. (2007) for the same sampling region and time period. Singh et al. (2003) observed a mean HCN enhancement ratio of 3.4 during measurements of Asian pollution outflow in 2001. Enhancement ratios of HCN in biomass burning plumes encountered in California during ARCTAS-CARB range from 2.1 to 4.1 HCN to CO (pptv / ppbv) (Table 4.1). The variability in HCN enhancement ratios may be explained by differences in combustion conditions and fuel type (Yokelson et al., 2007).

Christian et al. (2003) measured glycolaldehyde and hydroxyacetone emission ratios during laboratory studies of Indonesian and African fuels. Using the emission ratio of CO, HCN, glycolaldehyde, and hydroxyacetone to CO_2 determined by Christian et al. (2003), corresponding emission ratios relative to CO were estimated. The emission ratio of HCN, glycolaldehyde, and hydroxyacetone relative to CO (pptv / ppbv) is 12.3, 6.4, and 22.1, respectively, in fires from Indonesian fuels and 8.6, 3.2, and 3.3, respectively, in fires from African savanna fuels. Mean calculated enhancement

ratios of HCN, glycolaldehyde, and hydroxyacetone for the biomass burning plumes encountered in California and discussed in this work are 2.9, 5.7, and 1.5, respectively. These two sets of ratios were determined for fires of both different fuel and age. Postemission chemistry is expected to affect enhancement ratios, and fuel type is likely an important factor in the type and magnitude of emitted species. Nevertheless, the ARCTAS-CARB observations combined with previous laboratory observations demonstrate the range of emission ratios / enhancement ratios that may be measured from biomass burning sources.

4.6.2 BEARPEX 2009

The BEARPEX site is located on the western slope of the Sierra Nevada in a ponderosa pine plantation. The site is approximately five hours downwind of Sacramento, and a band of oak forests is located approximately halfway between Sacramento and the site. The prevailing daytime wind pattern transports anthropogenic volatile organic compounds (VOCs) and NO_x emissions from Sacramento and the Central Valley to the site. Isoprene, emitted from the band of oak forests, and MBO, emitted locally by the ponderosa pine forest, are added to the mixture. Wind direction reverses at night and brings clean air from the mountains to the site. Further details of the BEARPEX site can be found in Goldstein et al. (2000) and Dreyfus (2002).

Hydroxyacetone and glycolaldehyde concentrations are well correlated during the BEARPEX 2009 campaign (Fig. 4.8). The slope of the linear regression is 1.4, and the intercept is 0.80 pptv. $R^2 = 0.91$. The remarkable correlation is consistent with the hypothesis that hydroxyacetone and glycolaldehyde have similar sources (isoprene second-generation photooxidation) and sinks (reaction with OH and photolysis). The mean hydroxyacetone concentration measured during BEARPEX 2009 was 774 pptv, and the mean glycolaldehyde concentration was 986 pptv. Spaulding et al. (2003) measured average hydroxyacetone and glycolaldehyde concentrations of 420 pptv and 690 pptv, respectively, during an eight-day sampling period at the same site in August and September of 2000.

Using a simple box model, the ratio of glycolaldehyde to hydroxyacetone at the BEARPEX site

was calculated. VOCs represented in the model are isoprene and MBO; the concentrations of these VOCs simulate an isoprene source between Sacramento and the measurement site (the suburban oak tree belt) and a local source of MBO from the ponderosa pine plantation. The model was developed such that emissions from Sacramento (located at time = 0) and the surburban oak tree belt (located at time ≈ 150 minutes) are processed en route to the BEARPEX site (located at time ≈ 300 minutes) and modeled concentrations of these emissions are consistent with measurements conducted at the site. 300 minutes is chosen as the time representative of the measurement site, consistent with a 5-hour transport time from Sacramento to the site. Modeled concentrations of isoprene and MBO are shown in Fig. 4.9A. At 300 minutes, isoprene and MBO concentrations are both 2 ppbv.

Reaction rate constants are taken from IUPAC (Atkinson et al., 2004, 2006) and JPL (Sander et al., 2006) compilations. The rate constant for the reaction of isoprene-derived RO_2 and HO_2 discussed in Jenkin et al. (1997) has been used. Photolysis rates were calculated for the BEARPEX location using the Tropospheric Ultraviolet and Visible (TUV) radiation model (http://cprm.acd.ucar.edu/Models/TUV/). The isoprene oxidation mechanisms of Paulot et al. (2009a,b) have been followed with modifications and additions to mechanisms based on recent laboratory chamber experiments. The yield of hydroxyacetone from methacrolein oxidation in the presence of NO_x has been updated to 0.43 from 0.2 (Galloway et al., 2011). The mechanism describing MBO oxidation in the presence of NO_x from Chan et al. (2009) has been followed. A 0.15 yield of glycolaldehyde from MBO oxidation under low-NO_x conditions has been used as suggested by recent laboratory chamber experiments performed at Caltech. A unimolecular isomerization pathway for MACR that yields hydroxyacetone has been added and is the dominant formation pathway for hydroxyacetone in the model. When this pathway is excluded from the model, hydroxyacetone formation is dominated by NO oxidation of MACR. The model includes a smaller yield of hydroperoxide from MVK oxidation followed by HO_2 chemistry (0.3) than recommended by the Master Chemical Mechanism, MCM v3.2 (Jenkin et al., 1997; Saunders et al., 2003) and a large yield (0.6) of glycolaldehyde. This simple model does not include deposition.

Absolute concentrations of glycolaldehyde and hydroxyacetone calculated by the model are 1.1 and 0.9 ppbv, respectively, at 300 minutes and are similar to the mean observations from the campaign. The ratio of predicted glycolaldehyde concentration to hydroxyacetone concentration is shown in Fig. 4.9B. The predicted ratio resulting from only isoprene oxidation ranges from 1.1 to 1.3. The initial ratio is determined by the prompt formation of glycolaldehyde and hydroxyacetone via radical rearrangement as proposed by theoretical work (Dibble, 2004a,b) and recent laboratory chamber experiments (Paulot et al., 2009a; Galloway et al., 2011). The ratio increases when glycolaldehyde from MVK oxidation and hydroxyacetone from MACR oxidation are the dominant formation pathways. Since glycolaldehyde is formed from MBO oxidation and hydroxyacetone is not, the glycolaldehyde / hydroxyacetone ratio increases from 1.3 to 1.6 as more MBO is oxidized to form glycolaldehyde (250 – 600 minutes). The ratio of the production rate of glycolaldehyde to that of hydroxyacetone is shown in Fig. 4.9A and is mostly affected by increased glycolaldehyde production from MBO oxidation. Late in the model, oxidation of dihydroxyepoxides (IEPOX) of isoprene contributes to both hydroxyacetone and glycolaldehyde concentrations, highlighting the potential importance of the highly uncertain, late-generation isoprene oxidation chemistry at the site. The observed ratio of glycolaldehyde to hydroxyacetone at the BEARPEX site is 1.4 (Fig. 4.8), indicating predictions based only on isoprene and MBO chemistry are consistent with observations.

4.7 Conclusions

Chemical ionization mass spectrometry provides robust detection and quantification of hydroxyacetone and glycolaldehyde. The Caltech single quadrupole and tandem mass spectrometers are equally capable of the measurement of hydroxyacetone. Tandem mass spectrometry provides direct separation of the daughter ions of glycolaldehyde and acetic acid, enabling the differentiation of these mass analogues. This online method enables fast, in situ measurements with no sample processing. Ambient measurements of hydroxyacetone and glycolaldehyde were conducted during the ARCTAS-CARB 2008 campaign using the Caltech single quadrupole CIMS instrument. Enhancement ratios of hydroxyacetone, glycolaldehyde, and HCN were calculated for three biomass

burning plumes encountered in California during June 2008. Ambient measurements of hydroxyacetone and glycolaldehyde concentrations from oxidation of biogenic emissions were conducted during the BEARPEX 2009 campaign using the Caltech tandem CIMS instrument. The observed ratio of measured glycolaldehyde concentration to measured hydroxyacetone concentration is consistent with predictions from a simplified box model in which isoprene and MBO are the only VOCs represented.

4.8 Acknowledgements

G. S. Diskin and G. W. Sachse and A. H. Goldstein provided the ARCTAS-CARB and BEARPEX 2009 water measurements, respectively. The authors wish to thank the ARCTAS-CARB science team, the DC-8 crew, and the ARCTAS-CARB support team. The authors also wish to thank the BEARPEX science team and the UC Blodgett Forest Research staff. The hydroxyacetone, glycolaldehyde, and acetic acid measurements and their interpretation were made possible with the financial support of NASA (NAG: NNX-08AD29G) and the NSF (ATM-0934408).

Bibliography

Amelynck, C., Schoon, N., and Arijs, E.: Gas phase reactions of CF_3O^- and $CF_3O^- \cdot H_2O$ with nitric, formic, and acetic acid, International Journal of Mass Spectrometry, 203, 165–175, 2000.

Amelynck, C., Van Bavel, A. M., Schoon, N., and Arijs, E.: Gas phase reactions of CF_3O^- and $CF_3O^- \cdot H_2O$ and their relevance to the detection of stratospheric HCl, International Journal of Mass Spectrometry, 202, 207–216, 2000.

Atkinson, R., and Arey, J.: Gas-phase tropospheric chemistry of biogenic volatile organic compounds: A review, Atmospheric Environment, 37, S197–S219, doi:10.1016/S1352-2310(03)00391-1, 2003.

Atkinson, R., Baulch, D. L., Cox, R. A., Crowley, J. N., Hampson, R. F., Hynes, R. G., Jenkin, M. E., Rossi, M. J., and Troe, J.: Evaluated kinetic and photochemical data for atmospheric chemistry:

Volume I—gas phase reactions of O_x, HO_x, NO_x and SO_x species, Atmospheric Chemistry and Physics, 4, 1461–1738, 2004.

Atkinson, R., Baulch, D. L., Cox, R. A., Crowley, J. N., Hampson, R. F., Hynes, R. G., Jenkin, M. E., Rossi, M. J., and Troe, J.: Evaluated kinetic and photochemical data for atmospheric chemistry: Volume II—gas phase reactions of organic species, Atmospheric Chemistry and Physics, 6, 3625–4055, 2006.

Baker, B., Guenther, A., Greenberg, J., Goldstein, A., and Fall, R.: Canopy fluxes of 2-methyl-3-buten-2-ol over a ponderosa pine forest by relaxed eddy accumulation: Field data and model comparison, Journal of Geophysical Research—Atmospheres, 104, 26107–26114, 1999.

Bertschi, I., Yokelson, R. J., Ward, D. E., Babbitt, R. E., Susott, R. A., Goode, J. G., and Hao, W. M.: Trace gas and particle emissions from fires in large diameter and belowground biomass fuels, Journal of Geophysical Research—Atmospheres, 108, 8472, doi:10.1029/2002JD002100, 2003.

Butkovskaya, N. I., Pouvesle, N., Kukui, A., and Le Bra, G.: Mechanism of the OH-initiated oxidation of glycolaldehyde over the temperature range 233–296 K, Journal of Physical Chemistry A, 110, 13492–13499, doi:10.1021/JP064993K, 2006a.

Butkovskaya, N. I., Pouvesle, N., Kukui, A., Mu, Y. J., and Le Bras, G.: Mechanism of the OH-initiated oxidation of hydroxyacetone over the temperature range 236–298 K, Journal of Physical Chemistry A, 110, 6833–6843, doi:10.1021/JP056345R, 2006b.

Chameides, W. L., Lindsay, R. W., Richardson, J., and Kiang, C. S.: The role of biogenic hydrocarbons in urban photochemical smog: Atlanta as a Case Study, Science, 241, 1473–1475, 1988.

Chan, A. W. H., Galloway, M. M., Kwan, A. J., Chhabra, P. S., Keutsch, F. N., Wennberg, P. O., Flagan, R. C., and Seinfeld, J. H.: Photooxidation of 2-Methyl-3-Buten-2-ol (MBO) as a Potential Source of Secondary Organic Aerosol, Environmental Science & Technology, 43, 4647–4652, doi:10.1021/ES802560W, 2009.

Christian, T. J., Kleiss, B., Yokelson, R. J., Holzinger, R., Crutzen, P. J., Hao, W. M., Saharjo, B. H., and Ward, D. E.: Comprehensive laboratory measurements of biomass-burning emissions: 1. Emissions from Indonesian, African, and other fuels, Journal of Geophysical Research—Atmospheres, 108, 4719, doi:10.1029/2003JD003704, 2003.

Crounse, J. D., DeCarlo, P. F., Blake, D. R., Emmons, L. K., Campos, T. L., Apel, E. C., Clarke, A. D., Weinheimer, A. J., McCabe, D. C., Yokelson, R. J., Jimenez, J. L., and Wennberg, P. O.: Biomass burning and urban air pollution over the Central Mexican Plateau, Atmospheric Chemistry and Physics, 9, 4929–4944, 2009.

Crounse, J. D., McKinney, K. A., Kwan, A. J., and Wennberg, P. O.: Measurement of gas-phase hydroperoxides by chemical ionization mass spectrometry, Analytical Chemistry, 78, 6726–6732, 2006.

Dibble, T. S.: Intramolecular hydrogen bonding and double H-atom transfer in peroxy and alkoxy radicals from isoprene, Journal of Physical Chemistry A, 108, 2199–2207, doi:10.1021/JP0306702, 2004a.

Dibble, T. S.: Prompt chemistry of alkenoxy radical products of the double H-atom transfer of alkoxy radicals from isoprene, Journal of Physical Chemistry A, 108, 2208–2215, doi:10.1021/JP0312161, 2004b.

Dreyfus, G. B., Schade, G. W., and Goldstein, A. H.: Observational constraints on the contribution of isoprene oxidation to ozone production on the western slope of the Sierra Nevada, California, Journal of Geophysical Research—Atmospheres, 107, 4365, doi:10.1029/2001JD001490, 2002.

Galloway, M. M., Huisman, A. J., Yee, L. D., Chan, A. W. H., Loza, C. L., Seinfeld, J. H., and Keutsch, F. N.: Yields of oxidized volatile organic compounds during the OH radical initiated oxidation of isoprene, methyl vinyl ketone, and methacrolein under high NO_x conditions, Atmospheric Chemistry and Physics Discussions, 11, 10693–10720, 2011.

Goldan, P. D., Kuster, W. C., Fehsenfeld, F. C., and Montzka, S. A.: The Observation of a C_5

Alcohol Emission in a North American Pine Forest, Geophysical Research Letters, 20, 1039–1042, 1993.

Goldstein, A. H., Hultman, N. E., Fracheboud, J. M., Bauer, M. R., Panek, J. A., Xu, M., Qi, Y., Guenther, A. B., and Baugh, W.: Effects of climate variability on the carbon dioxide, water, and sensible heat fluxes above a ponderosa pine plantation in the Sierra Nevada (CA), Agricultural and Forest Meteorology, 101, 113–129, 2000.

Gray, D. W., Goldstein, A. H., and Lerdau, M. T.: The influence of light environment on photosynthesis and basal methylbutenol emission from *Pinus ponderosa*, Plant Cell and Environment, 28, 1463–1474, 2005.

Griffith, D. W. T.: Synthetic calibration and quantitative analysis of gas-phase FT-IR spectra, Applied Spectroscopy, 50, 59–70, 1996.

Grosjean, D., Williams, E. L., and Grosjean, E.: Atmospheric chemistry of isoprene and of its carbonyl products, Environmental Science & Technology, 27, 830–840, 1993.

Guenther, A., Hewitt, C. N., Erickson, D., Fall, R., Geron, C., Graedel, T., Harley, P., Klinger, L., Lerdau, M., McKay, W. A., Pierce, T., Scholes, B., Steinbrecher, R., Tallamraju, R., Taylor, J., and Zimmerman, P.: A global-model of natural volatile organic-compound emissions, Journal of Geophysical Research—Atmospheres, 100, 8873–8892, 1995.

Harley, P., Fridd-Stroud, V., Greenberg, J., Guenther, A., and Vasconcellos, P.: Emission of 2-methyl-3-buten-2-ol by pines: A potentially large natural source of reactive carbon to the atmosphere, Journal of Geophysical Research—Atmospheres, 103, 25479–25486, 1998.

Hornbrook, R. S., Blake, D. R., Diskin, G. S., Fuelberg, H. E., Meinardi, S., Mikoviny, T., Sachse, G. W., Vay, S. A., Weinheimer, A. J., Wiedinmyer, C., Wisthaler, A., Hills, A., Riemer, D. D., and Apel, E.C.: Observations of volatile organic compounds during ARCTAS—Part 1: Biomass burning emissions and plume enhancements, Atmospheric Chemistry and Physics Discussions, 11, 14127–14182, 2011.

Huey, L. G., Villalta, P. W., Dunlea, E. J., Hanson, D. R., and Howard, C. J.: Reactions of CF_3O^- with atmospheric trace gases, Journal of Physical Chemistry, 100, 190–194, 1996.

Jenkin, M. E., Saunders, S. M., and Pilling, M. J.: The tropospheric degradation of volatile organic compounds: A protocol for mechanism development, Atmospheric Environment, 31, 81–104, 1997.

Kroll, J. H., Ng, N. L., Murphy, S. M., Flagan, R. C., and Seinfeld, J. H.: Secondary organic aerosol formation from isoprene photooxidation, Environmental Science & Technology, 40, 1869–1877, doi:10.1021/ES0524301, 2006.

Lamanna, M. S., and Goldstein, A. H.: In situ measurements of C_2–C_{10} volatile organic compounds above a Sierra Nevada ponderosa pine plantation, Journal of Geophysical Research—Atmospheres, 104, 21247–21262, 1999.

Lee, Y. N., and Zhou, X. L.: Method for the determination of some soluble atmospheric carbonyl compounds, Environmental Science & Technology, 27, 749–756, 1993.

Lee, Y. N., Zhou, X. L., and Hallock, K.: Atmospheric carbonyl compounds at a rural Southeastern U.S. site, Journal of Geophysical Research—Atmospheres, 100, 25933–25944, 1995.

Li, Q. B., Jacob, D. J., Yantosca, R. M., Heald, C. L., Singh, H. B., Koike, M., Zhao, Y. J., Sachse, G. W., and Streets, D. G.: A global three-dimensional model analysis of the atmospheric budgets of HCN and CH_3CN: Constraints from aircraft and ground measurements, Journal of Geophysical Research—Atmospheres, 108, 8827, doi:10.1029/2002JD003075, 2003.

Matsunaga, S., Mochida, M., and Kawamura, K.: Growth of organic aerosols by biogenic semi-volatile carbonyls in the forestal atmosphere, Atmospheric Environment, 37, 2045–2050, doi:10.1016/S1352-2310(03)00089-X, 2003.

Moortgat, G. K., Grossmann, D., Boddenberg, A., Dallmann, G., Ligon, A. P., Turner, W. V., Gab, S., Slemr, F., Wieprecht, W., Acker, K., Kibler, M., Schlomski, S., and Bachmann, K.: Hydrogen peroxide, organic peroxides and higher carbonyl compounds determined during the BERLIOZ campaign, Journal of Atmospheric Chemistry, 42, 443–463, 2002.

Niki, H., Maker, P. D., Savage, C. M., and Hurley, M. D.: Fourier transform infrared study of the kinetics and mechanisms for the Cl-atom- and HO-radical-initiated oxidation of glycolaldehyde, Journal of Physical Chemistry, 91, 2174–2178, 1987.

Orlando, J. J., Tyndall, G. S., Fracheboud, J. M., Estupinan, E. G., Haberkorn, S., and Zimmer, A.: The rate and mechanism of the gas-phase oxidation of hydroxyacetone, Atmospheric Environment, 33, 1621–1629, 1999.

Paulson, S. E., Flagan, R. C., and Seinfeld, J. H.: Atmospheric photooxidation of isoprene Part 1: The hydroxyl radical and ground-state atomic oxygen reactions, International Journal of Chemical Kinetics, 24, 79–101, 1992.

Paulot, F., Crounse, J. D., Kjaergaard, H. G., Kroll, J. H., Seinfeld, J. H., and Wennberg, P. O.: Isoprene photooxidation: New insights into the production of acids and organic nitrates, Atmospheric Chemistry and Physics, 9, 1479–1501, 2009a.

Paulot, F., Crounse, J. D., Kjaergaard, H. G., Kurten, A., St. Clair, J. M., Seinfeld, J. H., and Wennberg, P. O.: Unexpected Epoxide Formation in the Gas-Phase Photooxidation of Isoprene, Science, 325, 730–733, doi:10.1126/science.1172910, 2009b.

Rothman, L. S., Jacquemart, D., Barbe, A., Benner, D. C., Birk, M., Brown, L. R., Carleer, M. R., Chackerian, C., Chance, K., Coudert, L. H., Dana, V., Devi, V. M., Flaud, J. M., Gamache, R. R., Goldman, A., Hartmann, J. M., Jucks, K. W., Maki, A. G., Mandin, J. Y., Massie, S. T., Orphal, J., Perrin, A., Rinsland, C. P., Smith, M. A. H., Tennyson, J., Tolchenov, R. N., Toth, R. A., Vander Auwera, J., Varanasi, P., and Wagner, G.: The HITRAN 2004 molecular spectroscopic database, Journal of Quantitative Spectroscopy & Radiative Transfer, 96, 139–204, 2005.

Sander, S. P., Friedl, R. R., Golden, D. M., Kurylo, M. J., Moortgat, G. K., Keller-Rudek, H., Wine, P. H., Ravishankara, A. R., Kolb, C. E., Molina, M. J., Finlayson-Pitts, B. J., Huie, R. E., and Orkin, V. L.: Chemical Kinetics and Photochemical Data for Use in Atmospheric Studies, Evaluation Number 15 JPL Publication 06-2, NASA Jet Propulsion Laboratory, California Institute of Technology, Pasadena, CA 2006.

Saunders, S. M., Jenkin, M. E., Derwent, R. G., and Pilling, M. J.: Protocol for the development of the Master Chemical Mechanism, MCM v3 (Part A): Tropospheric degradation of non-aromatic volatile organic compounds, Atmospheric Chemistry and Physics, 3, 161–180, 2003.

Schade, G. W., and Goldstein, A. H.: Fluxes of oxygenated volatile organic compounds from a ponderosa pine plantation, Journal of Geophysical Research—Atmospheres, 106, 3111–3123, 2001.

Schade, G. W., Goldstein, A. H., Gray, D. W., and Lerdau, M. T.: Canopy and leaf level 2-methyl-3-buten-2-ol fluxes from a ponderosa pine plantation, Atmospheric Environment, 34, 3535–3544, 2000.

Singh, H. B., Salas, L., Herlth, D., Kolyer, R., Czech, E., Viezee, W., Li, Q., Jacob, D. J., Blake, D., Sachse, G., Harward, C. N., Fuelberg, H., Kiley, C. M., Zhao, Y., and Kondo, Y.: In situ measurements of HCN and CH_3CN over the Pacific Ocean: Sources, sinks, and budgets, Journal of Geophysical Research—Atmospheres, 108, 8795, doi:10.1029/2002JD003006, 2003.

Spaulding, R. S., Schade, G. W., Goldstein, A. H., and Charles, M. J.: Characterization of secondary atmospheric photooxidation products: Evidence for biogenic and anthropogenic sources, Journal of Geophysical Research—Atmospheres, 108, 4247, doi:10.1029/2002JD002478, 2003.

Spencer, K. M., McCabe, D. C., Crounse, J. D., Olson, J. R., Crawford, J. H., Weinheimer, A. J., Knapp, D. J., Montzka, D. D., Cantrell, C. A., Hornbrook, R. S., Mauldin, R. L., and Wennberg, P. O.: Inferring ozone production in an urban atmosphere using measurements of peroxynitric acid, Atmospheric Chemistry and Physics, 9, 3697–3707, 2009.

St. Clair, J. M., McCabe, D. C., Crounse, J. D., Steiner, U., and Wennberg, P. O.: Chemical ionization tandem mass spectrometer for the in situ measurement of methyl hydrogen peroxide, Review of Scientific Instruments, 81, 094102, doi:10.1063/1.3480552, 2010.

Tuazon, E. C., and Atkinson, R.: A product study of the gas-phase reaction of methyl vinyl ketone with the OH radical in the presence of NO_x, International Journal of Chemical Kinetics, 21, 1141–1152, 1989.

Tuazon, E. C., and Atkinson, R.: A product study of the gas-phase reaction of isoprene with the OH radical in the presence of NO_x, International Journal of Chemical Kinetics, 22, 1221–1236, 1990a.

Tuazon, E. C., and Atkinson, R.: A product study of the gas-phase reaction of methacrolein with the OH radical in the presence of NO_x, International Journal of Chemical Kinetics, 22, 591–602, 1990b.

Washenfelder, R. A., Roehl, C. M., McKinney, K. A., Julian, R. R., and Wennberg, P. O.: A compact, lightweight gas standards generator for permeation tubes, Review of Scientific Instruments, 74, 3151–3154, doi:10.1063/1.1570949, 2003.

Yokelson, R. J., Crounse, J. D., DeCarlo, P. F., Karl, T., Urbanski, S., Atlas, E., Campos, T., Shinozuka, Y., Kapustin, V., Clarke, A. D., Weinheimer, A., Knapp, D. J., Montzka, D. D., Holloway, J., Weibring, P., Flocke, F., Zheng, W., Toohey, D., Wennberg, P. O., Wiedinmyer, C., Mauldin, L., Fried, A., Richter, D., Walega, J., Jimenez, J. L., Adachi, K., Buseck, P. R., Hall, S. R., and Shetter, R.: Emissions from biomass burning in the Yucatan, Atmospheric Chemistry and Physics, 9, 5785–5812, 2009.

Yokelson, R. J., Urbanski, S. P., Atlas, E. L., Toohey, D. W., Alvarado, E. C., Crounse, J. D., Wennberg, P. O., Fisher, M. E., Wold, C. E., Campos, T. L., Adachi, K., Buseck, P. R., and Hao, W. M.: Emissions from forest fires near Mexico City, Atmospheric Chemistry and Physics, 7, 5569–5584, 2007.

York, D., Evensen, N. M., Martinez, M. L., and Delgado, J. D.: Unified equations for the slope, intercept, and standard errors of the best straight line, American Journal of Physics, 72, 367–375, doi:10.1119/1.1632486, 2004.

Zhou, X. L., Huang, G., Civerolo, K., and Schwab, J.: Measurement of Atmospheric Hydroxyacetone, Glycolaldehyde, and Formaldehyde, Environmental Science & Technology, 43, 2753–2759, doi:10.1021/ES803025G, 2009.

Flight Date	$\frac{\Delta\text{HCN (pptv)}}{\Delta\text{CO (ppbv)}}$		$\frac{\Delta\text{GLYC (pptv)}}{\Delta\text{CO (ppbv)}}$		$\frac{\Delta\text{HAC (pptv)}}{\Delta\text{CO (ppbv)}}$		$\frac{\Delta\text{GLYC (pptv)}}{\Delta\text{HAC (pptv)}}$		Plume Age (Days)[a]
18 June	4.1	(0.99)	4.6	(0.91)	1.6	(0.98)	2.8	(0.88)	1
22 June	2.1	(0.93)	5.7	(0.56)	1.5	(0.77)	3.4	(0.52)	0.1
26 June	2.4	(0.96)	6.8	(0.93)	1.3	(0.96)	5.2	(0.94)	1

Table 4.1: Calculated enhancement ratios and the associated R^2 values (given in parentheses) of HCN, glycolaldehyde (GLYC), and hydroxyacetone (HAC) relative to long-lived plume tracer CO for three biomass burning plumes encountered during the ARCTAS-CARB campaign. The ratio of glycolaldehyde to hydroxyacetone in the plumes is included to enable comparison of the ratio of these compounds from biomass burning emissions and that of biogenic emissions, as measured during the BEARPEX 2009 campaign.
[a]Hornbrook et al. (2011)

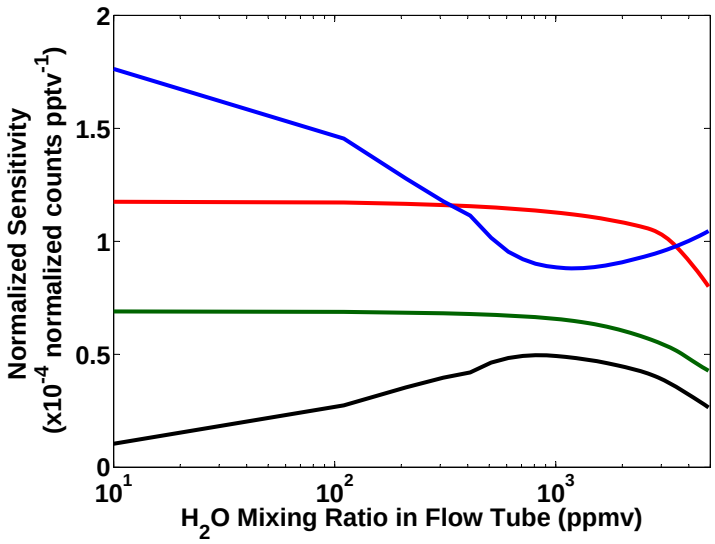

Figure 4.1: Single quadrupole CIMS instrument sensitivity curves for hydroxyacetone (red), glycolaldehyde (green), acetic acid fluoride transfer product (blue), and acetic acid cluster product (black) as a function of H_2O mixing ratio in the instrument flow tube. The sensitivity curves are used to calculate the final concentrations of the analytes. Typical H_2O mixing ratio values in the instrument flow tube were approximately 1500 ppmv during the ARCTAS-CARB campaign.

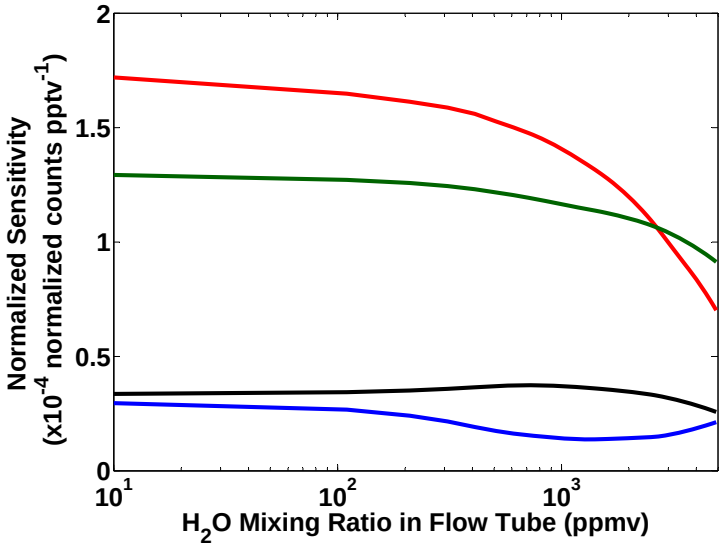

Figure 4.2: Tandem CIMS instrument sensitivity curves for hydroxyacetone daughter ion m159m85 (red), glycolaldehyde daughter ion m145m85 (green), acetic acid fluoride transfer daughter ion m79m59 (blue), and acetic acid cluster daughter ion m145m79 (black) as a function of H_2O mixing ratio in the instrument flow tube. The sensitivity curves are used to calculate the final concentrations of the analytes. Typical H_2O mixing ratio values in the instrument flow tube were approximately 1500 ppmv during the BEARPEX campaign.

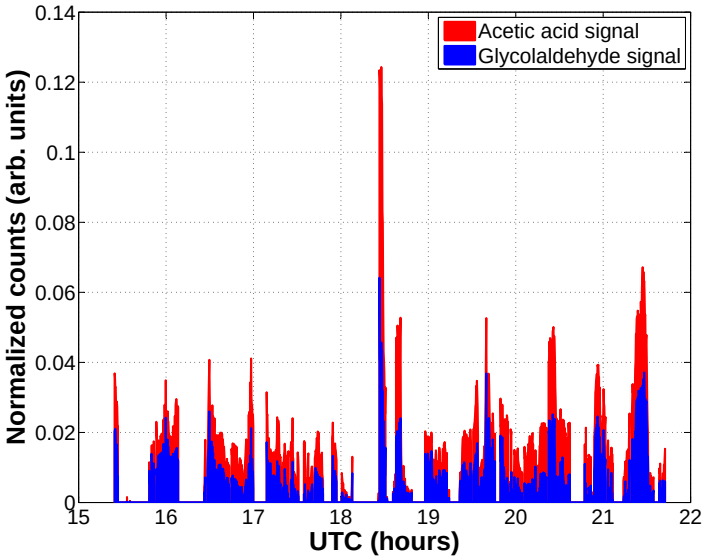

Figure 4.3: A time series of the contribution of acetic acid and glycolaldehyde to the m/z 145 signal detected by the Caltech single quadrupole CIMS instrument during the 18 June 2008 flight. The m/z 145 signal due to acetic acid is estimated from the m/z 79 acetic acid signal. The signal due to glycolaldehyde is determined by subtracting the signal due to acetic acid from the total m/z 145 signal.

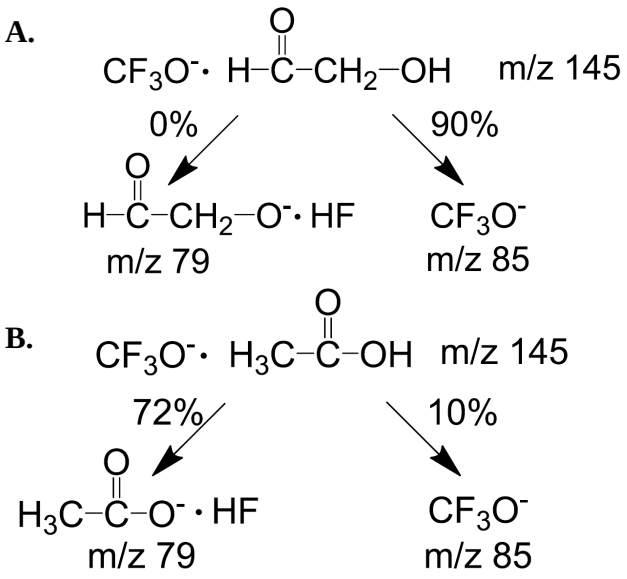

Figure 4.4: Collision-induced dissociation fragmentation pattern of glycolaldehyde (A) and acetic acid (B) including the percentage of m/z 145 parent ions that fragment to each of the daughter ions. The excellent separation of daughter ions enables the differentiation of glycolaldehyde and acetic acid.

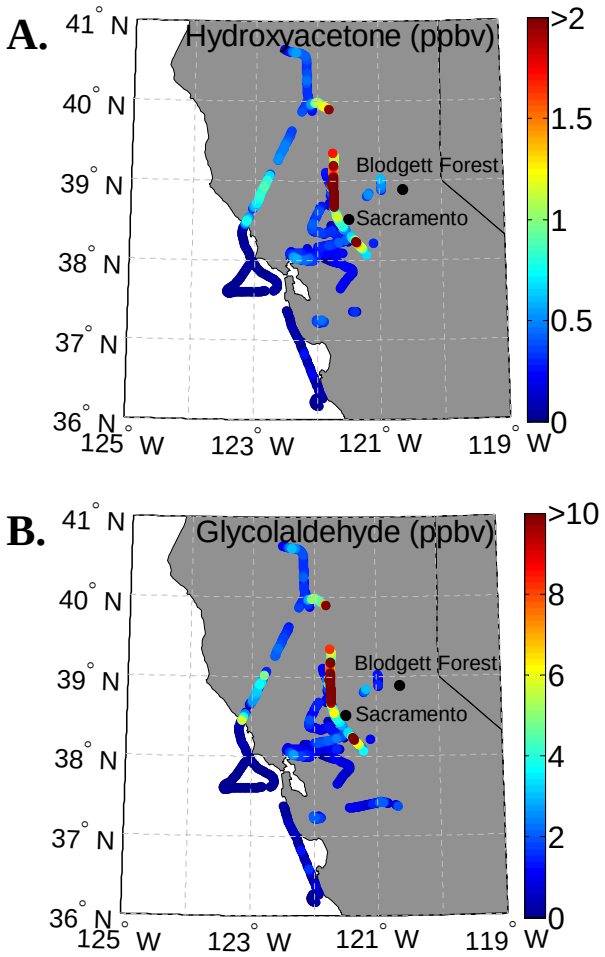

Figure 4.5: ARCTAS-CARB flight tracks colored by hydroxyacetone (A) and glycolaldehyde (B). Data presented are those when pressure altitude is less than 1.5 km. Observed concentrations of hydroxyacetone and glycolaldehyde are lowest along the coast and highest further inland, closer to biomass burning and biogenic sources.

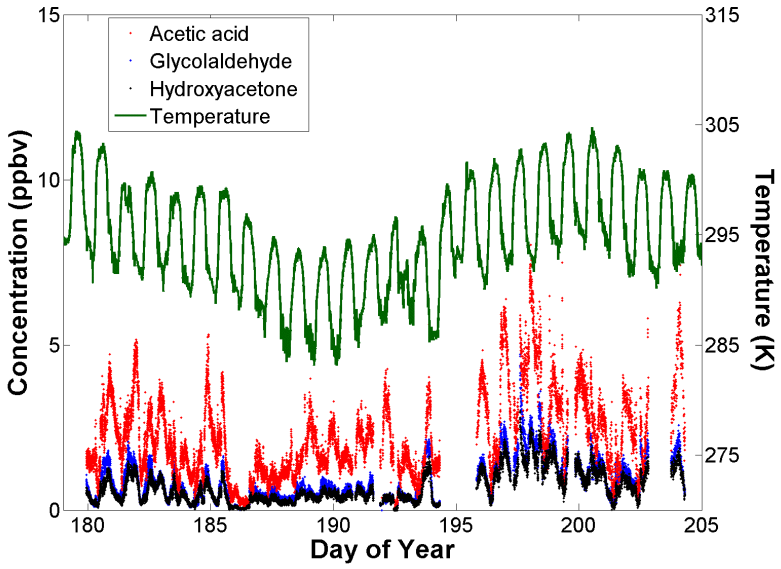

Figure 4.6: Concentrations of acetic acid (m145m79), glycolaldehyde (m145m85), and hydroxyacetone (m159m85) measured using the Caltech tandem CIMS instrument during the BEARPEX 2009 campaign.

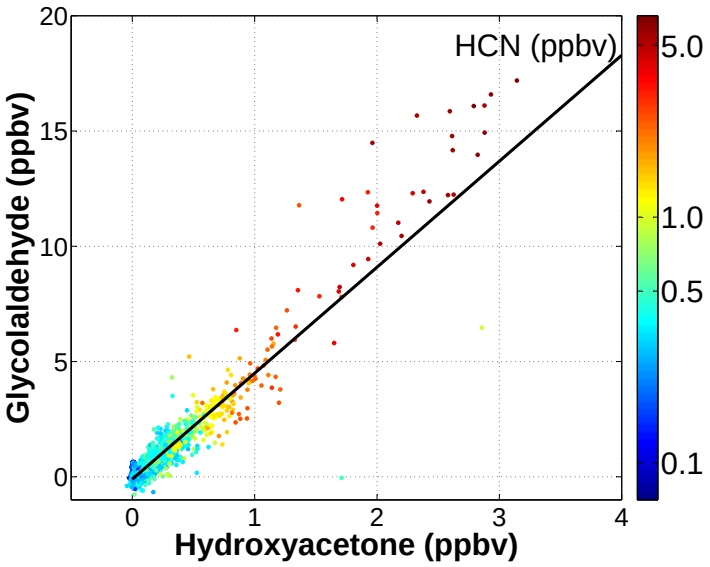

Figure 4.7: Glycolaldehyde concentration versus hydroxyacetone concentration colored by HCN concentration during the ARCTAS-CARB 2008 campaign. The slope of the linear regression is 4.6, and the intercept is -100 pptv. $R^2 = 0.87$.

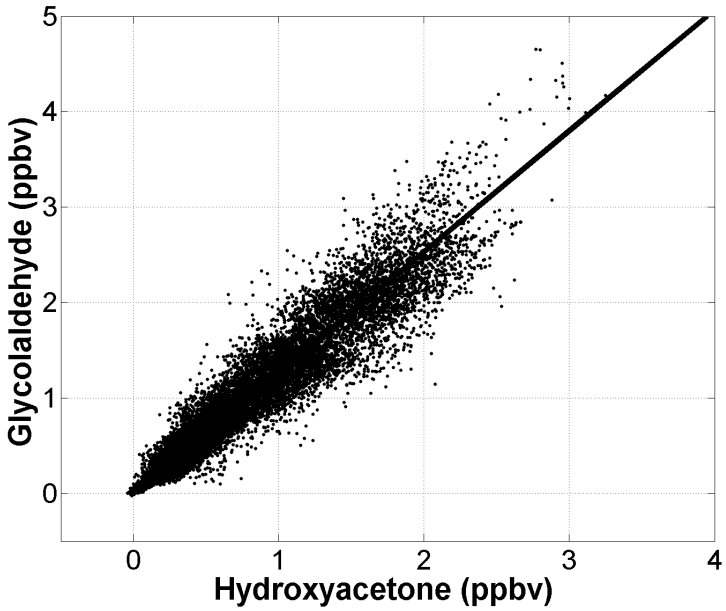

Figure 4.8: Glycolaldehyde concentration versus hydroxyacetone concentration during the BEARPEX 2009 campaign. The slope of the linear regression is 1.4, and the intercept is 0.80 pptv. $R^2 = 0.91$. The correlation is consistent with the hypothesis that hydroxyacetone and glycolaldehyde have similar sources and sinks.

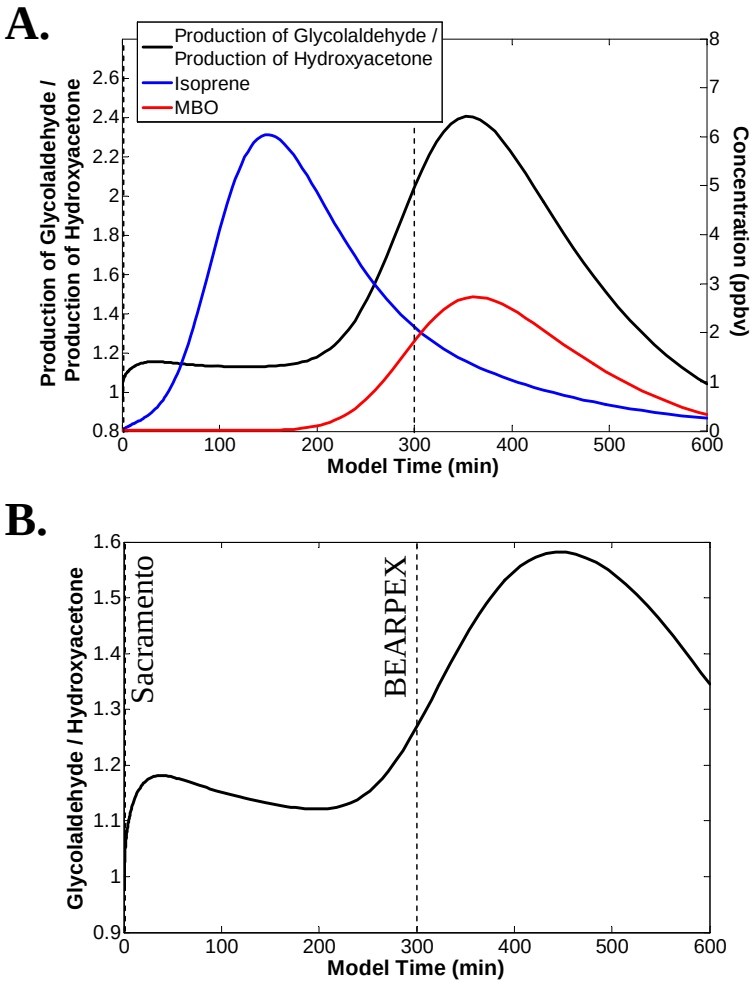

Figure 4.9: Ratio of the production of glycolaldehyde to the production of hydroxyacetone and concentration of isoprene and MBO (A) as predicted by a simple box model of the BEARPEX 2009 campaign. Ratio of glycolaldehyde concentration to hydroxyacetone concentration (B). As the BEARPEX site is approximately five hours downwind of Sacramento, CA, model oxidation time of 300 minutes is expected to correspond to site conditions.

Chapter 5

Conclusions

Ambient measurements of atmospheric trace gases and particulate matter are critical for extending our current knowledge of atmospheric processes. As discussed in this work, currently, models cannot accurately predict concentrations of airborne species under all conditions. Carefully collected, well-calibrated measurements are required to identify discrepancies between predicted and actual values. Close coupling of the experimental and modeling communities enables identification of errors and voids in our understanding. By working together, these groups have the opportunity to design and execute field and laboratory experiments aimed at answering outstanding atmospheric chemistry questions. The body of work in this thesis demonstrates progress toward understanding atmospheric chemical systems by means of in situ observations.

Chapter 2 illustrated the effectiveness of coupling observations and model predictions. A method for estimating the rate of ozone production in Mexico City using accurate measurements of three trace gases was described. This method does not require knowledge of volatile organic compound emissions, peroxyradical concentrations, or meteorological conditions. A comparison of measurements and predictions from a full photochemical box model indicated a discrepancy at high NO_x levels. In situ observations implied further NO_x controls may yield reductions in city smog levels while the effectiveness of this tool for smog control was not indicated by model predictions. Further investigation, using both measured data and modeled output, is required to determine why HO_x concentrations are generally underestimated at high NO_x levels for the conditions studied in Mexico City and what impact this underestimation may have on pollution-control strategies.

Regulatory efforts aimed at reducing particulate matter concentration in the Los Angeles basin have included measures enacted to reduce concentrations of gas-phase SO_2, the precursor of particulate sulfate. By combining aircraft observations, ground-based measurements, and modeled output, trends in airborne sulfur concentrations in the Los Angeles basin were identified and quantified. As described in Chapter 3, a substantial decrease in SO_2 concentration and a modest reduction in sulfate concentration occurred between 2002 and 2008. Future efforts to evaluate the effectiveness of efforts aimed at reducing particulate concentrations in the Los Angeles Basin will require additional measurements and model predictions of airborne species.

The ability to conduct more accurate measurements is facilitated by the development of innovative techniques. Chapter 4 detailed the use of triple quadrupole mass spectrometry to separate and quantify two exact mass analogues—glycolaldehyde and acetic acid. As glycolaldehyde is a precursor of glyoxal, both a tracer for and direct contributor to the formation of secondary organic aerosol, more accurate quantification of glycolaldehyde enables better predictions of secondary organic aerosol concentration and composition. The triple quadrupole chemical ionization mass spectrometry technique is a particularly valuable tool in efforts to better quantify concentrations of isobaric species. Continual development of instrumentation is necessary for increasing accuracy of ambient measurements and better constraining atmospheric models.